EVALUATING SATELLITE-BASED AEROSOL RETRIEVALS OVER MOUNTAINOUS REGIONS OF THE U.S.

A Thesis
by
IAN A. KRINTZ

Submitted to the School of Graduate Studies
at Appalachian State University
in partial fulfillment of the requirements for the degree of
MASTER OF SCIENCE

May 2021
Department of Physics and Astronomy

EVALUATING SATELLITE-BASED AEROSOL RETRIEVALS OVER MOUNTAINOUS REGIONS OF THE U.S.

A Thesis
by
IAN A. KRINTZ
May 2021

APPROVED BY:

James Sherman, Ph.D.
Chairperson, Thesis Committee

Christopher Thaxton, Ph.D.
Member, Thesis Committee

Jennifer Burris, Ph.D.
Chairperson, Department of Physics and Astronomy

Mike McKenzie, Ph.D.
Dean, Cratis D. Williams School of Graduate Studies

Abstract

EVALUATING SATELLITE-BASED AEROSOL RETRIEVALS OVER MOUNTAINOUS REGIONS OF THE U.S.

Ian Krintz
B.S., Appalachian State University
M.S., Appalachian State University
M.Sc., Management Center Innsbruck

Chairperson: Dr. James Sherman

Model-based predictions of the Earth's future climate rely on a series of assumptions and measurements to calculate the net global radiation balance. One of the largest sources of uncertainty in these measurements are the direct and indirect effects of atmospheric aerosols on the radiation budget (Intergovernmental Panel on Climate Change, 2014). Quantification of aerosol optical depth (AOD) with low uncertainty is achieved by surface-based sunphotometers which are geographically isolated. Alternatively, polar orbiting satellite-based platforms can provide near-global coverage on timescales of days to weeks. These satellite retrievals are limited by the need for cloud screening and the difficulty of separating the relative contributions from aerosols, trace gases, and surface reflectance to the observed top-of-atmosphere (TOA) radiances. Low aerosol loading, mountainous terrain, and snow or ice-covered surfaces exacerbate these retrieval challenges (Kahn, 2012; Levy et al., 2010; Sherman et al., 2016). Validation of satellite-based AOD retrievals against surface-based "ground truth" measurements is performed by collocating the results within a spatio-temporal window. This window is typically selected based on the estimated spatial and temporal extent over which a given air mass is measured by both the satellite and ground-based sensors. Often, such a window may not be optimized for the unique topography and surface properties at the ground site.

In this work, we evaluate satellite-based retrievals from NASA's Moderate Resolution Imaging Spectrometer (MODIS) and NASA's Multi-angle Imaging Spectrometer (MISR) above four

mountainous U.S. sites: (1) Appalachian State University (APP-Boone, NC); (2) Walker Branch, TN (WB); (3) Storm Peak Laboratory (SPL-Steamboat Springs, CO); and (4) University of Nevada (Reno, NV). Satellite AOD products evaluated include MODIS Dark Target (DT) at 3 km and 10 km resolutions, MODIS Deep Blue (DB) 10 km, MODIS combined DT / DB (COMBINED) 10 km, and the MISR 4.4 km product. Multiyear ground-based measurements are made at each site by either a Cimel sunphotometer or Multifilter Rotating Shadowband Radiometer (MFRSR). We (1) examine the influence of spatial and temporal variability in aerosol and surface properties on satellite / sunphotometer agreement, (2) apply and assess an automated method for optimizing collocation window and radius in the context of variability in surface properties and AOD, and (3) compare the performance of satellite AOD products above the four sites, and examine factors influencing their performance (season, surface properties, etc.).

Maps of the Normalized Differential Vegetation Index (NDVI), topography, and land cover are used to characterize the surface properties within a 50 km radius of each site. At the eastern sites (APP and WB), satellite-sunphotometer mean bias is primarily influenced by topography, urban regions, and water bodies for most products. Collocations at the western sites (SPL, Reno) are complicated by heterogeneous surface types and NDVI. The collocation window optimization algorithm is insensitive to temporal window size and insensitive to radius for the eastern sites if urban terrain is avoided. The algorithm is less successful at optimization for the western sites, particularly at Reno due to gaps over urban areas surrounding the site. Averages performed at the selected collocation window size for each resolution and site indicate little seasonal influence in agreement metrics at APP and WB, however fewer collocations are made during winter at western sites (esp. SPL). The DT algorithm tends to overestimate AOD in the summer and underestimate in the winter. Aqua MODIS products perform as well as Terra during summer but underestimate AOD more than Terra during winter. The mean bias of MODIS Terra DT AOD is ~0.02 to 0.04 more positive than MODIS Aqua for all sites and seasons. The MODIS DT 3 km product performs about equally to the DT 10 km product at APP, WB, and SPL.

Acknowledgments

This research was funded by a GRAM award. Thanks to the many students, faculty, and staff who have contributed to research at AppalAIR.

Dedication

To Dr. Sherman, who helped provide many opportunities for personal and professional growth as a member of the AppalAIR research team. His dedication to the advancement of students and science facilitated presentations at conferences and travel to other states and countries.

To my wife Jessica, who has always been a support throughout my academic career. Her never wavering faith, love, and patience provided space and time for the completion of my degrees and thesis.

Table of Contents

Chapter 1: Introduction

1.1 Overview of Atmospheric Aerosols

There is an ever-growing body of evidence that the Earth's climate is changing as a result of natural and anthropogenic factors which cause disturbances to the global radiation budget. In order to determine the net effect and how it will affect the future climate, scientists must combine measured and assumed parameters as inputs to computer models. The resulting estimate is inevitably limited by the uncertainties of the inputs. The Intergovernmental Panel on Climate Change (IPCC, 2014) states that the direct and indirect effects of atmospheric aerosols on the global radiation budget are one of the largest sources of uncertainty in climate models. Aerosols are solid or liquid particles suspended in the air which often appear as smoke, dust, or haze. These particles directly affect the solar radiation budget by scattering or absorbing incoming radiation. Aerosols also serve as cloud condensation nuclei and indirectly effect solar radiation budget by modifying cloud albedo, lifetimes, and precipitation potential (Twomey, 1977; Albrecht, 1989). Aerosols can be produced by either primary or secondary means and their sources can be either anthropogenic (human activities) or natural. Black carbon emitted directly by diesel vehicles or biomass burning and sulfate and secondary organic aerosols (SOA) produced via chemical processing of anthropogenic precursor gases from combustion processes are examples of anthropogenic aerosols, although SOA is also produced by interactions involving biogenic and anthropogenic precursor gases (Goldstein et al., 2009). Aerosols are also naturally occurring as a result of atmospheric or biological processes, such as wind-dust, volcanic ash, sea salt, or pollen. As a consequence of the regional nature of aerosol sources, aerosols are typically localized geographically and tend to reside within or near the planetary boundary layer, although favorable atmospheric conditions may transport aerosols to the upper troposphere and across great distances (Val Martin et al., 2010; VanCuren & Cahill, 2002; Yu et al., 2012). Most aerosols have

lifetimes on the order of days to weeks as a result of common removal mechanisms such as settling or rainout and are subject to seasonal and annual variability.

1.2 Aerosol Direct and Indirect Effects on Solar Radiation

There are generally three properties that govern how a particle will directly interact with electromagnetic (EM) radiation – the ratio of particle size divided by wavelength of incident radiation (size parameter, d/λ), particle shape, and the particle's wavelength-dependent complex refractive index. The light scattering and absorption coefficients of particles (σ_{sp} and σ_{ap}) generally exhibit a power law dependence $1/\lambda^{\alpha}$, where the α_{sp} and α_{ap} are called the scattering and absorption Angstrom exponents, respectively. If the particle is much smaller than the wavelength of incident radiation (i.e. $d/\lambda << 1$), Rayleigh theory adequately describes the interaction, for which $\alpha_{sp}=4$ and $\alpha_{ap}=1$. However, if the particle diameter is close to the wavelength of the radiation, Mie theory must be applied to predict the behavior. The composition of the particle also determines the scattering and absorptive capabilities: the real part of the refractive index of the particle provides information on the scattering properties, while the imaginary part is proportional to aerosol light absorption coefficient. In the case of a purely scattering aerosol, the imaginary part will be zero. In the case of non-spherical particles, such as dust, Mie theory cannot be applied and T-matrix (Dubovik et al., 2002) and other techniques are necessary to model the interactions.

Aerosol direct radiative effect (DRE) is typically used to quantify the direct effects of scattering and absorption on solar radiation budget. It is defined as the difference in the net downwelling solar flux (downwelling minus upwelling) with aerosols minus the net downwelling flux without aerosols (units Wm^{-2}). It must be specified at a given altitude, usually the top of the atmosphere (TOA) or the Earth's surface. A negative DRE value indicates an increase in net upwelling radiation with aerosols than without aerosols (i.e. cooling effect) while a positive DRE value indicates a reduction in net upwelling radiation in presence of aerosols. Brighter aerosols produce cooling effects at both the TOA and surface while darker aerosols lead to a warming effect at the TOA but a cooling effect at the surface (Hansen et al., 1980). The DRF effect at the TOA also

depends (to a lesser extent) on the backscatter fraction and surface albedo (Sherman & McComiskey, 2018), where a given aerosol may have a cooling effect over darker surfaces, yet a warming effect over brighter surfaces (Haywood & Shine, 1995).

The first indirect effect of aerosols, termed the cloud albedo or Twomey Effect, is a result of aerosols acting as cloud condensation nuclei. Intuitively, a larger number of smaller droplets means a greater density of surfaces for potential interaction (seen as "whiter" clouds) and results in a net negative radiative effect. However, cloud thickness is an important factor; for sufficiently thick clouds a net warming effect may be observed (Twomey, 1977). Increases in cloud lifetimes, heights, and suppression of light rain events together comprise the second indirect effect of aerosols (Albrecht, 1989; Pincus & Baker, 1994). Finally, the semi-direct effect of aerosols is a reduction in cloud formation as a result of the absorptive heating of the aerosol particles (Ackerman, 2000). The direct and indirect effects of aerosols are illustrated in Figure 1 below.

Figure 1

The Effects of Aerosols on the Earth's Energy Balance

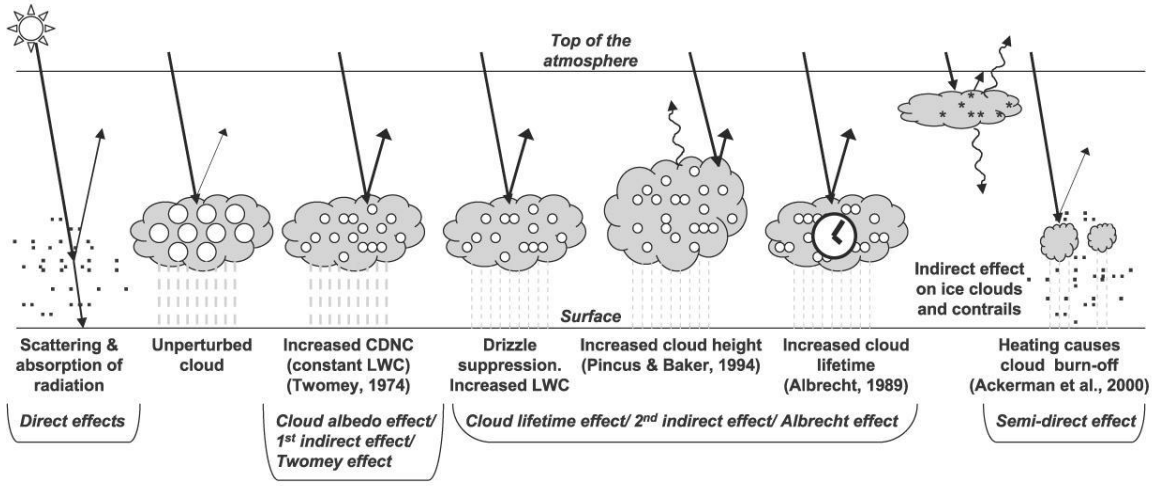

Note. Aerosols' direct effects are the scattering and absorption of radiation. Indirect effects include increased cloud droplet number concentration (CDNC) at a constant liquid water content (LWC), drizzle suppression with an increased LWC, modification of cloud heights and lifetimes, and cloud burn-off due to absorptive heating. Image credit: IPCC 4th Assessment Report, Working Group 1.

1.3 Aerosol Properties Used in Radiative Transfer Models

Radiative transfer models (RTMs) are used to quantify aerosol DRE and are also used as part of satellite-based aerosol retrieval algorithms. The models require several important aerosol properties as inputs in order to properly evaluate their interactions with EM radiation, including the spectral dependence of aerosol optical depth (AOD) and single scattering albedo (SSA), along with some proxy for the size distribution. AOD is a dimensionless measure of the column-integrated light extinction coefficient ($AOD = \int_{z=0}^{TOA} \sigma_{ep}\, dz$), where extinction is the sum of scattering plus absorption. It is a measure of the amount of aerosol in the atmospheric column, in an optical sense. The AOD can also be expressed as the negative natural logarithm of the ratio of the transmitted flux by aerosols to the total incident flux. Single scattering albedo, also a dimensionless quantity, is the ratio of scattering to extinction coefficient ($SSA = \frac{\sigma_{sp}}{\sigma_{ep}} = \frac{\sigma_{sp}}{\sigma_{sp}+\sigma_{ap}}$) where a value of 1 indicates a purely scattering aerosol and a value near zero indicates a purely absorbing aerosol. The size distribution of aerosols is commonly measured with instruments such as a scanning mobility particle sizer (SMPS). When such instruments are not available, a proxy such as scattering asymmetry parameter (g) may be used to gather information regarding the distribution. Asymmetry parameter is the average of the cosine of the angle of scattering; it is a measure of the directionality of scattering by the particle. If light is scattered equally in the forward and backward hemispheres then the asymmetry parameter will be near zero, indicating aerosols falling into the Rayleigh size regime where the aerosol is very small relative to the wavelength of EM radiation. Conversely, if the asymmetry parameter is close to 1, this indicates that the aerosol particles are approximately the same size – or larger – than the wavelength. While AOD generally has the largest influence on DRE, the SSA can exert a comparable influence for higher aerosol loading conditions (Sherman & McComiskey, 2018).

Aerosols are generally grouped into two regimes: fine mode, with particle diameters ranging from ~5 nm to 1 μm, and coarse mode for particles with diameters larger than 1 μm. The fine mode is

sometimes further subdivided into the nucleation / Aitken mode (< 0.1 μm) and the accumulation mode (0.1 μm to 1 μm). The accumulation mode aerosols dominate the radiative effects of fine mode aerosols. Given these distributions, short wavelength radiation is affected by aerosols of all sizes, while longer wavelengths (e.g. the thermal infrared) interact with larger aerosols.

Angstrom exponent (AE or α) describes the spectral dependence of AOD, via the equation

$$AOD(\lambda) = AOD(\lambda_{ref}) \cdot \lambda^{AE} \quad (1)$$

In practice, AE is often estimated as the negative slope of the least-squares regression fit of the natural logarithm of the measured AOD versus the natural logarithm of wavelength, although the choice of visible / near-IR wavelength range used in the regression can influence the calculation of AE for dust-dominated aerosol regions (Eck et al., 1999). Since the spectral dependence of AOD is greater for fine-mode aerosols than for coarse-mode aerosols, AE can provide some information on particle size distribution, with larger (smaller) AE values corresponding to size distributions more influenced by smaller (larger) particles. Values of AE > 2 are typically associated with fresh biomass burning (Kaufman et al., 1992) while values of AE < 1 indicate aerosol populations largely influenced by dust or sea salts (Holben et al., 1991; Eck et al., 1999). Values of AE between 1-2 are typical for background continental aerosols in non-desert regions, which are primarily influenced by mixtures of aged (and hence larger) accumulation-mode particles often resulting from transported pollution and biomass burning.

1.4 Ground and Satellite-Based Platforms for Measuring Aerosol Properties

Aerosol properties may be measured in-situ using near-surface or airborne sampling methods or remotely from either the Earth's surface or aboard satellite-based platforms. In-situ systems can measure aerosol intensive properties – those which are independent of aerosol amount, such as SSA, size distribution, and g – to a high degree of accuracy (Sherman et al., 2015) but lack the ability to quantify AOD. Conversely, surface-based remote sensing is capable of low uncertainty AOD measurements, yet intensive properties are much more difficult to calculate reliably. The key advantage to both surface-based remote and in-situ measurements over satellite based remote sensing

methods are their high temporal resolutions. However, being point measurements, they are extremely limited in their ability to represent the spatial distribution of aerosols and their properties. As a solution to the spatial limitation, satellite-based platforms can provide near-global coverage but with a much longer gap between retrievals relative to the ground-based measurements. Each of these platforms are discussed in more detail in the following subsections.

1.4.1 Satellite-Based Aerosol Retrievals

Satellite-based platforms provide near-global coverage of aerosols with temporal intervals on the order of approximately one week or less, and spatial resolutions of around 3 to 20 km depending on the instrument and orbital characteristics. Most satellites derive aerosol properties by determining the self-consistent set of aerosol optical properties which (when used as inputs to an RTM) yield the best agreement of calculated upwelling TOA spectral radiance with measured upwelling TOA solar radiance. The calculated radiances are stored in a look-up table for each solar and sensor zenith angle and light scattering angle over a wide range of AOD, SSA, and size distributions. The lookup table must also be able to separate the contributions of TOA radiances due to aerosols from those of the surface, which require some assumptions of surface type for the region (Levy et al., 2007). The difficulties associated with separating the contributions to TOA radiances due to surface, trace gases, and aerosols, along with screening the effects of clouds, are limiting factors in the satellite-based aerosol retrievals. Currently, only AOD is retrieved with an accuracy close to that needed for low-uncertainty DRE studies (Kahn, 2012; Sherman & McComiskey, 2018), and is also being used in estimates of sub-2.5 μm surface particulate matter (PM 2.5) concentrations for air quality applications (Chu et al., 2003; van Donkelaar et al., 2016).

Two satellite instruments are considered here: NASA's Moderate Resolution Imaging Spectrometer (MODIS; Levy et al., 2007b) and NASA's Multi-angle Imaging Spectrometer (MISR; Kahn & Gaitley, 2015). Both have been validated at the global level against networks of low uncertainty "ground truth" stations, however there are significant discrepancies at the regional scale. These inconsistencies occur over mountainous terrain due to the difficulties in separating the surface

and atmospheric contributions to the observed radiances, particularly at low aerosol loading (Levy et al., 2010; Sherman et al., 2016) and over snow and ice-covered surfaces (Kahn, 2012). Absolute uncertainties for satellite AOD retrievals are currently about 0.05 (e.g. Levy et al., 2010) and improving, although the uncertainty required to estimate DRF to within approximately 1 Wm^{-2} is 0.02 (McComiskey et al., 2008; Sherman & McComiskey, 2018). Satellites are also very limited in their ability to quantify aerosol intensive properties, however recent improvements show that aerosol type and SSA may be at least qualitatively estimated from MISR retrievals (Kahn & Gaitley, 2015). The algorithm-specific retrieval method and unique characteristics of each instrument are discussed in Chapter 2.

1.4.2. Ground-Based Remote Sensing

Remote sensing devices for measuring AOD – named sunphotometers – have been around since the early 18th century (Shaw, 1983), and have gone through significant advances. Although possessing varying degrees of complexity, sunphotometers all measure direct solar radiances at multiple wavelengths and the AOD algorithms invert the measured radiances, using the Beer-Lambert-Bouger equation (Shaw, 1983). The inversion requires knowledge of the signal that the instrument would measure at the TOA, which is typically obtained via a Langley method calibration (Shaw, 1983). It also requires knowledge of optical depth (OD) contributions due to Rayleigh scattering from the static atmospheric gases (oxygen, nitrogen, carbon dioxide) and absorption by trace gas pollutants (ozone, nitrogen dioxide). Rayleigh OD can be calculated from measurements of surface pressure and temperature (Bodhaine et al., 1999). The ozone and nitrogen dioxide OD are zero for all but a few UV-visible bands and can be estimated from either satellite or climatological data. The inversion assumes that cloud OD is zero, which is satisfied if there are no clouds along the instrument's line of sight. Similar to satellite-based retrievals, contamination from thin clouds near or in line of sight poses challenges for AOD retrieved by ground-based sunphotometers. Federated sunphotometer networks such as NASA's Aerosol Robotic Network (AERONET; Holben et al., 1998) and NOAA's Surface Radiation Budget Network (SURFRAD) have been used as "ground-

truth" for validating satellite-retrieved AOD since 2002, due to the low AOD uncertainty of ~0.01-0.02 measured by Cimel sunphotometers used by AERONET (Eck et al., 1999; Michelsky, 2002) and the Multifilter Rotating Shadowband Radiometers (MFRSR) used by SURFRAD (Michelsky, 2002). While the SURFRAD network is only located within the continental U.S., AERONET has several hundred permanent stations worldwide and therefore is the most common network for global validation of satellites. Using advanced algorithms, sunphotometers are also able to estimate aerosol intensive properties (SSA, g), although these measurements are subject to higher uncertainty at low AOD (Dubovik et al., 2000).

1.4.3 Evaluation of Satellite-Measured AOD by Ground-Based Sunphotometers

The use of ground-based AOD measurements made by sunphotometers to evaluate AOD retrieved from satellite platforms is complicated by the fact that the upward pointing sunphotometer samples air conditions along the sun line of sight at regular temporal intervals (for example, ~15 min for AERONET sites during mid-day), whereas the downward pointing satellite instrument averages the AOD over a given spatial pixel size (for example, ~10 km x 10 km) at a given time. Furthermore, the AERONET measurement times typically do not coincide precisely with the time that the satellite passes nearest to the ground site and the closest satellite pixel is rarely centered exactly over the ground site. Spatio-temporal collocation involves selecting spatial and temporal-averaging windows such that the air masses sampled by both instruments can be assumed to be similar enough that the AOD measurements may be directly compared. A choice of spatio-temporal window not optimized for the region surrounding the ground site and the satellite sensor capabilities can induce a bias in the AOD comparisons that is nearly impossible to quantify.

Many global evaluations of MODIS AOD above AERONET sites have used spatio-temporal windows based on similar reasoning to that outlined in Ichoku et al (2002). In their study, Ichoku et al. did not observe a systematic bias in global MODIS / AERONET AOD comparisons induced by varying the spatial averaging window size from 30 km x 30 km to 90 km x 90 km. They chose a 50 km x 50 km spatial window so as to optimize spatial statistics (i.e. averaging over 5x5=25 of the 10

km x 10 km pixels) without increasing the likelihood for errors due to topographic or aerosol type inhomogeneity. Such assumptions may not be valid over individual sites with complex terrain. In selecting a temporal window size, Ichoku et al. used summer observations of long-range aerosol transport from Africa over the Atlantic to estimate a typical air mass velocity of ~50 km/h. Based on this, they compared AERONET-measured AOD averaged over a temporal window of 1 h (centered on time of MODIS overpass) to MODIS-measured AOD averaged over a 50 km x 50 km spatial window, centered at the ground site. Kovacs (2006) selected a temporal window of 1 h as well. Though the intention of their study was not the analysis of a spatio-temporal collocation method for validation of satellite swath measurements, a radius of 20 km was mentioned to be in good agreement with ground truth data. Furthermore, one site in the Kovacs study (Boulder, CO) performed poorly relative to the others, which was attributed to the complex terrain and sub-optimal surface reflectance. Zhao et al. (2002) optimized the spatio-temporal window for MODIS AOD validation studies over the ocean using 13 island AERONET sites and found a temporal window of 1 h and spatial window of 100 km to be optimal, although a circle of 25 km was removed from the satellite data over the site to reduce the effects of land and shallow water. The larger window size over water was unsurprising, since the ocean surface is more homogeneous than many land surfaces. Based on these other studies, a spatial window on the order of 100 km or less and a temporal window of around 1 h are reasonable starting points for a spatio-temporal collocation optimization algorithm over land.

1.5 Objectives and Significance

The over-arching objective of this thesis work is to perform a detailed evaluation of satellite-based AOD retrievals made by the MODIS and MISR instruments above four mountainous U.S. sites: (1) Appalachian State University (APP-Boone, NC); (2) Walker Branch, TN (WB); (3) Storm Peak Laboratory (SPL-Steamboat Springs, CO); and (4) University of Nevada (Reno, NV). Each location is home to either a CIMEL sunphotometer (as part of NASA AERONET) or MFRSR for evaluating the satellite retrieved AOD and the four sites collectively represent aerosol loading and surface type conditions over mountainous U.S. regions. Specifically, we

1. Examine the influence of spatial and temporal variability in aerosol and surface properties on satellite / sunphotometer AOD agreement.
2. Apply and assess an automated method for optimizing collocation window and radius, in the context of variability in surface properties and AOD.
3. Compare the performance of satellite AOD products above the four sites, and examine factors influencing their performance (season, surface properties, etc.).

The results of this project have implications for localized aerosol studies, where the level of agreement between the satellite and ground-measured AOD is often influenced by the selection of a spatio-temporal window used for collocating the two measurements. To the best of our knowledge, no studies have been conducted analyzing the effects of choice of such a window on AOD agreement over mountainous terrain. Most satellite AOD validation studies apply a spatio-temporal collocation window calculated based on the spatial and temporal extent that the same air mass would be expected to be 'seen' by both the ground and satellite-based sensors (e.g. Ichoku, 2002), which may not apply to the region under study.

1.6 Thesis Structure

The thesis is structured as follows. The four mountainous sites used in the study and the data products available at each site are introduced in Chapter 2. The spatio-temporal collocation method is described in Chapter 3, including algorithm development, site characterization, and optimization of the window for each site. A detailed discussion of results from the study is presented in Chapter 4, followed by a summary of findings, limitations of our study, and suggested directions for future work.

Chapter 2: Data and Sites

Land-based AOD and AE measurements are performed by two types of instrumentation at the four sites: Cimel sunphotometers located at APP, WB, and RENO as part of the NASA AERONET federated network, and a MFRSR located at SPL. Satellite retrievals of AOD used in this study include the outputs of four MODIS products and one MISR algorithm. Table 1 provides a summary of these ground and satellite-based datasets including the AOD expected error and the wavelengths at which AOD is reported. Sections 2.1-2.2 detail the operational parameters and algorithm specifics for each satellite-based data set, while Section 2.3 describes the ground-based instrumentation. Supporting satellite-derived datasets utilized to characterize the surface properties (NDVI, land cover type) at each ground site are identified in Section 2.4, followed by a brief description of each site in the context of these surface properties, topography, and other noteworthy characteristics.

Table 1

Remote Sensing Datasets Used in this Study

Name	Resolution	Source	Properties	Wavelengths	AOD Expected Error
MODIS DB	10	satellite	AOD	550	$\pm(0.05 + 0.20 \cdot AOD)$[f]
MODIS DT	10	satellite	AOD	470, 550, 660	$\pm(0.05 + 0.15 \cdot AOD)$[e]
MODIS DT	3	satellite	AOD	470, 550, 660	$\pm(0.05 + 0.20 \cdot AOD)$[c]
MODIS COMBINED	10	satellite	AOD	550	$\pm(0.05 + 0.15 \cdot AOD)$[e]
MISR	4.4	satellite	AOD	550	± 0.05 or $\pm(0.2 \cdot AOD)$[d,g]
AERONET	N/A	ground	AOD, AE	340, 380, 440, 500, 670, 875, 1020, 1640	± 0.01 to ± 0.02[b]
MFRSR	N/A	ground	AOD, AE	500, 615, 673, 870	± 0.01[a]

Note. The wavelengths (in nm) listed here are those included in the product and are not necessarily indicative of the full spectral capabilities of the instrument. Instrument pixel resolutions are reported in km.

[a]Alexandrov et al. (2008).

[b]Eck et al. (1999).

[c]Gupta et al. (2018).

[d]Kahn et al. (2010).

[e]Levy et al. (2013).

[f]Sayer et al. (2019).

[g]The larger of the two values is chosen as the expected error.

2.1 MODIS Aerosol Optical Depth

The MODIS instruments are located aboard the sun-synchronous, polar-orbiting NASA Earth Observing System (EOS) satellites Terra (since 2000) and Aqua (since 2002). MODIS provides near-global coverage daily thanks to a wide 2330 km swath width at nadir and an approximately 99-minute orbital period. Terra is a "morning" satellite with a 10:30 a.m. local standard time (LST) descending node equatorial crossing, while Aqua is an ascending node "afternoon" satellite with an equatorial crossing around 1:30 p.m. LST. Raw top-of-atmosphere (TOA) radiances in 36 spectral bands ranging from 410 nm to 14.5 μm (14500 nm) are measured with nadir resolutions varying from 250 m to 1 km, although it should be noted that pixels become larger at the edges of the scan. A calibration is then applied to the raw radiances from which many downstream products are derived. Two algorithms have been developed for aerosol studies: Dark Target (DT) and Deep Blue (DB), which are detailed in the following sections along with a new combined DT / DB product (COMBINED).

2.1.1 Dark Target (DT) Algorithm

The MODIS Dark Target (DT) algorithm is designed for retrieving AOD over "dark" surfaces – those which are generally non-reflective in the visible and some parts of the shortwave infrared (SWIR), such as vegetated landscape or open ocean. The 470 nm, 660 nm, and 2120 nm channels are used to identify satellite pixels suitable for retrieval using DT algorithm. The following is a brief description of the DT algorithm; additional information may be found in Levy et al. (2007a) as well as the Algorithm Theoretical Basis Document (ATBD; Levy et al., 2009). Note that the algorithm differs slightly between the 3 km versus the 10 km resolution products, primarily in the pixel grouping, minimum pixel count for retrieval, and quality assurance (QA) definitions. Furthermore, while a discussion of the geometric requirements for satellite retrieval are beyond the scope of this paper, it is important to note their necessity in accurate retrieval algorithms.

Initially, the calibrated and geolocated radiances, with pixel resolution of 0.5 km x 0.5 km at nadir, are grouped into 20-by-20 (6-by-6) boxes for the 10 km (3 km) product and classified as land, ocean, or "other". If any pixel is classified as "other" but no land pixels are found, then no retrieval is

attempted. If all pixels are ocean, then the ocean algorithm (not detailed here) is chosen. If at least one pixel is land, then the land algorithm is selected. Further filtering is performed to screen out pixels containing snow, ice, clouds, bright land, streams, and other cases which are unsuitable for the algorithm. Over land, the brightest 50% and darkest 20% of the remaining pixels are then removed to reduce the potential of outliers. For the 10 km (3 km) algorithm, at least 12 (5) of the maximum 120 (12) pixels remaining must pass in order to proceed with the retrieval or else a quality flag of 0 is assigned to the data. Corrections for atmospheric gas absorption (H_2O, O_3, etc.) are applied and the resulting top-of-atmosphere (TOA) spectral reflectances are then averaged over the entire box to improve signal-to-noise. The major uncertainty in the MODIS AOD retrieval algorithm lies in separating the contributions of surface and atmosphere to the TOA spectral reflectance. The MODIS DT algorithm makes use of the fact that nearly all reflectance in the 2.1μm band is due to the surface and that there are well-established relationships between surface reflectance at 2.1μm band to that in the 0.47 μm and 0.66 μm bands for a given surface type and viewing geometry (solar and satellite viewing angles) and season (Kaufman et al., 1997). The algorithm uses the TOA reflectance at 2.1μm and these relationships to subtract off the surface contributions at 0.47 μm and 0.66 μm. The measured TOA reflectances at the three wavelengths are then compared with those in a look-up table (LUT) of simulated atmospheric TOA spectral radiances computed using different mixtures of fine and coarse aerosols specific to the region and season of the retrieval. Aerosol optical depth and fine mode fraction are estimated by minimizing the differences between the LUT and the observations.

A variety of factors may contribute to the quality flag (QA flag) assigned to the retrieval box. These QA flags are contained in the scientific data set (SDS) field “Land_Ocean_Quality_Flag”. Values between 0 and 3 may be assigned to the 10 km product to indicate reduced levels of quality, with 3 corresponding to the highest level of confidence in the retrieved AOD and 0 corresponding to the lowest level of confidence. The 3 km product is only specified as of ‘good’ (QA flag = 3) or ‘poor’ (QA flag = 0) quality. The DT algorithm reports AOD at 470, 550, and 660 nm. The SDS

names for these fields are “Corrected_Optical_Depth_Land_xxx”, where xxx indicates the wavelength.

2.1.2 Deep Blue (DB) Algorithm

Named for its ability to estimate AOD over surfaces which are “dark” in the near-UV region of the EM spectrum (MODIS band at 0.41 μm) and bright over most of the visible spectrum, the Deep Blue (DB) aerosol retrieval algorithm is designed for use over regions characterized by little vegetation, bright soil, or urban areas. The DB algorithm is implemented on multiple satellite-based instruments, including MODIS, the Advanced Very High Resolution Radiometer (AVHRR), and the Visible Infrared Imaging Radiometer Suite (VIIRS). The MODIS DB algorithm only reports AOD at 550 nm (“Deep_Blue_Aerosol_Optical_Depth_550_Land”) and uses a QA flag system like that for the DT algorithm (“Deep_Blue_Aerosol_Optical_Depth_550_Land_QA_Flag”), with values ranging from 3 (highest quality assurance) to 0. Currently only a 10 km resolution DB product is available. As with the DT algorithm, a full description is available within the ATBD and recent literature (Hsu et al., 2013) while an abridged explanation follows.

The calibrated pixel data is first checked for clouds, and the surface is screened to remove pixels identified as snow or ice. The surface is then classified as vegetated, urban, or arid using the Normalized Difference Vegetation Index (NDVI) calculated from the 650 and 860 nm channels. See Section 2.4.1 and Equation 2 below for more information regarding the NDVI. Surfaces categorized as arid use a LUT to determine surface reflectance. Vegetated surfaces use the SWIR NDVI method employed by the DT algorithm. Urban or transitional-type regions use a combination of the arid and vegetated methods. An aerosol model is then selected, either a dust model (coarse aerosols) or a fine / mixed model, based on a maximum likelihood algorithm given the region of the retrieval. The AOD is then estimated from the LUT of aerosol properties associated with this model and observed reflectance. If the coarse model is chosen, SSA is also reported, while the fine / mixed model instead reports the AE.

2.1.3 Combined DT and DB Product

A combined product is also available, which selects the best product for the given surface type based on the monthly mean NDVI, taken over multiple years. The DT product is used for NDVI ≥ 0.3 and the DB product is used if NDVI ≤ 0.2. The product with a higher quality flag is used for NDVI values between 0.2 and 0.3 unless the quality flag is the same for both products. In this case, the results are averaged (Sayer et al., 2014). Since there is no DB product at 3 km resolution, the combined product is also only available at 10 km under the name "Dark_Target_Deep_Blue_Optical_Depth_550_Combined", with a corresponding quality flag ("AOD_550_Dark_Target_Deep_Blue_Combined_QA_Flag").

2.2 MISR Aerosol Optical Depth

The MISR instrument is also located aboard the EOS Terra spacecraft and provides global coverage with a period of approximately nine days, due to the much smaller swath width of MISR (350 km), relative to MODIS. The unique feature of MISR are its nine cameras, each measuring at four wavelengths (446, 558, 672, and 866 nm). One camera points to the nadir, while four are oriented at angles of 26.1°, 45.6°, 60.0°, and 70.5° relative to the Earth's surface and are symmetric in both the forward and aft directions. This allows multiple images of the same scene with different optical path lengths, reducing the uncertainty in AOD retrievals due to surface assumptions. The time between the images of the first and last camera is around 7 minutes. Each pixel covers an area of approximately 275 m x 275 m and pixels are grouped into a 16-by-16 box such that the nominal product resolution is 4.4 km as of version 23.

The retrieval method is summarized as follows. The observations have a detrending function applied (i.e. subtraction of the average) to generate so-called Empirical Orthogonal Functions (EOFs) of the angular shape of TOA radiances. The average, along with the observations, are used to derive aerosol optical property constraints as inputs to a LUT of forward radiative transfer calculations. The angular shape of the directional reflectance function is then also computed from the difference between the LUT data and the observations. Minimization of the difference between the EOF-derived

and LUT-derived angular dependence allows selection of an aerosol model and AOD (Martonchik & Diner, 1992).

Version 23 of the MISR Level 2 Aerosol Product is used in this study, where the AOD at 550 nm is reported in the SDS "Aerosol_Optical_Depth". It is important to note that no quality assurance field is explicitly available for this product, and that at moderate to high AOD, MISR retrievals are more susceptible to errors (Kahn & Gaitley, 2015). However, the SDS "Aerosol_Retrieval_Screening_Flags" may provide useful information when the retrieval fails due to topography, clouds, or geometric problems. While an uncertainty range is provided with the product, this study uses the AOD expected error envelope corresponding to the larger of ± 0.05 or $0.2 \cdot AOD$ (Kahn et al., 2010) to be more consistent with the uncertainty method applied to other products.

2.3 Ground-Based AOD and Angstrom Exponent

2.3.1 NASA AERONET

The NASA AERONET AOD algorithm (Holben et al., 1998) calculates AOD through measurement of the direct solar radiance made by Cimel sunphotometers at nine wavelengths (see Table 1). Direct-sun measurements are performed at optical air mass intervals of 0.25, which corresponds to roughly every 15 minutes near noon and more frequently during sunrise and sunset. Each measurement is the average of a triplet of readings taken within a short time window (~1 min), which provides a means of cloud screening and statistical robustness. The AERONET instruments are routinely calibrated (approximately once per year) using the Langley method (Shaw, 1983) against a reference Cimel sunphotometer at a high-altitude site in Mauna Loa, HI. The Level 2 data product is cloud screened, quality-assured, and applies the most recent calibration. The resulting uncertainty of around 0.01 to 0.02 is low enough to be considered ground-truth for studies against satellite-derived AOD (Eck et al., 1999; Levy et al., 2010). Aerosol optical depth at other wavelengths is calculated from AOD at the measured wavelengths via a quadratic fit of ln(AOD) versus ln(λ), as suggested by Eck (1999). Angstrom exponent of the AOD is computed as the negative slope of ln(AOD) versus ln(λ), typically using wavelengths between 440 and 870 nm. Column-averaged aerosol intensive

properties such as SSA and size distribution are derived from almucantur scans of the sky (Holben et al., 1998). Single scattering albedo retrieved by AERONET is not included in this analysis since it is subject to large uncertainties for low AOD conditions (Dubovik et al., 2000), which is characteristic of the selected sites throughout most of the study period.

2.3.2 Multifilter Rotating Shadowband Radiometer (MFRSR)

Originally developed for the Department of Energy's Atmospheric Radiation Measurement (ARM) program, the MFRSR measures direct solar radiance at six wavelengths to compute spectral AOD (Harrison et al., 1994; Michalsky et al., 2001). Measurements are performed more frequently than AERONET, often reported as one-minute averages. In the case of this study, cloud screening and quality assurance are undertaken by the principal investigators (PIs) of the site. The AOD uncertainty in a well-calibrated instrument is close to that of the AERONET Cimel at 0.01. Like the AERONET measurements, a second-order polynomial fit may be used to interpolate AOD to satellite wavelengths.

2.4 Surface Reflectance and Type

2.4.1 Normalized Differential Vegetation Index (NDVI)

According to the ATBD (Huete et al., 1999), the MODIS NDVI is the ratio of the difference between the reflectance in the near infrared (NIR) and the reflectance in the red part of the visible EM spectrum to the sum of these reflectances:

$$NDVI = \frac{NIR-Red}{NIR+Red} \quad (2)$$

Desert and sparsely vegetated surfaces typically have NDVI values near zero, while an NDVI close to 1 indicates dense vegetation. This is due to the fact that photosynthetically active pigments absorb blue and red wavelengths but are highly reflective in the near-IR. NDVI reported at 250 m resolution is available in the products MOD13Q1 and MYD13Q1 (Didan 2015) from the Terra and Aqua satellites respectively at the Land Processes Distributed Active Archive Center (LPDAAC). The best

result for each pixel over a 16-day period is then projected on a sinusoidal grid. NDVI was also averaged within a 40 km-by-40 km box for each site to construct monthly averages.

2.4.2 Surface Land Cover Maps

A supervised classification scheme using data from the MODIS satellites has been developed which produces land cover type maps for many of the common classification schemes. Here, the results from International Geosphere-Biosphere Programme (IGBP) scheme are used to characterize the region of interest around the sites. The land cover maps are produced on an annual interval with a pixel size of 500 m by combining data from both Terra and Aqua. The data are available at the LPDAAC under the product name MCD12Q1 (Friedl & Sulla-Menashe, 2019).

2.5 Sites

The regions surrounding the four sites in this study contain a variety of topographic and surface properties, which along with sufficient aerosol loading make them good candidates for areas expected to pose difficulties for satellite-based aerosol retrievals. Two eastern U.S. sites were selected which possess low to moderate elevation changes and spatially consistent land cover. In contrast, the two western U.S. sites are generally characterized by greater elevation differences and heterogeneous surface properties. When aligned, the ground and satellite-based data record spans at least 5 years at each site. Details for each site are provided in the following sections.

2.5.1 Appalachian State University (APP)

The APP site (36.2 N, 81.7 W) is located on the Appalachian State University campus in the mountains of Boone, NC, at approximately 1080 m above mean sea level (ASL). The region consists primarily of deciduous forests and spans an elevation range of around 1800 m. Aerosol loading has a strong seasonal influence, with summer maxima (Sherman et al., 2015; Sherman et al., 2016) due to secondary organic aerosols and sulfates and the low-loading winter months largely influenced by biomass burning for residential heating (Link et al., 2015). The AERONET site is stationed on top of a parking deck near the campus library and has been active since July 2010. Aside from gaps due to

maintenance or calibration, the data record used in this study spans nearly 8 years. Additional information on the APP site is available in Sherman et al. (2015).

2.5.2 Walker Branch (WB)

Located about 230 km west of APP, the Walker Branch, TN AERONET site (35.958 N, 84.287 W, 365 m ASL) collected data from 1997 to 2009. The local topography is generally flat with elevations ranging from 300 to 900 m. Like the APP site, a significant portion of the land cover within 50 km of the site consists of deciduous broadleaf forests, however there are more savanna and urban / build-up lands along with some rivers and lakes. Two cities are nearby: Knoxville, TN approximately 33 km the east and Maryville, TN about 37 km to the southeast. One major aerosol source in the area is the 870 MW Bull Run coal power plant operated by the Tennessee Valley Authority (U.S. Energy Information Administration, https://www.eia.gov/state/?sid=TN), located about 14 km northeast of the site. Although the WB site altitude may not qualify it as 'mountainous' and the measurement period has little overlap with the other sites, we include the site in our study for the following reasons: (1) it is the closest to a high-elevation mountainous U.S. site with a record of sufficiently high AOD for examining the aerosol model assumptions made by satellite retrieval algorithms; (2) its inclusion offers a second eastern U.S. site for comparison with the two high-elevation western U.S. sites which possess different surface topography and vegetation types.

2.5.3 Storm Peak Laboratory (SPL)

Storm Peak Laboratory (40.455 N, 106.745 W, 3220 m ASL) is situated at the top of Mount Werner near Steamboat Springs, CO. The region is topographically complex, with elevations ranging from 2 to 4 km ASL. The land cover type is primarily grasslands and savannas with some patches of evergreen needleleaf forests. A Yankee Scientific MFRSR collected data from March 1999 to May 2013, although there is a gap in the data during the year 2012 when the instrument was down for maintenance (Hallar et al., 2015).

2.5.4 Reno (RENO)

The Reno AERONET station (39.541 N, 119.814 W, 1410 m ASL) is located on the roof of the physics building at the University of Nevada, Reno and has been active since 2012. The regional land cover consists of mostly desert grasslands, along with some savanna, evergreen needleleaf, and barren areas. Unlike SPL, roughly half of the region within a 12 km radius of the site is classified as urban / build-up land. The city of Reno has a population of around a quarter million, approximately 20 times that of Steamboat Springs near SPL.

Chapter 3: Methods

The following sections describe the data retrieval, processing, and collocation scheme as well as the approaches we use to predict a suitable spatio-temporal collocation window for each site. Plots and maps of surface (NDVI, land cover, topography) and aerosol properties (AOD and AE) in both space and time provide a means of estimating the region over which satellite retrievals are likely representative of the surface measurements at each site. This graphical method also provides insight into factors influencing agreement and provides support for underlying assumptions. An automated method for optimizing the spatio-temporal window is presented, along with the metrics utilized to assess the performance of this scheme.

3.1 Spatial and Temporal Variability in Aerosol and Surface Properties

In Sections 4.1-4.2, plots of temporal and spatial variability of aerosol and surface properties are presented. The annual cycles of monthly-averaged AOD (at 550 nm) at each of the ground sites and monthly-averaged NDVI averaged over 40 km x 40 km box centered at each ground site are plotted (Sect. 4.1.1) to provide information on their seasonal variability. These serve as visual guides for predicting which satellite AOD products may be expected to perform best at the sites during given season(s). Monthly-averaged AOD plots are also useful for determining whether aerosol model or surface model assumptions used by the satellite AOD retrieval algorithms exert a greater influence on the retrieved AOD, which is more sensitive to particle property (surface model) assumptions for AOD larger than (smaller than) roughly 0.15 at 550 nm (Levy et al., 2010). We also include monthly-averaged Angstrom exponent (AE) measured at the ground sites as a semi-qualitative indicator of aerosol size distribution and its annual cycle.

In Section 4.1.2, AOD and AE are binned by hour of day and averages are formed for each hour, which are plotted for each site / season. The degree of variability for hours near Terra and Aqua overpass times (LST hours ~10:30-12:15 for Terra and ~12:45-14:30 for Aqua) is useful for estimating the sensitivity of satellite / sunphotometer collocations to size of the temporal collocation window. Temporal AOD variability measured by sunphotometers on timescales of a few hours or less

can also serve as a rough indicator of the degree of spatial aerosol variability over the ground site. The satellite AOD algorithms assume spatial homogeneity within a given pixel, which may or may not typically hold true above a given ground-truth site.

In Section 4.2, we examine the spatial dependence of satellite-sunphotometer AOD agreement near the ground sites. The objectives are to (1) identify satellite AOD retrieval biases above each site and compare the biases of the different satellite AOD products; (2) examine the potential roles of landcover type, NDVI, and topography on these biases; (3) estimate the extent of the region surrounding each ground site over which the AOD retrieved by satellite is likely representative of ground-measured AOD, and how this varies amongst the AOD products. To accomplish this, we place all satellite AOD retrievals within a 50 km radius of each ground site into spatial bins of 5 km x 5 km for the 10 km AOD products (MODIS DB and DT 10 km and their COMBINED product) and 3 km x 3 km bins for the high-resolution products (MODIS DT 3 km and MISR). We also take the average of sunphotometer-measured AOD within a 1h window centered at each satellite overpass time. For each spatial bin, we calculate the mean satellite-sunphotometer AOD difference for each satellite product. We also count the number of collocations for each bin. From these bins, we form spatial plots of mean AOD difference and number of collocations for the 50 km radius surrounding the ground site. The bin sizes are selected as a compromise between spatial resolution and adequate number of collocations.

The mean difference between satellite and ground-measured AOD in the immediate vicinity of the site is likely a true mean satellite AOD bias, since both sensors are expected to sample the same air mass. For parts of the region further away from the site, the mean AOD difference could be due to spatial variability in aerosol loading and additional satellite retrieval biases due to differences in vegetation, elevation, and land cover type. We use the extent of the region surrounding the site for which the mean AOD difference is the same as at the site as an estimate of the spatial extent of the representativeness of AOD measured at the ground site and hence the optimal collocation radius. We examine the similarity of AOD difference spatial patterns in relationship to the spatial dependence of

surface elevation, surface cover type, and NDVI to gain insight into their potential role in satellite AOD retrieval biases. Though we refer to the mean satellite-sunphotometer AOD differences as a 'bias', the spatial variability in mean AOD differences could be due in part to different aerosol conditions and due to spatial variability in factors influencing the satellite AOD retrievals (Sect. 4.2) such as vegetation, land cover type, topography and spatial variability in sampling. For this reason, we place the spatial variability in 'AOD bias' in the context of maps of (a) monthly-averaged NDVI; (b) surface elevation; and (c) landcover type.

3.2 Spatio-Temporal Collocation Algorithm

We use the MATLAB programming language for developing the automated spatio-collocation algorithm, along with the subsequent data processing, based largely on familiarity with the MATLAB programming environment and its ability to handle large data volumes. The first preliminary step is to download the satellite and ground-based AOD products and place them into a form suitable for further processing. This step involves generating a data query to the MODIS and MISR websites for the data period under study, along with downloading the AOD data for each AERONET site. The MFRSR AOD data is provided by SPL site Principal Investigator (PI) Gannett Hallar. In the case of MODIS, we request all data within the period of the surface remote sensing data set, but spatially constrain the results to a 1-degree by 1-degree box centered on the site. Additional automation of the download process, such as recursively searching for missing files in the local database, is performed using scripts written for MATLAB. MISR uses a path system to identify each satellite overpass; sample files from each path are downloaded and checked for any spatial bias, as some may have a portion of the region to the East or West of the site missing. Once the unbiased paths are identified, a temporal subset of the data matching the ground measurements is requested. MODIS files are natively stored in the HDF-4 format, while the MISR Version 23 data are in an HDF-5 compatible format.

AERONET and MFRSR data are ordered from the AERONET online database and provided by the site PI, respectively. The AERONET data needs to be extracted from the text files and

formatted into MATLAB matrices, which is accomplished using a custom import script that also applies a second-order polynomial fit to generate new columns of data interpolated to the wavelengths of the satellite data (Eck et al., 1999). All AOD comparisons made in this study are performed at 550 nm. The results are then stored in MATLAB structures with a standardized format so that they can be efficiently loaded into the workspace during the collocation process.

The satellite data require further reduction, as the full swath of data is not needed to perform collocations within a much smaller spatial window. A maximum radius of 80 km is used to further subset the data based on the assumption that the topography, land cover, and aerosol sources are well characterized within this region around the site. At the same time, such a window should be small enough that it does not substantially increase the probability of aerosol fronts in the retrieval that are not sampled by the ground station. This sub-setting method is performed in MATLAB during the extraction process from the native file format to either intermediate comma-separated values (CSV) files or directly to MATLAB structures. First, the latitude and longitude SDS are read and used to create a matrix of distances from the site via the haversine formula. Based on the indices of this distance matrix which fall within the maximum radius, the corresponding indices of other SDS are extracted and written to a MATLAB structure. To reduce processing time, as there are many files and computer resources are limited, use of parallel processing and datastores are implemented in MATLAB.

Once the data are prepared, the structures for the surface and satellite data are then used as inputs to the collocation function, along with additional parameters. The input data are filtered based on quality flag, minimum AOD threshold, and maximum radius from the site (spatial window). The minimum AOD threshold is set at -0.05 to avoid introducing a bias to the data (Levy et al., 2007b). The collocation algorithm is designed so that the inputs can also be filtered based on any user-defined criteria of the available SDS, such as including only points with a certain elevation range or cloud-to-pixel distance, although no additional filtering is implemented in this study. Next, the satellite data timestamps are adjusted so that the date and time for each pixel belonging to a single retrieval

matches that of the pixel closest to the site. The filtered data is then iteratively searched for all surface measurements that fall within the specified time window relative to each satellite overpass. An additional criterion is then imposed, like that used by Ichoku et al. (2002): at least two surface measurements are needed to allow the collocation to be accepted, with a similar restriction for the number of satellite pixels required. However, rather than adopting a static value for the number of satellite pixels, a value based on the spatial window is used since multiple resolutions are available:

$$Npixels_{min} = ceiling\left[0.2\left(2 \cdot \frac{r_{max}}{res}\right)^2\right] \quad (3)$$

where r_{max} [km] is half the spatial window, res [km] is the resolution of the satellite product (e.g. 10 km), and $Npixels_{min}$ is the minimum number of satellite pixels required for the collocation to pass. Note that this criterion is designed for square retrieval boxes, and this study used circular regions; therefore, the minimum number of pixels required is larger than necessary, which is expected to provide a more robust result. Once all passing collocations are accumulated, statistical information such as the mean, median, standard deviation, number of each type of data point in the collocation, and other diagnostic information are then output from the function. A flow chart of the collocation procedure is depicted in Figure 2 below.

Figure 2

Flow Chart of the Collocation Procedure

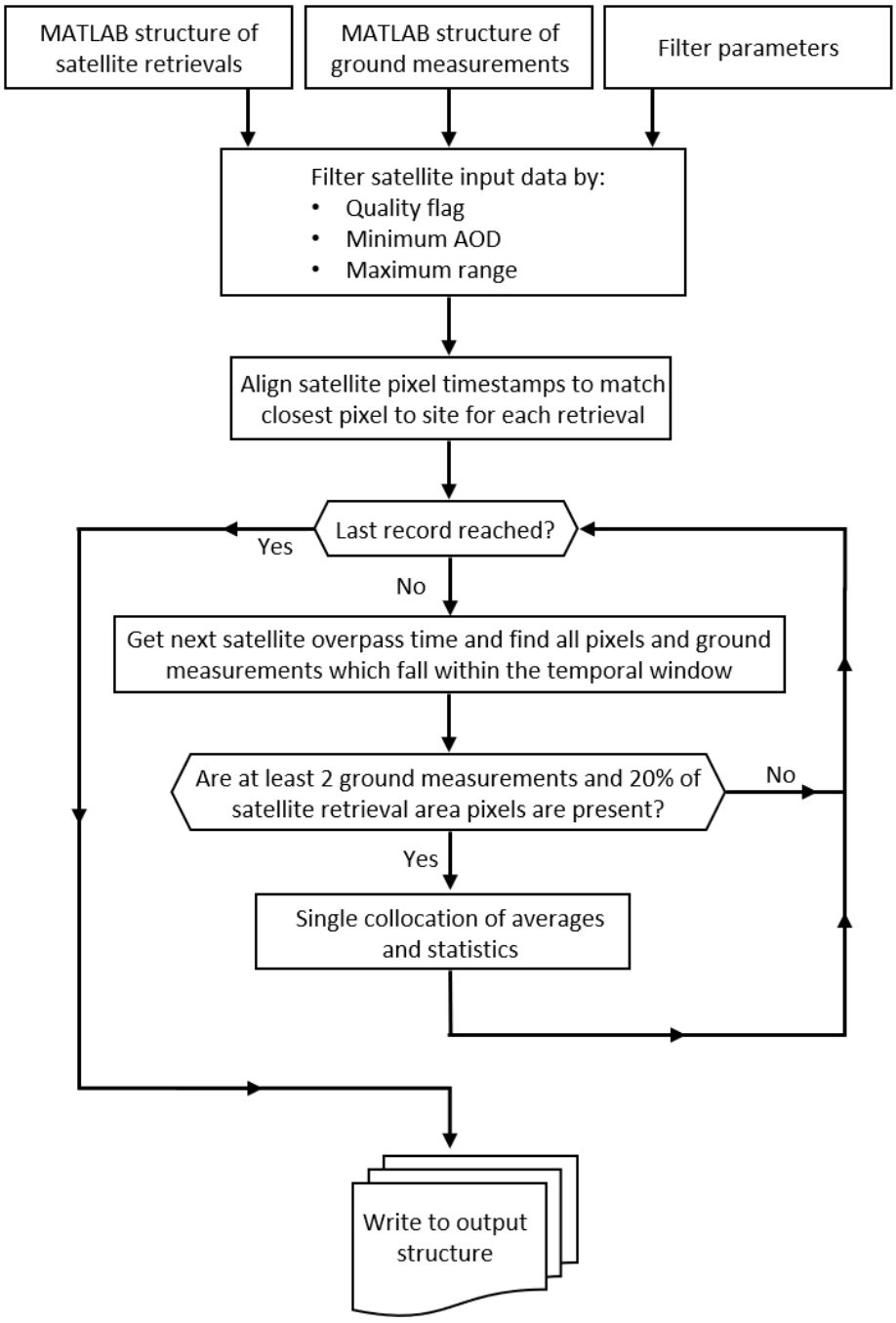

3.3 Scheme for the Optimization of the Spatio-Temporal Window

After analysis of the factors influencing spatio-temporal collocations to obtain an estimate of reasonable window sizes, the spatio-temporal window is optimized for each site included in the study using an iterative approach. Four separate temporal windows are selected: 30, 60, 90, and 120 minutes, centered on the satellite overpass time (e.g. a 30-minute temporal window is defined as the period consisting of the 15 minutes preceding and the 15 minutes following the satellite overpass). For each temporal window, iterations are performed over a series of circular spatial windows with radii ranging from 1 to 50 km. Collocation results from each iteration are placed in a structure, so that the agreement between the satellite data and the ground data can be evaluated. Several different metrics for assessing the agreement are chosen, including:

1. linear regression results such as slope, intercept, and correlation coefficient
2. mean AOD bias
3. percent of collocations within the expected error (EE; see Table 1)
4. root-mean-square error (RMSE)
5. number of collocations

Linear regression results are provided at the 95% confidence level. The mean AOD bias is defined in the same manner as in Gupta et al. (2018):

$$Mean\ Bias = \frac{1}{N}\sum(Satellite\ AOD - Ground\ AOD) \qquad (4)$$

These metrics are calculated for each iteration and collected within a single matrix in MATLAB, then plotted as a function of radius and time window. This iterative procedure is outlined in Figure 3 below.

Figure 3

Iterative Routine for the Optimization of the Spatio-Temporal Window

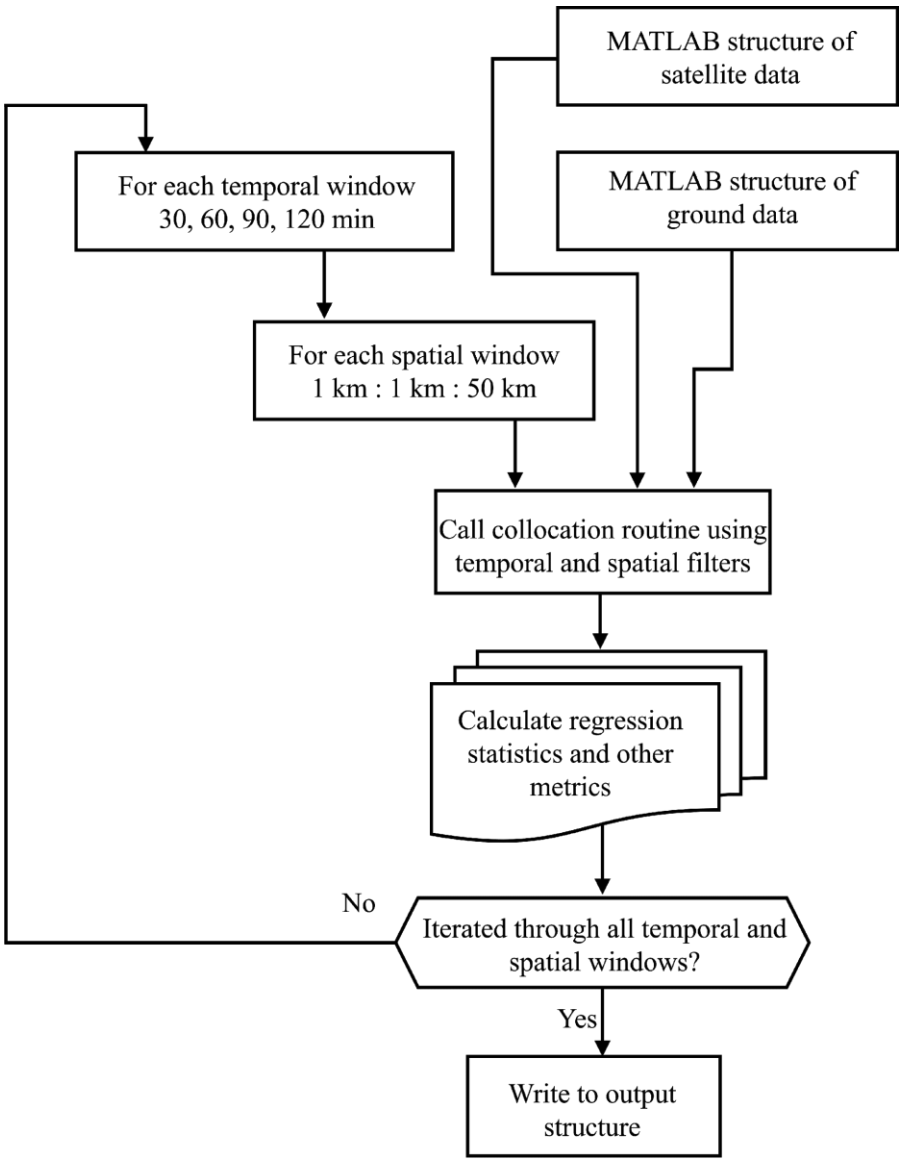

Chapter 4: Results and Discussion

Plots of the temporal variability in surface and aerosol properties on diurnal and annual timescales are presented in Section 4.1. Based on these plots, we estimate an upper bound for the collocation temporal window and make predictions as to which satellite algorithms are expected to perform best for a given site and season. In Section 4.2, we explore how maps of land cover, NDVI (January and June), and topography can provide context for maps of satellite retrieval frequency and AOD 'mean bias'. These relationships ultimately influence the spatial collocation window over which the satellite retrieval is representative of the site. An analysis of the spatio-temporal window optimization algorithm output in the context of spatial and temporal variability plots / maps is used to derive a site- and resolution-specific estimate of the collocation window. The overall performance and seasonal performance of each satellite product for collocations performed at the 'optimal' spatio-temporal window is then discussed.

4.1. Temporal Variability in Surface and Aerosol Properties

4.1.1 Annual Cycle in Monthly-Averaged Aerosol Properties and NDVI

Aerosol optical depth is generally low during the cooler months and higher during the summer, more so for the eastern U.S. sites, particularly for the WB site (Figure 4). There is less seasonal AOD variability and lower overall AOD for the western U.S. sites. Higher AOD for SPL and Reno in summer, along with lower Angstrom exponent, is consistent with presence of biomass-burning aerosols (Hallar et al., 2015). Values of AOD less than ~0.15 for most sites and seasons means that the AOD retrievals will be more influenced by surface reflectance and topography assumptions used by the satellite retrieval algorithms (with exception of WB and perhaps APP in summer) than by their assumed aerosol type (Levy et al., 2010). Angstrom exponent values of 1-2 for most sites / seasons are consistent with a larger fraction of fine-mode aerosols while values less than 1 during non-summer months at SPL (and to lesser extent winter and spring at Reno) are consistent with large influence from coarse-mode aerosols (i.e. dust) in the western U.S., which has been reported by Hallar et al. (2015). Higher NDVI values during April-October at all sites but Reno are

due to the presence of green vegetation while lower values at Reno are the result of less green vegetation, namely desert. Based on this, algorithms optimized for bright, desert surfaces such as MODIS DB would be expected to perform worse than those for greener surfaces (MODIS DT) at all sites except at Reno and (during winter) SPL. The MISR AOD retrieval algorithm should not be as affected by NDVI as MODIS, due to the use of multiple viewing angle (in addition to multi-wavelength) in the MISR algorithm.

Figure 4

Monthly-Averaged AOD, AOD Angstrom Exponent (AE), and NDVI for All Sites

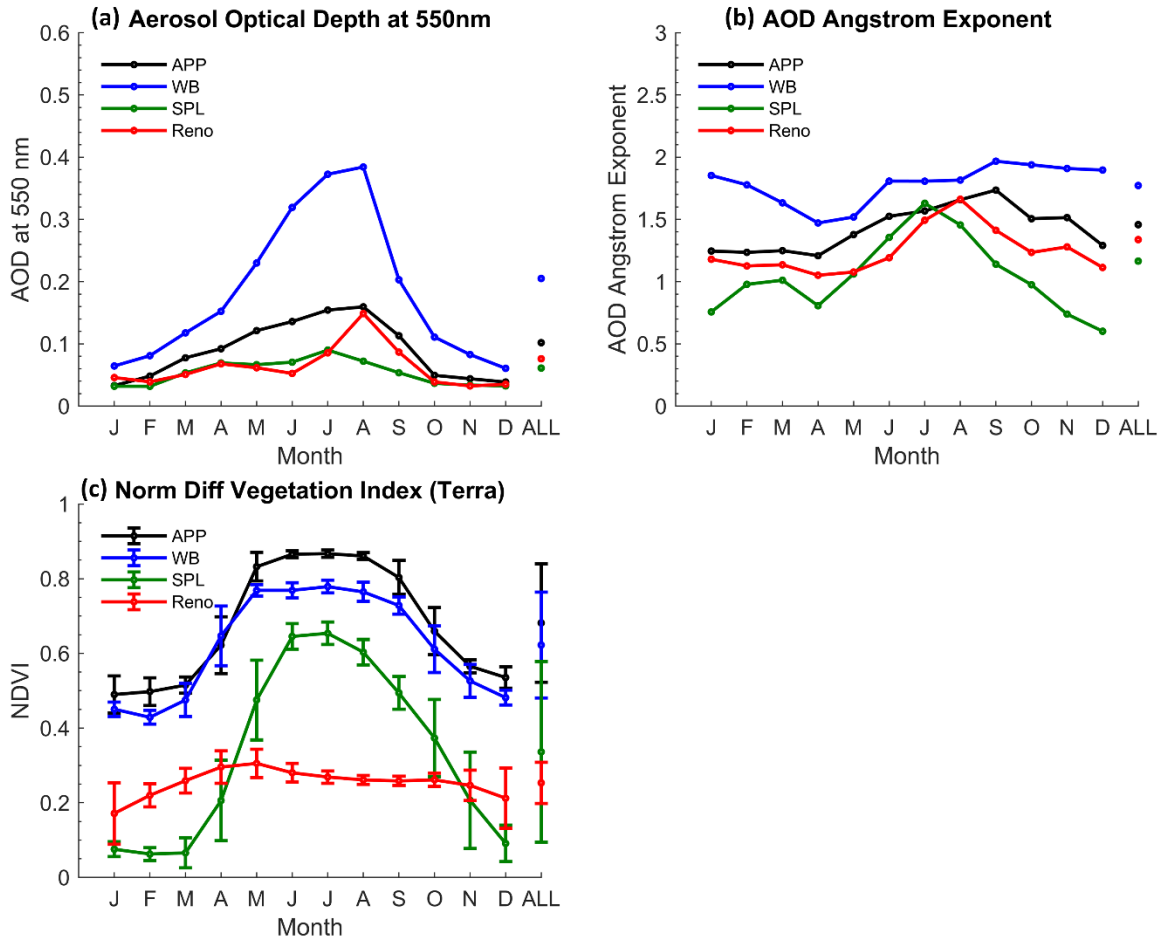

Note. Error bars on the NDVI traces represent standard deviations. The standard deviations are larger for AOD and AE plots and are thus not included to highlight the annual cycle of mean values.

4.1.2 Diurnal Cycle in Aerosol Properties at All Sites

Hourly-averaged AOD and AOD Angstrom exponent are shown for each site / season in Figure 5. If there is small diurnal variability for a given site / season, we would expect less dependence of the satellite-sunphotometer AOD agreement on the temporal collocation window size than for sites / seasons with larger diurnal variability, primarily near hours of satellite overpass. There is very little diurnal variability in AOD and Angstrom exponent (AE) at the APP, WB, and Reno sites during hours near the Terra and Aqua overpass times (LST hours ~10:30-12:15 and ~12:45-14:30, respectively). This seems to imply that temporal window sizes up to 2 h centered at satellite overpass times could potentially be used for collocations at these sites, especially for instruments aboard Terra (MODIS Terra, MISR). The lack of mid-day temporal aerosol variability may also be an indicator of spatial aerosol homogeneity at / near the sites. Aerosol homogeneity within a given pixel is used by the satellite AOD retrieval algorithms.

Figure 5

Diurnal Variability of AOD and AOD Angstrom Exponent at APP, WB, SPL, and Reno

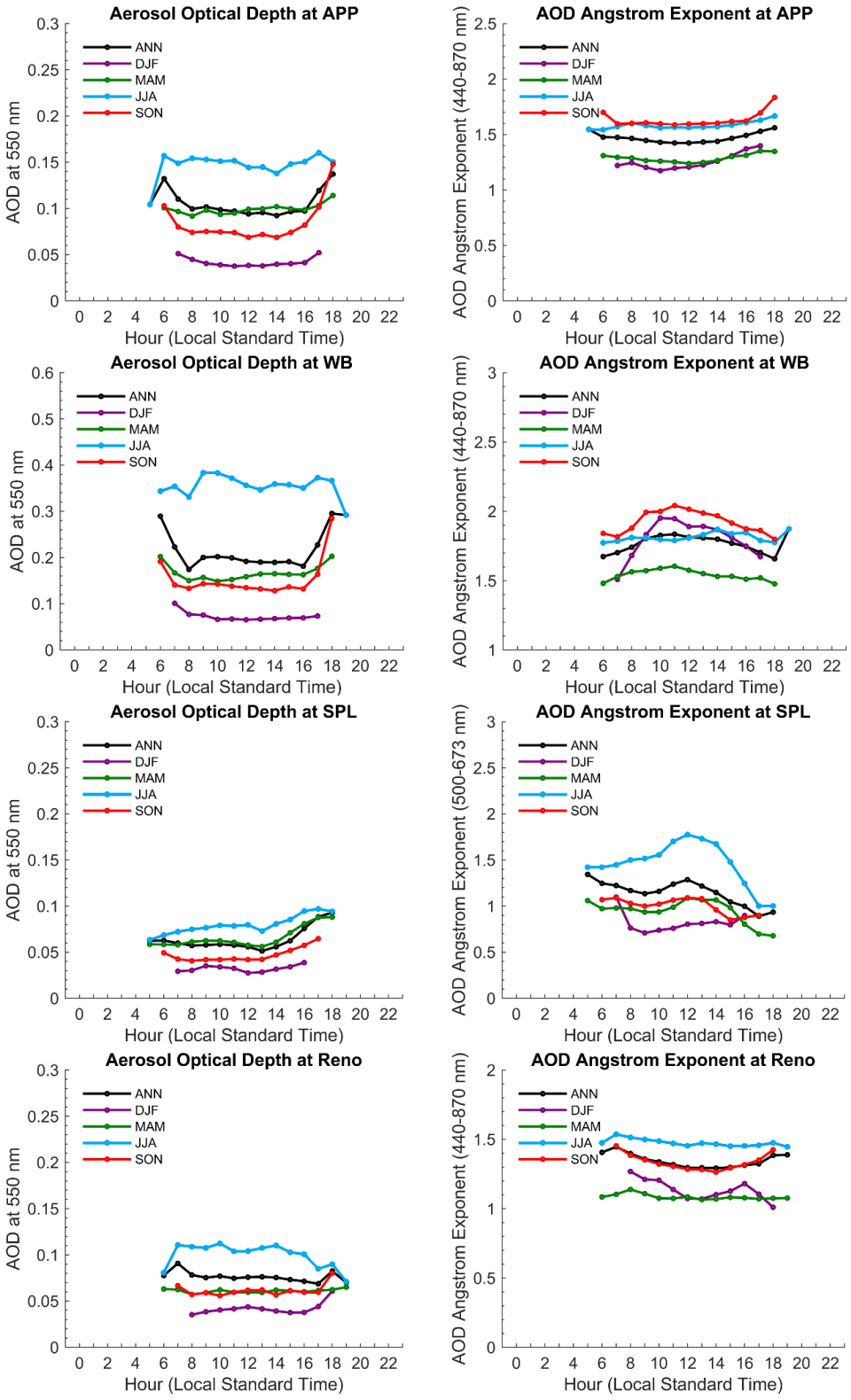

Aerosol optical depth at SPL is relatively constant in the morning, with modest afternoon increases (~0.03-0.04) for all seasons except winter (Figure 5). The afternoon AOD increases are accompanied by decreases in AE, with values less than one in spring and fall indicative of large dust particles. This could be the result of afternoon upslope flow conditions which transport dust from lower elevations. Less variability in AOD and particle size distribution during morning hours lead us to speculate that the satellite-MFRSR AOD agreement is relatively insensitive to the size of temporal collocation window for instruments on the Terra satellite (MISR, MODIS Terra) but the tendency to shift to higher AOD and larger particles over the afternoon hours may lead to some sensitivity of MODIS Aqua AOD performance to the size of temporal collocation window.

4.2 Spatial Variability in Surface Properties and their Influence on Collocations

4.2.1 APP

Maps of surface elevation, land cover type, and NDVI during January and June for the region surrounding APP are shown in Figure 6. The high NDVI values associated with dense deciduous forests (Figure 6b) and the high degree of spatial NDVI homogeneity at APP (Figures 6c-d), especially during heavily vegetated warm season months, are favorable for satellite products such as MODIS DT, which perform best over dark, vegetated regions (Levy et al., 2013). The topography within the region (Figure 6a) is not as complex as near the western U.S. sites but contains enough heterogeneity that the higher spatial resolution AOD products (MODIS DT 3 km and MISR 4.4 km) could conceivably perform just as well as MODIS 10 km products, despite more noise resulting from less spatial averaging (Gupta et al., 2018). Significant elevation decreases are present beginning ~20 km to the southeast of the APP site (Figure 6a), along with some urban terrain (the city of Hickory, NC) ~60 km from the site.

Figure 6

Maps Used to Characterize the APP Site

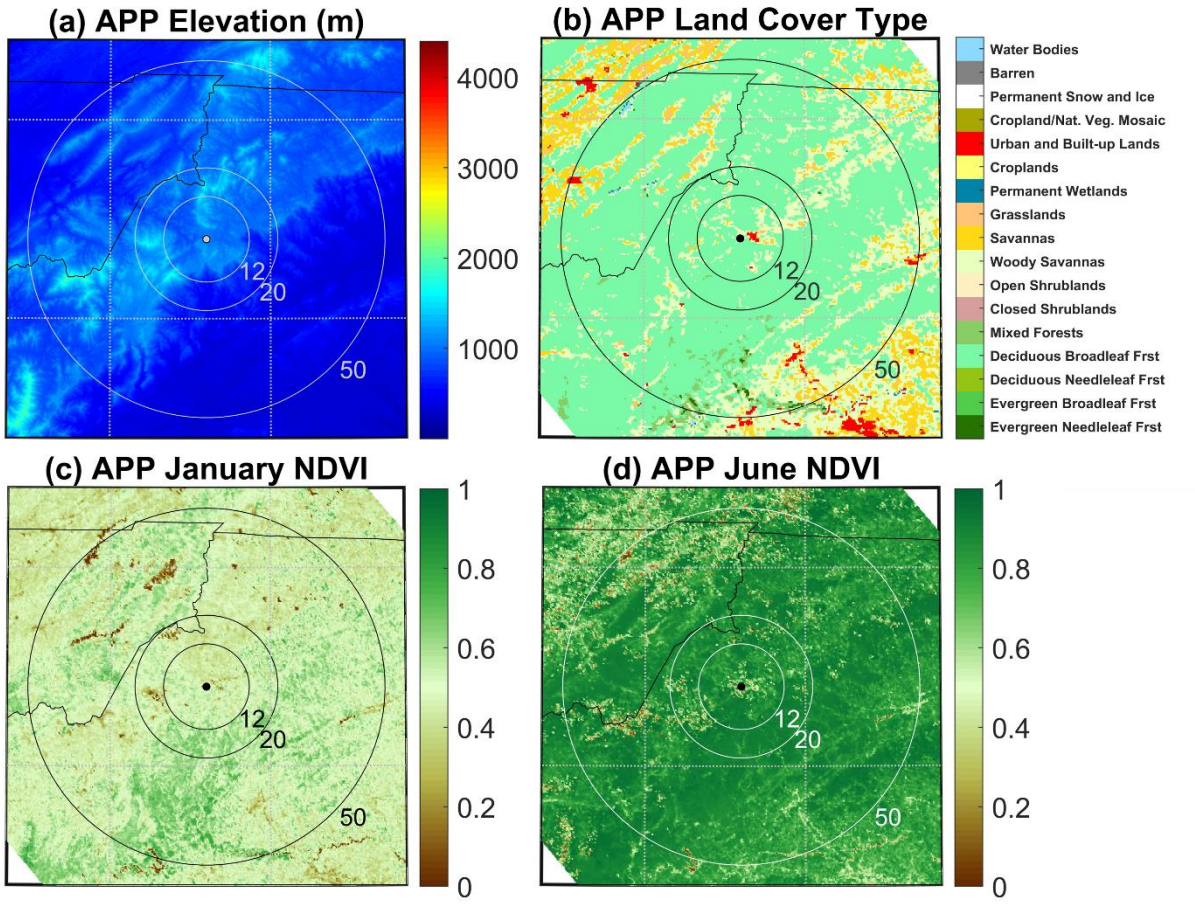

Note. The four maps are derived from: (a) USGS 1 arc-second elevation data, (b) 2004 MODIS-derived land cover type, (c) January 2004 MODIS Terra 16-day NDVI, (d) June 2004 MODIS Terra 16-day NDVI. The numbered rings indicate a circle of constant radius (12, 20, and 50 km) around the site.

There are no major spatial sampling gaps in the pixels contributing to satellite-AERONET collocations for any satellite product in the 50 km radius circle centered at APP (Figure 7). The overall sampling for MODIS Terra is higher than that of Aqua. The high-resolution MODIS DT 3 km product has a few small gaps over small urban areas and water bodies, while the coarse resolution 10 km products still retrieve over these small-scale fluctuations. There are nearly twice as many satellite-AERONET collocations above the low-elevation southeast sector as above APP and the rest of surrounding region for all products (Figure 7). The higher SE sampling is mainly at radii larger than

~12 km for the high-resolution products (MISR, MODIS DT 3 km) and at radii larger than ~20 km for the 10 km MODIS products. The spatial sampling inhomogeneities are a bit less for MISR than for MODIS.

Figure 7

Maps of the Spatial Distribution of Satellite-Sunphotometer Collocations at the APP Site

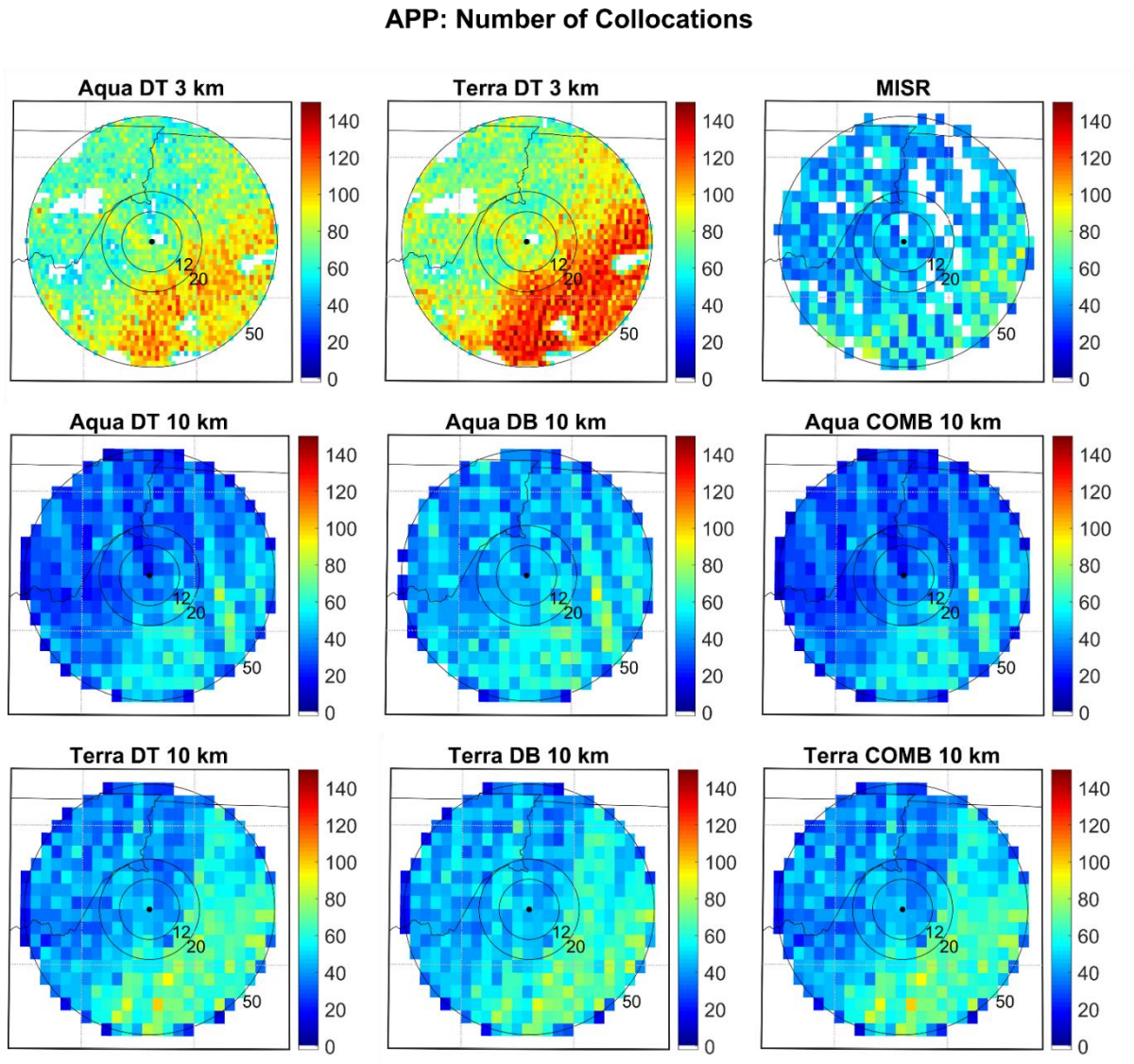

Maps of mean satellite-AERONET AOD differences at / near APP are shown in Figure 8. The magnitudes of the differences for all products are ~0.03 or less in the ~10-15 km region surrounding the APP site, suggesting only small AOD measurement / algorithm biases in the satellite retrievals above APP. The positive biases are slightly smaller for MISR and Terra DT 10 km (≤ 0.02) than for Terra DT 3 km (≤ 0.03). The Aqua DT AOD biases are less negative (~ -0.01 to -0.02) than that of the Aqua and Terra DB (~ -0.02 to -0.03). The spatial variability in mean satellite-AERONET AOD differences for APP largely follows the elevation map (Figure 6a). All satellite AOD products exhibit a more positive mean AOD bias (relative to AERONET) for the low elevation regions > 20 km to the south, east, and northwest of APP than near the APP site, which likely indicates that the aerosol loading in these regions are less representative of that measured above the APP AERONET site. The largest mean satellite-AERONET AOD differences are over the small urban areas to the south and to the east (Figure 8). Since the landcover type and NDVI over most of this lower elevation region are similar to at APP (Figures 6b-d), the higher AOD biases are likely due to a longer atmospheric path length and urban influence and not due to appreciable terrain-dependent satellite retrieval biases. The Terra DT AOD bias is ~0.02-0.03 larger than Aqua over most of the region at similar elevation to APP but the Terra-Aqua difference is slightly larger at the lower elevations (~0.04-0.05). The spatial variability in MISR AOD bias is smaller than that of the MODIS products. A larger satellite-AERONET AOD difference in the lower-elevation SE region, coupled with more frequent sampling for this region (Figure 7), indicates that including this region (r > 20 km) in satellite-AERONET collocations could bias satellite AOD evaluations over APP.

Figure 8

Maps of Mean Satellite-Sunphotometer AOD Difference at the APP Site

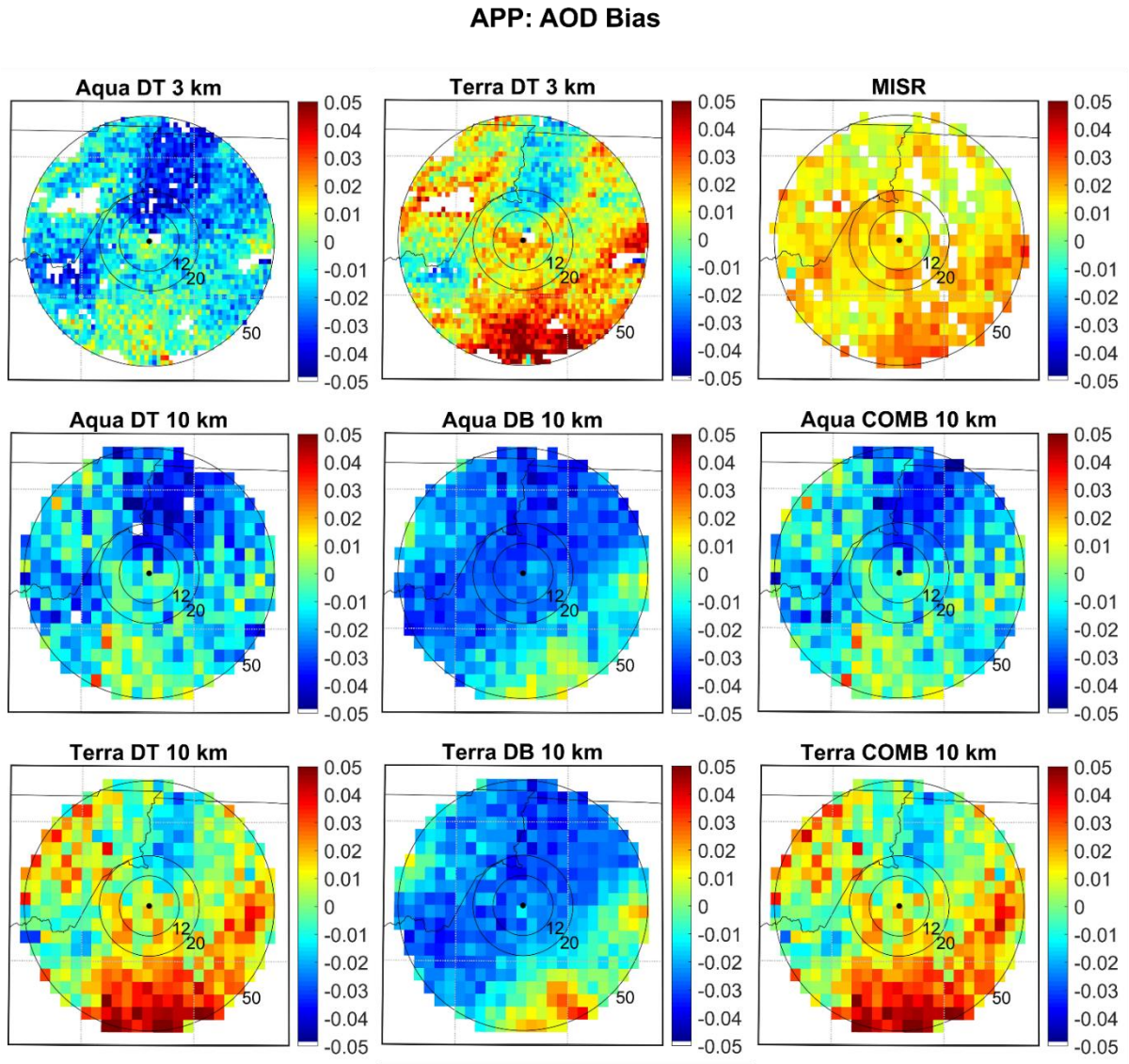

4.2.2 WB

Walker Branch is like APP in that the NDVI is quite high throughout the year (Figure 9c). There is more land cover spatial heterogeneity (Figure 9b) than near APP, with broadleaf deciduous forest over much of the region within ~12 km of WB and to the north and west, savannas and urban influences (mainly the city of Knoxville) to the south and southeast, and major rivers south / southwest of WB, along with smaller rivers near the site. Still, the NDVI is for the most part spatially

homogeneous during both winter (Figure 9c) and summer (Figure 9d). Major rivers are apparent in the January NDVI map (Figure 9c) as areas of near-zero NDVI, which occur mostly within the southern half of the study region. The small river immediately to the south of the site which runs to the northeast is expected to interfere with retrievals near the site, as these pixels are likely to be screened as water or heterogeneous land. Topographically, the WB site is the most homogeneous of the four mountain sites studied in this work, except for some small elevation increases to the north (Figure 9a).

Figure 9

Maps Used to Characterize the WB Site

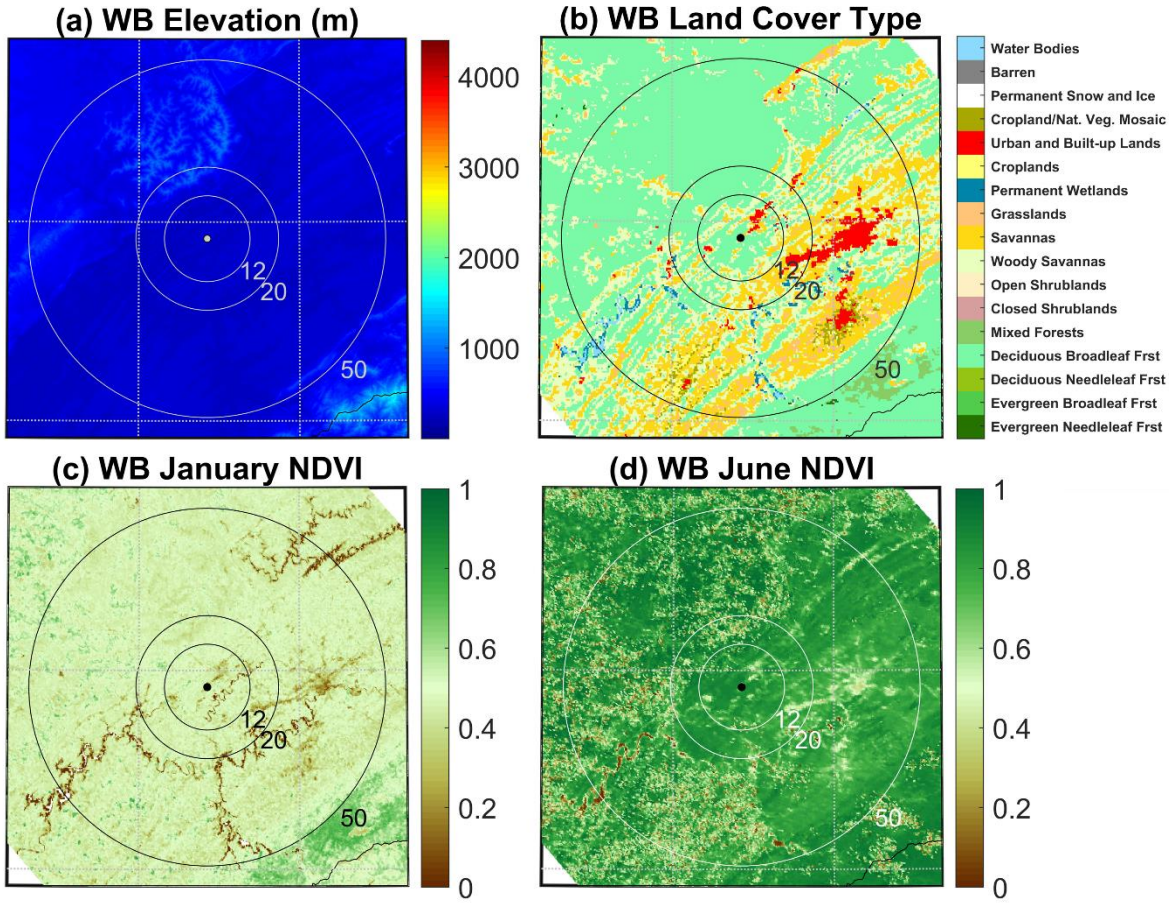

Note. The four maps are derived from: (a) USGS 1 arc-second elevation data, (b) 2004 MODIS-derived land cover type, (c) January 2004 MODIS Terra 16-day NDVI, (d) June 2004 MODIS Terra

16-day NDVI. The numbered rings indicate a circle of constant radius (12, 20, and 50 km) around the site.

Urban areas and rivers are reflected in the sampling gaps of satellite AOD products over the region surrounding WB (Figure 10). As expected, MODIS DT does not retrieve above rivers and urban areas (Figures 9b, 10). The MODIS COMBINED product contains the same sampling gaps as DT, due to its use of the DT algorithm results in this region of generally high NDVI. All satellite products retrieve less (by factor of ~2) over the variable-elevation, forested regions >15-20 km to the north-northwest of the WB site (Figures 9a-b) than over other areas of the 50 km radius circle centered at WB site, where the spatial variability in the number of satellite-AERONET collocations is generally small (Figure 10). Exceptions to this are the DT spatial sampling gaps near urban areas and rivers. MODIS Terra retrieves more than MODIS Aqua over the entire region.

Figure 10

Maps of the Spatial Distribution of Satellite-Sunphotometer Collocations at the WB Site

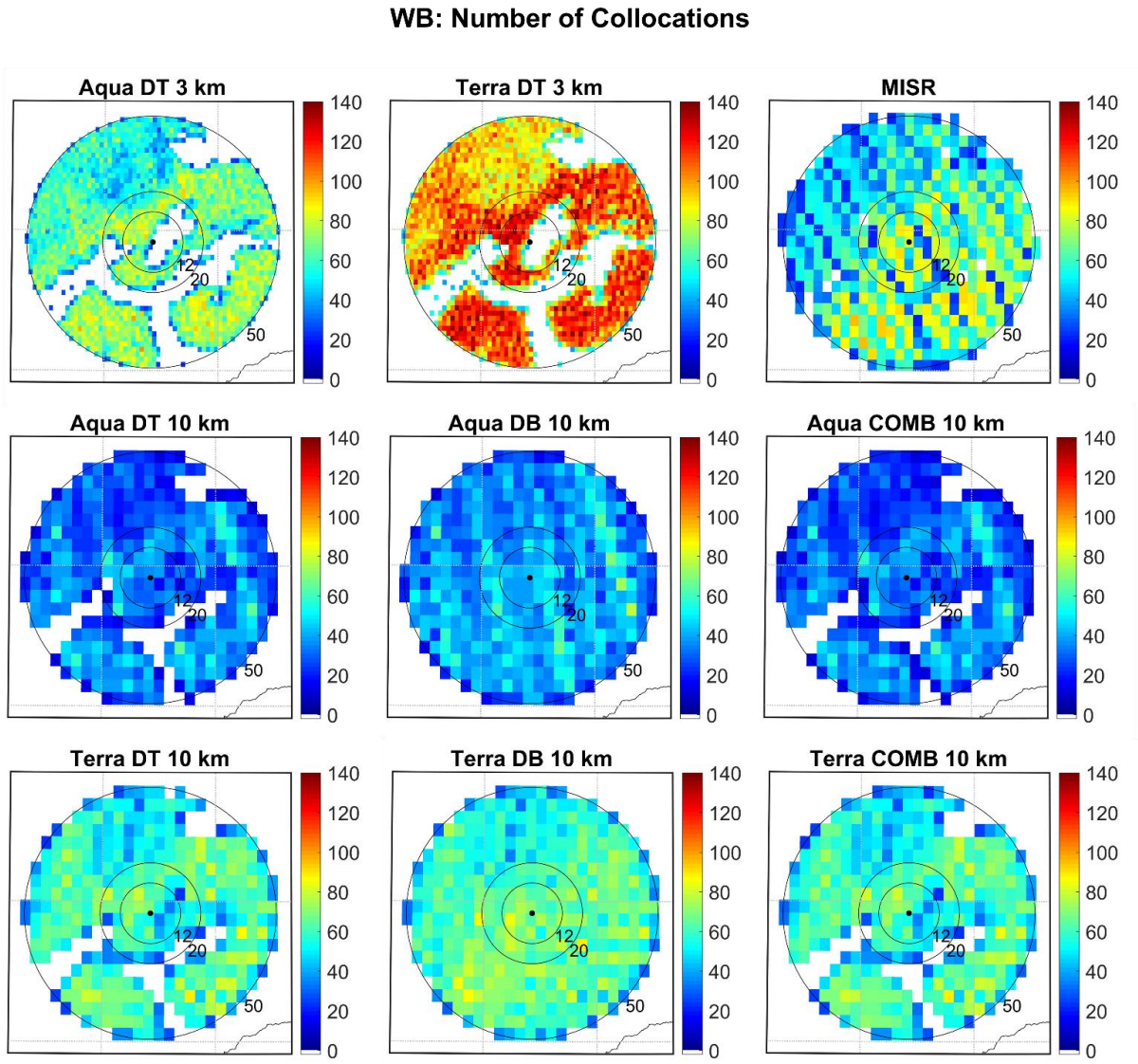

Maps of mean satellite-AERONET AOD differences at / near WB are shown in Figure 11. MODIS Terra DT AOD retrievals appear to be biased about 0.03 higher than Aqua DT for most of the 50 km region surrounding WB, for both the 3 km and 10 km products. By contrast (similar to APP), the MODIS Terra-Aqua DB differences are small over nearly all of the region. The mean satellite-AERONET AOD differences become more negative for all satellite AOD products in the higher-elevation northwest quadrant at distances larger than ~15-20 km from WB than near the site,

with the possible exception of MISR. This likely indicates that AOD in this region is generally lower and not representative of conditions at WB.

The mean satellite-AERONET AOD differences for the urbanized area to east-southeast of WB are more positive than near WB for both Aqua and Terra DB (by ~0.02-0.03). The differences in this area are also more positive overall for Terra and Aqua DT 3 km and 10 km, although there are some 10 km pixels near Knoxville that are more negative. These pixels lie on the edges of urban areas where no retrievals were attempted and therefore could be due to pixel contamination. The higher-resolution MODIS 3 km product performs better near these discontinuous regions and (like the DB product) yields higher AOD near the boundaries of urbanized region. The mean MISR-AERONET difference increases by ~0.02 for the Knoxville area but otherwise is actually more negative over much of the urbanized area to east-southeast of WB. This could be due to different surface assumptions made by MISR.

Regardless of sensor and AOD product, the plots in Figure 11 indicate that inclusion of the higher-elevation areas to west-northwest of WB and the urbanized areas to the east-southeast in satellite-AERONET collocations at WB could potentially bias the results. The radius of representative conditions at the site is likely ~12-15 km, although MISR may be less sensitive to the choice of collocation radius than MODIS. The MODIS DT 3 km sampling gaps at / near WB could potentially add noise to the collocation statistics (through less pixels to average) but the mean AOD differences in the ~12 km region surrounding WB are sufficiently uniform (especially Aqua) that the sampling gaps would likely not bias the collocation statistics for radii less than 12 km. The MODIS DB algorithm appears to perform better than the MODIS DT 10 km product near boundaries of urban / savanna / river surface types, at least near WB.

Figure 11

Maps of Mean Satellite-Sunphotometer AOD Difference at the WB Site

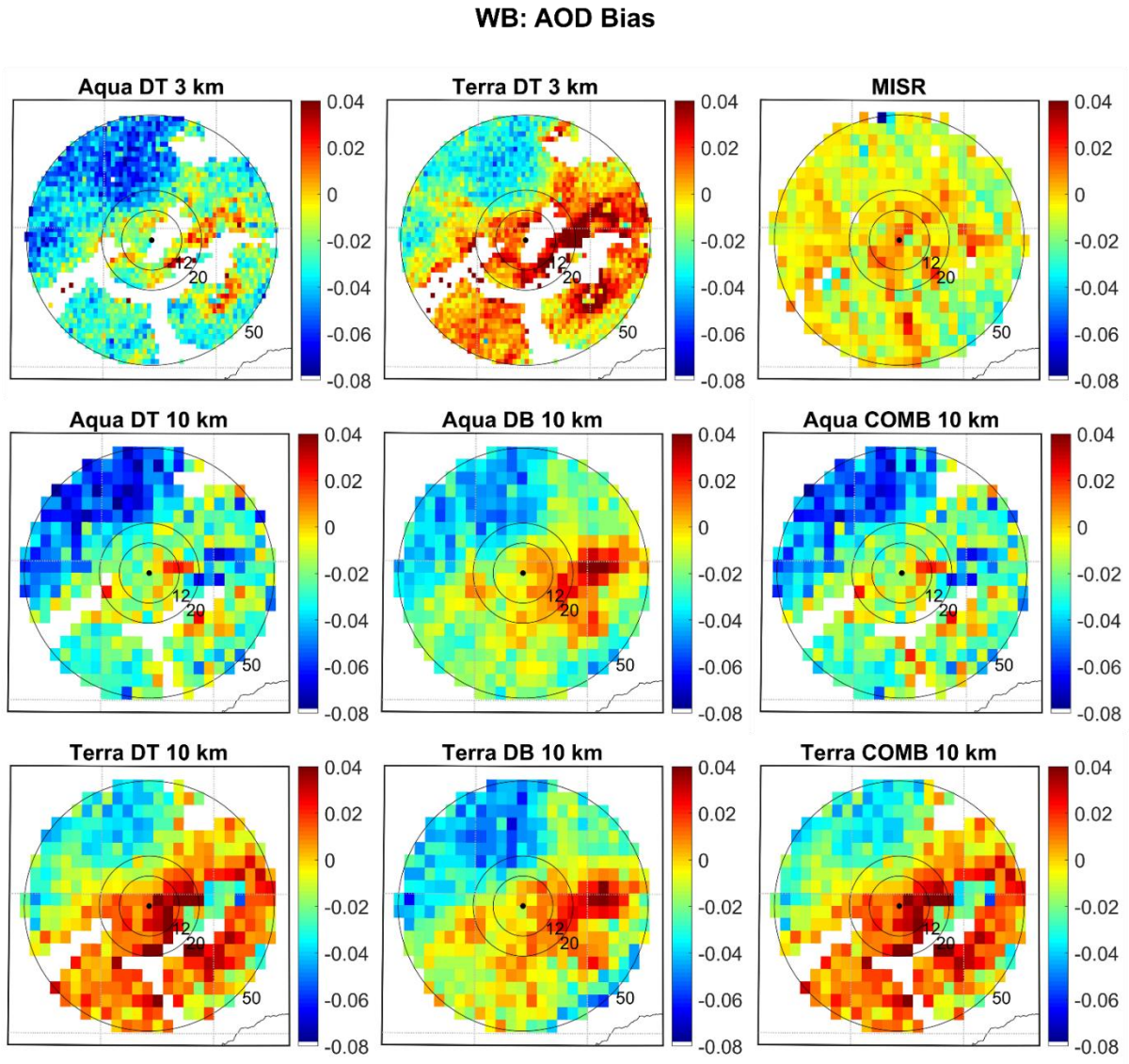

4.2.3 SPL

The region at / near the high-elevation SPL site is home to sizable small-scale elevation gradients of ~1000-2000 m (Figure 12a), which complicate satellite-based AOD retrievals. In particular, MISR does not retrieve over terrain where the standard deviation of surface elevation exceeds 500 m (Garay, et al., 2017). The land cover type and NDVI are also highly heterogenous (Figures 12b-d), ranging from very high-NDVI evergreen forests to moderately high-NDVI savannas

and woody savannas to grasslands with moderate-to-lower NDVI (summer NDVI ~0.20-0.50). Evergreen needleleaf forests tend to grow on the north or northeast facing slopes of the mountains below about 3300 m. High summer NDVI is more favorable to the MODIS DT AOD retrieval algorithm than MODIS DB. The SPL site is unique out of the sites in our study in that there are less than ~10 winter AOD collocations for all satellite products except MODIS Terra DB, for which there were 16 satellite-sunphotometer collocations. This heavy warm-season sampling bias is likely due to snow during the winter months and our results and discussion for SPL will focus primarily on summer and the surrounding months.

Figure 12

Maps Used to Characterize the SPL Site

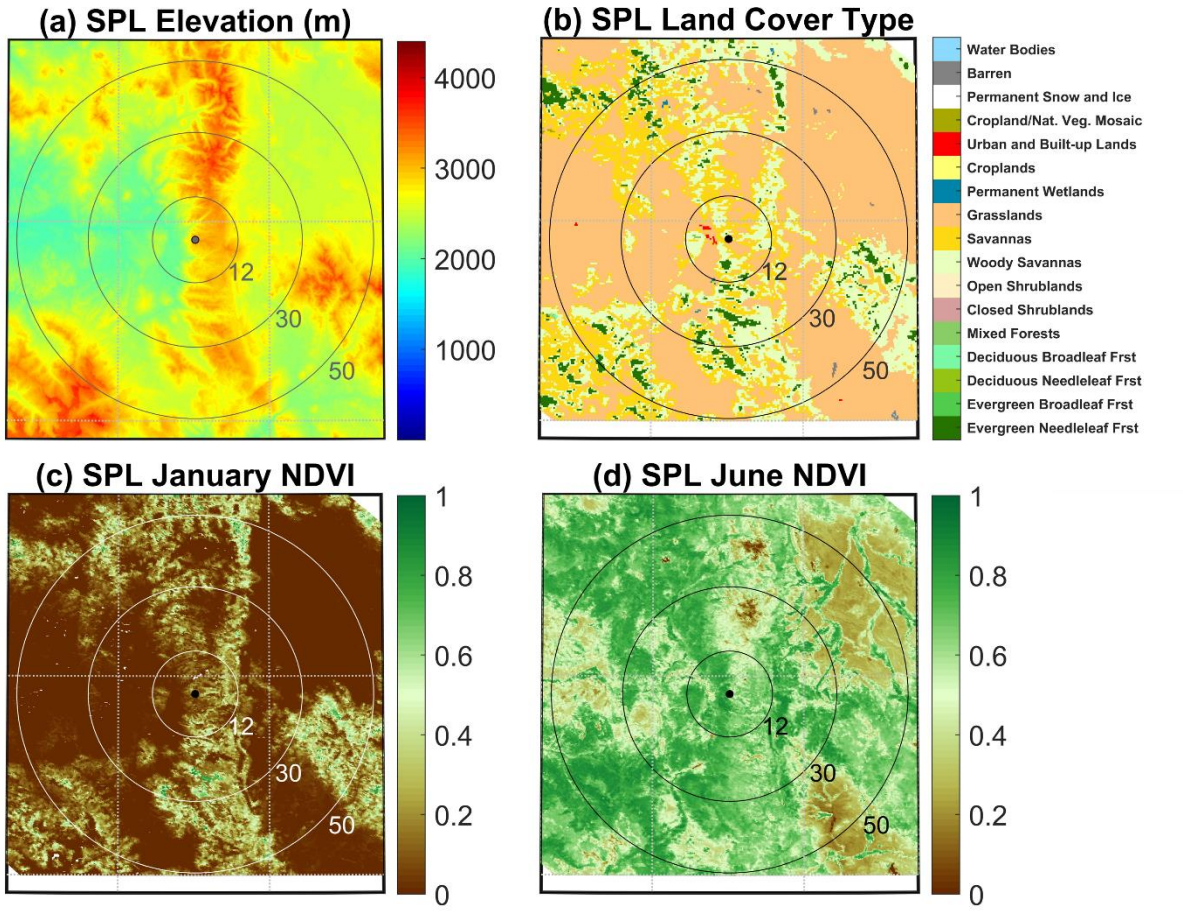

Note. The four maps are derived from: (a) USGS 1 arc-second elevation data, (b) 2004 MODIS-derived land cover type, (c) January 2004 MODIS Terra 16-day NDVI, (d) June 2004 MODIS Terra 16-day NDVI. The numbered rings indicate a circle of constant radius (12, 30, and 50 km) around the site.

From Figure 13, it is seen that there are multiple portions of the highly heterogeneous terrain surrounding SPL with reduced collocations for the various satellite instruments. MISR often does not retrieve in the region greater than ~20 km to the southeast-to-southwest of SPL. This region possesses sizable small-scale elevation gradients of ~1000-2000 m along with gradients in landcover type but MISR is able to retrieve for similar topography and land cover type to the north of SPL. The regions where MODIS DT retrieves less frequently are largely confined to the less vegetative grassland areas

>20 km to the northeast-to-southeast of SPL (Figures 12b-d, 13), along with mountain peaks. The summer NDVI for all of these regions is typically less than ~0.30. The DT spatial sampling gaps are larger for Aqua than for Terra and larger for the 10 km product (especially Aqua) than for the 3 km product. Large spatial sampling differences are also present for Aqua and Terra DB products. While Terra DB has the most complete spatial sampling coverage of all satellite products, Aqua has gaps near the high-elevation regions to the north, east, and southeast of SPL (Figure 12a). The coincidence of some Aqua DT and DB gaps in these regions could possibly be due to a mountain shadowing effect during the afternoon Aqua overpass times. The MODIS 3 km products indicate reduced sampling over the town of Steamboat Springs to the west / northwest of the study site.

The number of AOD retrievals for all satellite products is greatest in the lower elevation grasslands west of the SPL site (Figures 12a, 13), with at least 1.5-2 times the number of retrievals as anywhere else in the 50 km radius circle surrounding the site (Figure 13). Satellite-sunphotometer collocations at SPL thus are disproportionately influenced by this region which is bounded by the surrounding mountains. Terra retrieves approximately twice as often as Aqua except where (as mentioned above) topography and NDVI limit retrievals. The MODIS 10 km COMBINED product is nearly identical to that of DT over the 50 km region surrounding SPL (Figure 13), indicating that it nearly always uses DT despite the presence of low-NDVI areas in the region.

Figure 13

Maps of the Spatial Distribution of Satellite-Sunphotometer Collocations at the SPL Site

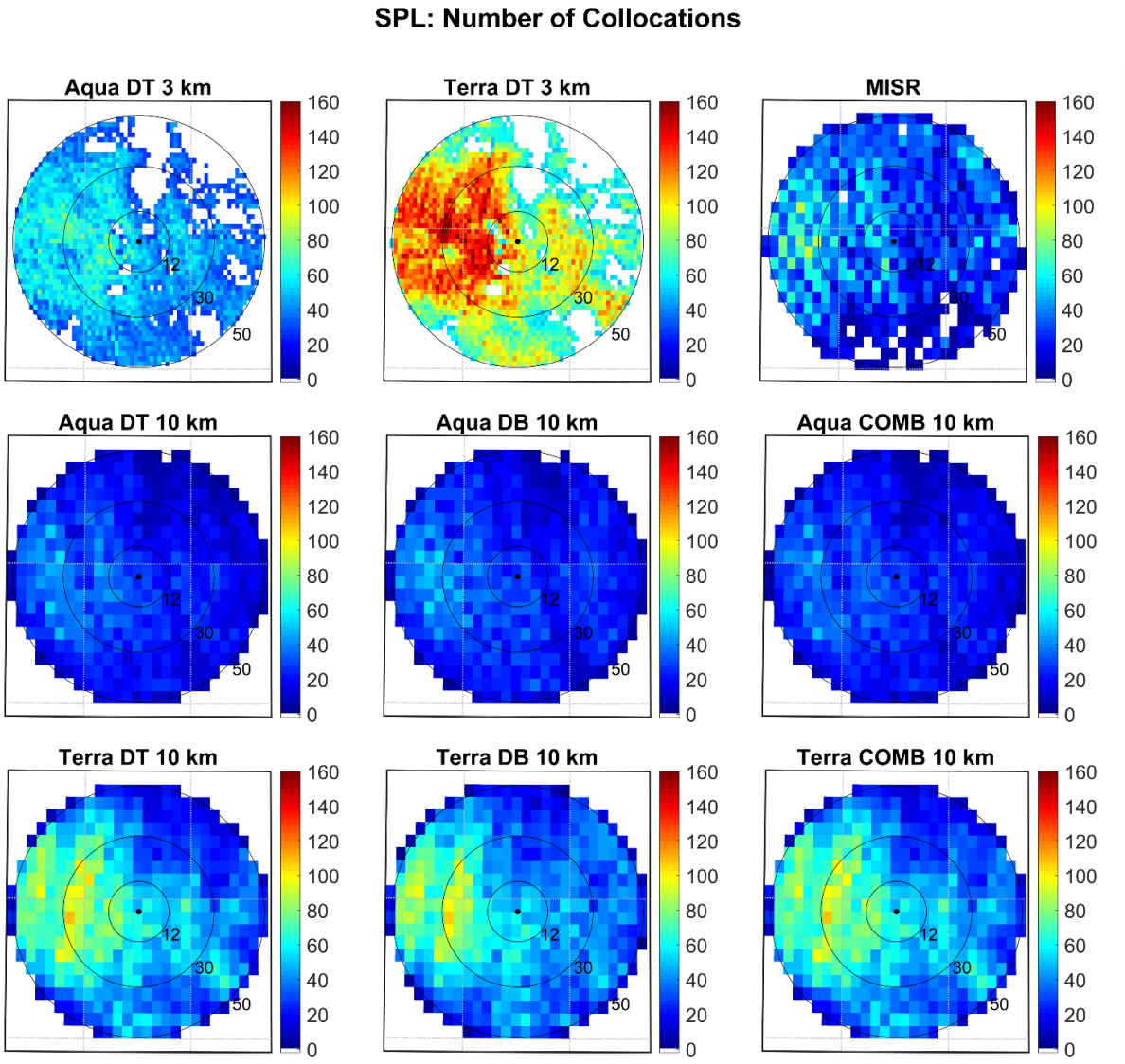

Maps of mean satellite-MFRSR AOD differences over a 50 km radius circle centered at SPL site are shown in Figure 14. The spatial variability is very small for MODIS DB, with values of -0.02 to -0.04 throughout most of a ~20-30 km radius surrounding SPL for Terra DB and slightly less negative (0.00 to -0.02) for Aqua DB. The mean AOD difference actually approaches zero for both Terra and Aqua DB at larger distances (30-50 km) from SPL.

Figure 14

Maps of Mean Satellite-Sunphotometer AOD Difference at the SPL Site

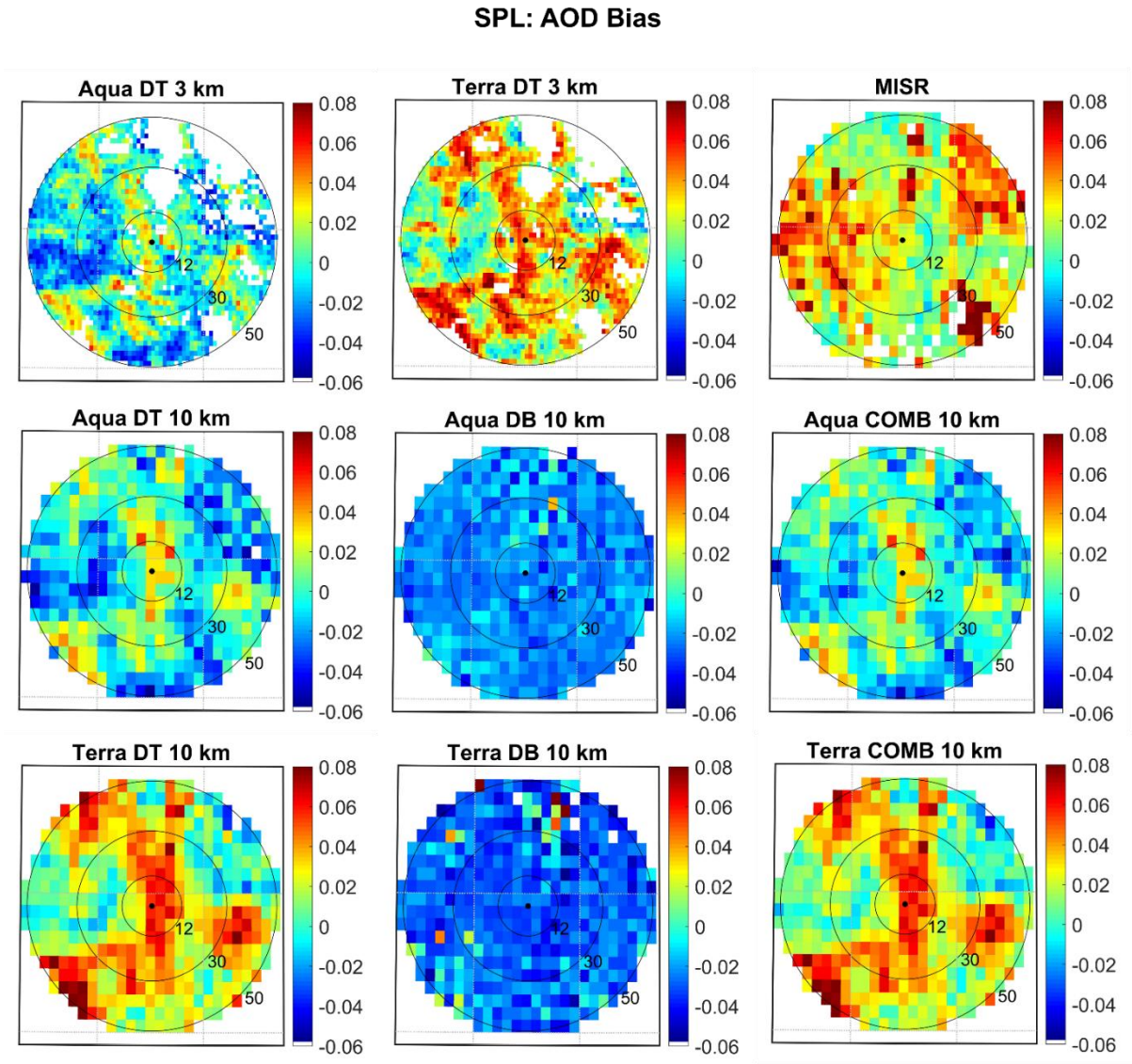

In contrast to MODIS DB, the mean satellite-MFRSR AOD differences for the high-resolution satellite products (MODIS Terra and Aqua DT 3 km and MISR) have the same spatial dependence as land cover type (Figure 12b) and summer NDVI (Figure 12d). The coarser DT 10 km products also show a similar spatial dependence, albeit not as visually obvious. MODIS DT possesses a large positive AOD bias with respect to MFRSR over highly vegetated (summer NDVI greater than ~0.60) terrain, including savannas, woody savannas, and evergreen forests. The mean AOD bias over

these regions is ~0.05-0.08 for Terra DT and ~0.02-0.05 for Aqua DT, with the highest biases over the evergreen forests. The Terra and Aqua DT AOD biases are slightly less positive over moderately vegetated regions (NDVI ~0.50-0.60) and is near zero for Terra DT and slightly negative for Aqua DT in regions with NDVI ~0.40. The reduced MODIS DT retrievals for sparsely vegetated grasslands (NDVI less than ~0.20-0.30) are seen in Figure 13. The spatial pattern of MISR AOD bias near SPL differs from that of MODIS DT, with the least positive MISR bias (~0.00-0.03) over the most highly vegetated regions and most positive MISR bias (0.04-0.08) over the less-vegetated grassland regions with NDVI less than ~0.40.

Since most of the terrain in immediate vicinity of SPL site (within ~12 km) is moderate to highly vegetated (with summer NDVI greater than ~0.50), the MODIS Terra DT products (3 km and 10 km) possess the largest positive mean bias (0.03-0.06) near the SPL site ($r < 12$ km) compared to the MFRSR (Figure 14). Aqua DT and MISR have a very small positive bias within this same area (~0.00-0.03). Aqua DB has a very small negative bias (~0.00 to -0.02) while that of Terra DB is slightly more negative (~ -0.02 to -0.04). The disproportionately large number of collocations for all satellite AOD products in the less-vegetated grassland region to the west of SPL, along with the apparent AOD biases in this region, would likely impact MODIS DT and MISR AOD evaluations that include this region (i.e. collocation radius beyond ~15-20 km). It would also impact evaluation of the MODIS COMBINED product, which is largely derived from DT for SPL. The impact would likely make the Terra DT product appear to perform better (by reducing the positive bias) and the Aqua DT and MISR products appear to perform worse (by making the bias negative and more positive, respectively). Increasing the collocation radius beyond ~15-20 km would likely have minimal effect on evaluations of DB AOD at SPL.

4.2.4 RENO

Reno presents different challenges than the other mountain sites for satellite AOD retrieval and spatio-temporal collocation optimization algorithms, due to the large contrast in land cover types and NDVI at / near the Reno AERONET site relative to most of the region west and southwest of the

site. The terrain is largely urban at / near the site, but the immediate area is largely surrounded by sparse vegetation (desert grasslands possessing low NDVI, Figures 15c-d). Much of the high-elevation terrain to the west and southwest of the site consists of more vegetated savannas, high-NDVI evergreen forests, and Lake Tahoe (Figure 15b). The aggregated effect of these landcover types is low 40 km x 40 km average NDVI during all seasons (Figure 4c) but with considerable spatial inhomogeneity, especially during summer and the surrounding months (Figure 15d). The urban terrain poses problems for both MODIS DT and DB while the bright, low-NDVI desert terrain violates the surface property assumptions used by the DT algorithm (Levy et al., 2013). The number of satellite-sunphotometer AOD collocations over the region centered at Reno during winter is (depending on satellite and product) several times smaller than summer. Though the seasonal discrepancy is not as large as at SPL, the heavy warm-season sampling bias leads us to focus primarily on summer and the surrounding months.

Figure 15

Maps Used to Characterize the RENO Site

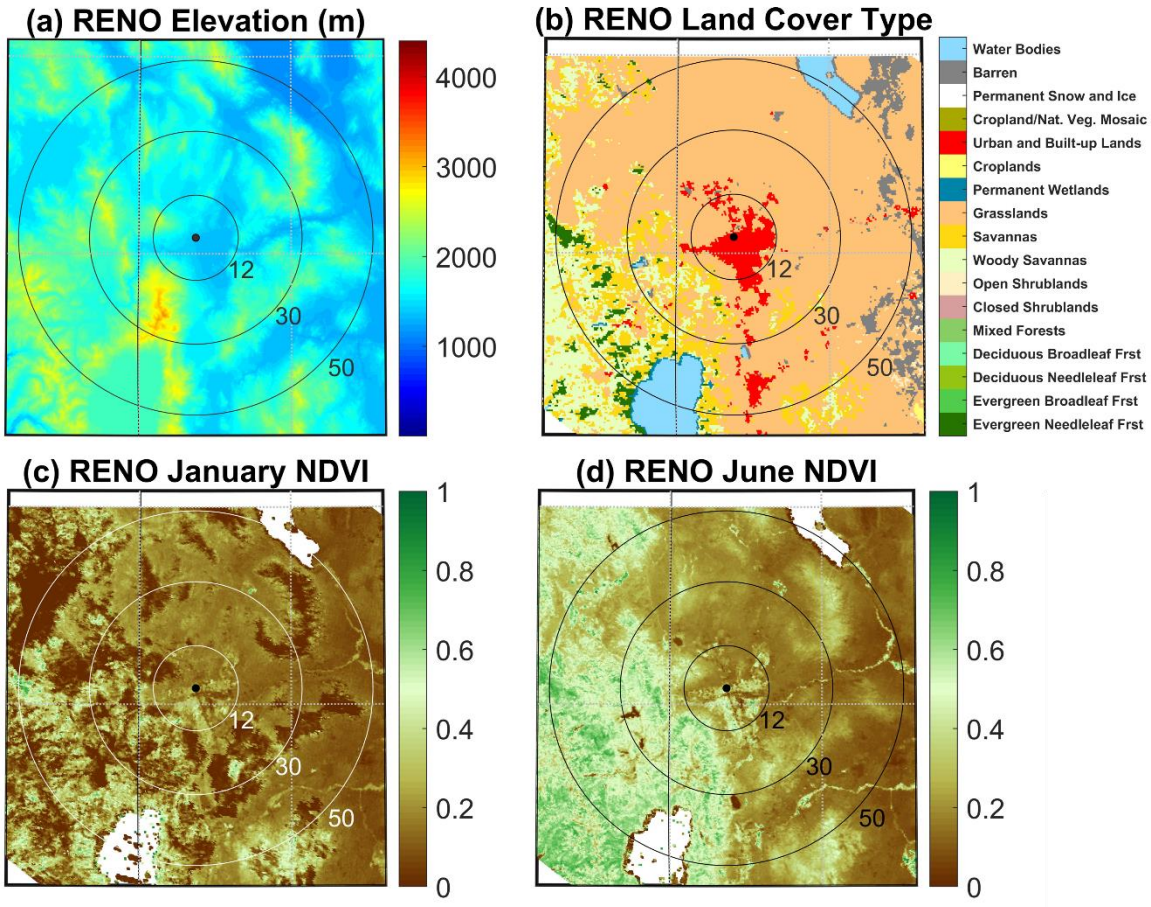

Note. The four maps are derived from: (a) USGS 1 arc-second elevation data, (b) 2004 MODIS-derived land cover type, (c) January 2004 MODIS Terra 16-day NDVI, (d) June 2004 MODIS Terra 16-day NDVI. The numbered rings indicate a circle of constant radius (12, 30, and 50 km) around the site.

Reduced sampling in both MODIS DT and DB AOD retrievals for the 50 km radius circle surrounding Reno AERONET site exist over the much of the urban terrain, Lake Tahoe to the southwest, and areas of low NDVI (Figure 16). The urban sampling minima near the Reno site are larger for DB than for DT 10 km. However, this may be influenced by inclusion of some non-urban subpixels in the 10 km product, as seen by comparison of the number of DT 3 km and 10 km collocations near the Reno site and other urban boundaries. The DT 3 km sampling gaps clearly

follow the areas of urban landcover type (Figure 15b). By contrast, MISR is able to retrieve over all land cover types (Figure 16) with the exception of Lake Tahoe.

Figure 16

Maps of the Spatial Distribution of Satellite-Sunphotometer Collocations at the RENO Site

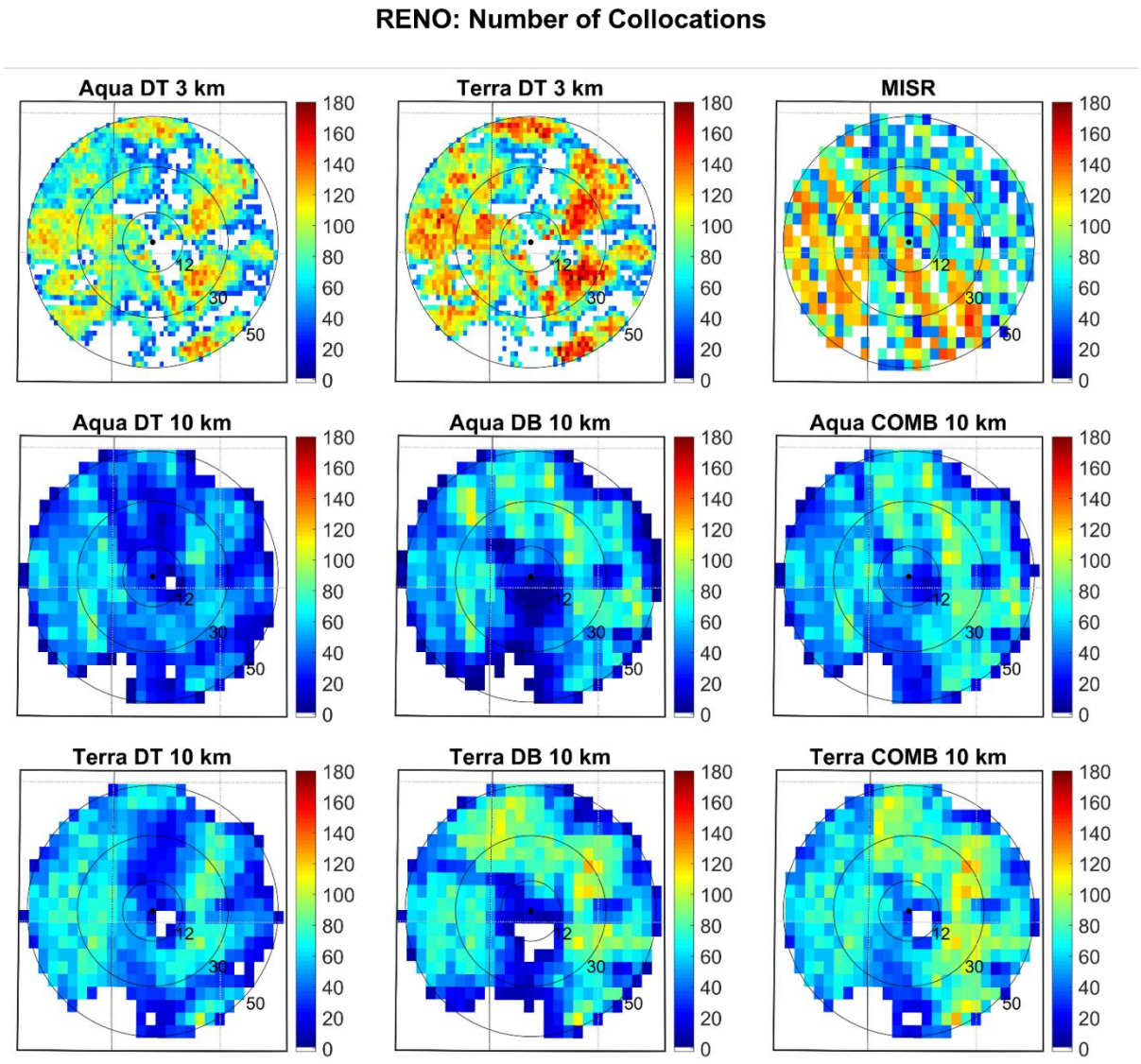

The largest number of MODIS DT and MISR collocations with AERONET are above the savannas and forests to the southwest (at distances greater than ~10 km from site) and above small patches of savannas and more vegetated grasslands at distances greater than ~20 km from site (Figure 16). The higher resolution DT 3 km product has more collocations than the DT 10 km product near boundaries of different land cover type. The number of collocations for DB is highest over the northwest to east sector at a distance greater than ~20 km from Reno site. Reno is only site in our study where the MODIS COMBINED product contains appreciable contributions from both DT, DB, and averages of the two (Figures 16-17). The major contribution to the COMBINED product from DB is over the less-vegetated grasslands in the region running clockwise from north to southeast (Figure 17b) while DT contributes more over the more vegetated savannas and forests along the southeast to northwest region (Figure 17a). Dark Target also helps to fill in some of DB's sampling gaps in the somewhat more vegetated grassland areas (NDVI ~0.30-0.50) and in some urban areas, including the immediate vicinity south and west of the Reno site. Areas to the north and southeast of the Reno site are the primary locations where the DB and DT algorithms are averaged and assumed to be the best AOD approximation by the COMBINED algorithm (Figure 17c).

Figure 17

Maps of the Spatial Distribution of Satellite-Sunphotometer Collocations at the RENO Site for Each Algorithm Selected by the Terra 10 km COMBINED Product

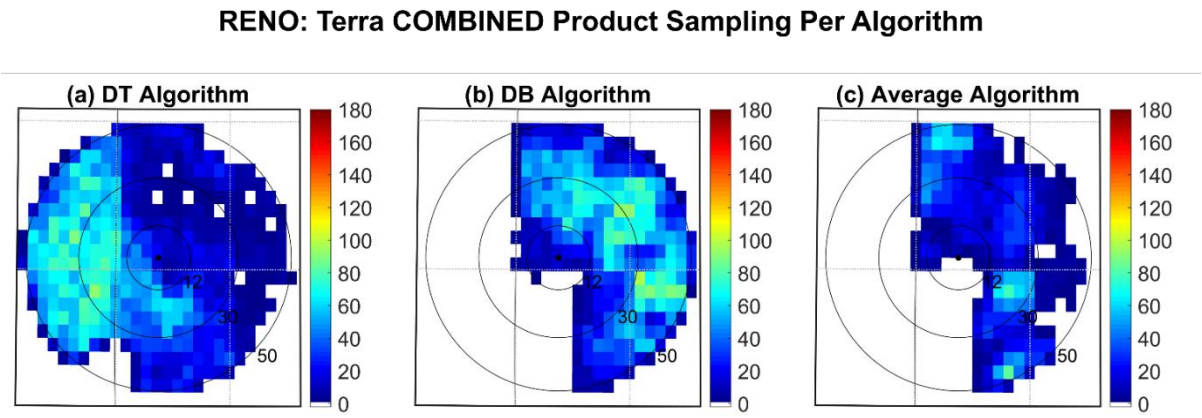

Note. Similar results were observed for the Aqua 10 km COMBINED product.

Maps of mean satellite-AERONET AOD differences over a 50 km radius circle centered at the Reno AERONET site are shown in Figure 18. MISR possesses a positive mean bias (0.02-0.06) at / near the Reno site (r < 12 km) compared to AERONET, in addition to over most of the less vegetated desert grasslands and urban areas primarily located to the east of the site. The mean MISR-AERONET AOD difference is close to zero (-0.02 to 0.02) over much of the savannas, forests, and moderately vegetated grasslands primarily to the west / southwest. Excellent MISR agreement with ground-truth over moderate and highly vegetated terrain (NDVI greater than ~0.40-0.50) and higher positive bias over less vegetated terrain (NDVI less than ~0.40) by MISR near Reno are similar to results observed near SPL. Evaluation of MISR AOD using the Reno AERONET site may display some sensitivity to collocation radius at values larger than 12 km, due to lower mean MISR AOD bias to the west of the site and the higher number of MISR retrievals in that region, which if included would likely decrease the mean MISR AOD bias.

Figure 18

Maps of Mean Satellite-Sunphotometer AOD Difference at the RENO Site

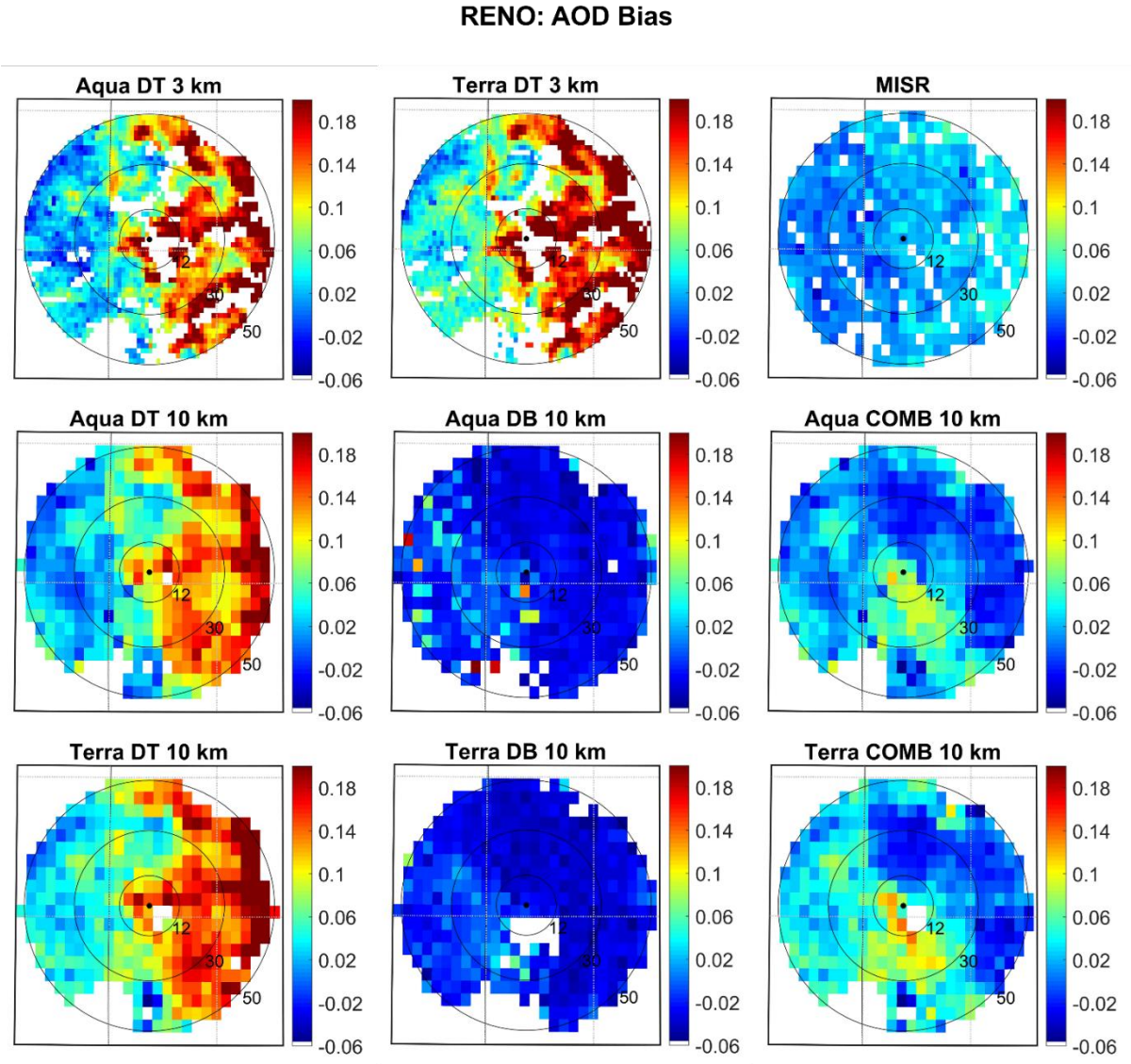

MODIS Terra and Aqua DT both possess large positive AOD biases (0.10-0.20) over the desert grasslands (NDVI less than ~0.30), with smaller positive biases for the more vegetated grasslands, savannas, and forests to the west of Reno site (~0.02-0.10 for Terra and ~0.00-0.06 for Aqua). The small DT AOD biases over moderately vegetated terrain is also like that at SPL, although the magnitudes of these biases are larger at Reno. The reduced sampling of MODIS DT over the urban areas at / near the AERONET site complicates MODIS DT evaluations over Reno and the large

DT bias for the DT-retrieved pixels near the site would certainly lead to poor agreement with AERONET. The competing effects of high positive DT AOD bias to the east and lower positive bias values to the west would also make interpretation of the results difficult for collocation radii larger than ~15 km.

Both Terra and Aqua DB have fairly uniform negative biases (~ -0.02 to -0.06) with respect to AERONET over the less vegetated desert grasslands in the region. Terra DB agrees very well with AERONET over much of the more vegetated grasslands, savannas, and forests to the west while Aqua DB exhibits (in general) a small high bias over this terrain. Similar to MODIS DT, the reduced number of DB retrievals in the urban areas at / near the Reno site (less than ~12 km) complicates attempts to collocate it with AERONET, as the expected agreement would likely improve with increasing collocation radius to include regions to the west of the site.

The MODIS COMBINED product improves upon the DT and DB AOD retrievals above Reno through the use of primarily DT over the more vegetated western portions of the region and DB over the less vegetated eastern areas, in addition to averaging of the two products over savanna and semi-vegetated grassland covered regions to the north and southeast of the Reno site, where the NDVI is between ~0.20-0.30 (Sayer et al., 2014). The resulting Terra and Aqua COMBINED products perform similarly overall, with small positive bias (~0.02-0.06) over the more vegetated western terrain and a small, mostly negative bias (~ -0.02 to -0.06) over much of the desert grasslands east of Reno site. The averaging of DB and DT over the urbanized region to south-southeast of Reno site still yields a larger mean AOD difference than that of MISR. In addition, the coincident spatial sampling gaps in the urbanized areas near the Reno site complicate efforts to evaluate the COMBINED AOD product at Reno. That being said, the spatial distribution of mean COMBINED-AERONET AOD over a ~20-25 km radius does seem more representative of that near the Reno site than that of either DT or DB alone, which should make realistic collocations possible.

4.3 Spatio-Temporal Optimization Algorithm Results

The statistical satellite AOD performance metrics of satellite-sunphotometer collocations (Sect. 3.3) demonstrate minimal sensitivity to temporal window size at the four sites under study. The insensitivity of the satellite AOD performance metrics to temporal collocation window size is consistent with the overall lack of aerosol variability at the sites near satellite overpass hours (Sect. 4.1.2). We select a temporal window of 1 h to increase the number of collocations relative to the 30 min window, without allowing for such a large window that changing atmospheric and aerosol loading conditions (Figure 5) are likely. The following discussion will hence refer to the results from this 1 h window. In contrast to the relative insensitivity to temporal window size, some satellite AOD performance metrics demonstrate sensitivity to spatial collocation window radius, more so for the western U.S. mountain sites (SPL and Reno). This spatial dependence at SPL and Reno is likely due to the dependence of satellite-retrieved AOD on topography and NDVI (at least for MISR and MODIS DT), as discussed in Sect. 4.2. Furthermore, the spatial dependence sometimes varies amongst metrics and satellite AOD products, making it difficult to identify the 'best metrics' for use in optimizing the spatial collocation radius. For brevity, we only include (1) AOD RMS difference; (2) percent of satellite retrievals with agreement to within, above, and below the expected error envelope (Table 1) of the satellite AOD product; (3) mean AOD bias (Eq. 4); (4) linear correlation coefficient of the regression; along with (5) number of collocations. The plots of collocation radius dependence of the other statistical parameters (slope and y-intercept of linear regression) do not add additional information for optimizing spatial collocation radius, at least for the sites in this study.

4.3.1 APP

The agreement between satellite and AERONET-retrieved AOD at APP is relatively insensitive to spatial radius used for the collocations, as seen from the statistical parameters shown in Figure 19. The percent of retrievals with AOD agreement lying within satellite AOD product error envelopes (Figure 19b) exhibits a modest dependence on collocation radius, with slightly worse agreement for radii larger than ~20-25 km for most AOD products. Two of the high-resolution

products (MISR and the MODIS Aqua 3 km DT) have best agreement for radii less than ~12 km (Figures 19a, b). It should be noted that the MODIS DB product performs better with increasing collocation radius (Figures 19b, d). We choose a collocation radius of 12 km for the high-resolution products (MISR, MODIS Terra DT 3 km, and MODIS Aqua DT 3 km) and a radius of 20 km for the 10 km products based on these considerations. The relative insensitivity to collocation radius at APP is not surprising, given the fairly uniform vegetation and the lack of large aerosol spatial gradients (Figure 8). Slightly worse MODIS DT and MISR AOD agreement with AERONET and slightly better agreement for MODIS DB for collocation radii larger than ~20-25 km are both likely due to inclusion of the lower elevation pixels to the southeast of the APP AERONET site (Figure 8). The results are consistent with the spatial distribution of mean satellite-AERONET AOD differences presented in Sect. 4.2.1.

Figure 19

Statistical Parameters of Satellite Versus AERONET-Measured AOD as a Function of Collocation Radius Centered on the APP AERONET Site

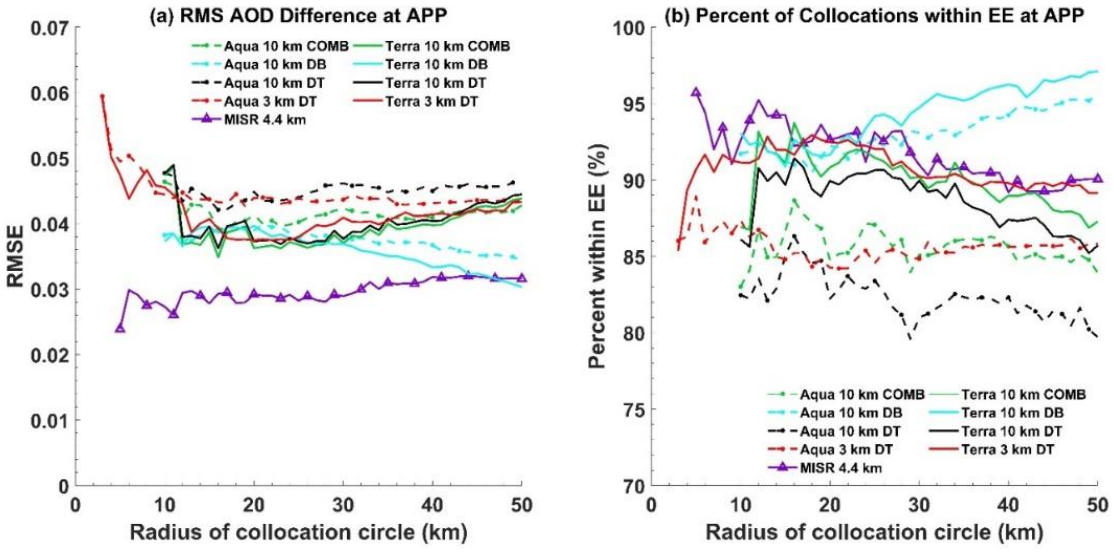

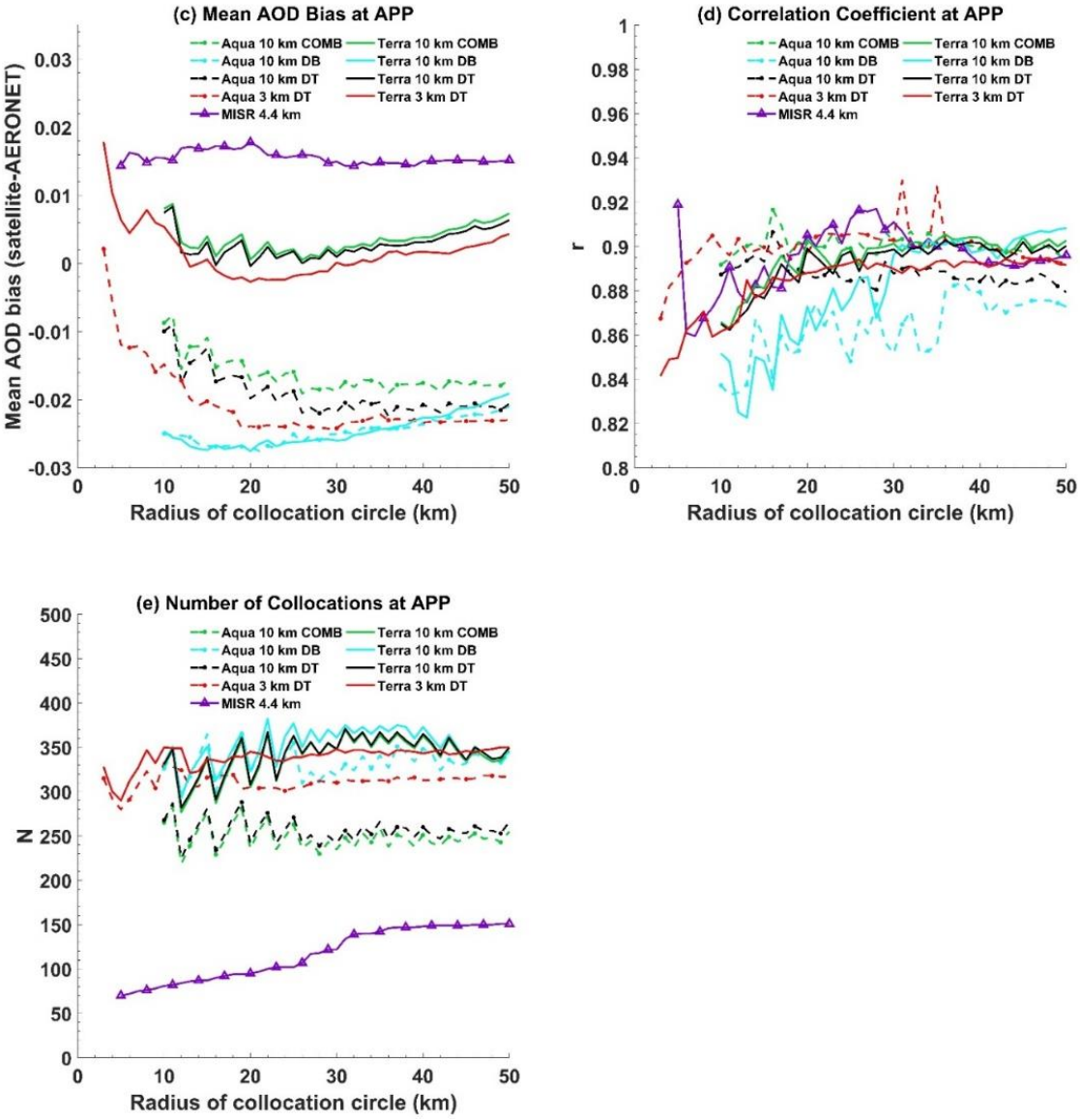

Note. AOD comparisons are made at 550 nm. EE indicates the satellite AOD product expected error envelope.

4.3.2 WB

Similar to APP, the agreement between satellite and AERONET-retrieved AOD at WB is relatively insensitive to spatial radius used for the collocations. The RMSE (Figure 20a) and percent of retrievals with AOD agreement lying within satellite AOD product error envelopes (Figure 20b) are slightly worse for collocation radii less than 10-15 km for the high-resolution MODIS products. This could be due to the smaller number of collocations for radii < 10 km (Figure 20e) as a result of

the collocation sampling constraints (Eq. 3) and reduced collocations over the region immediately east of the site. The mean AOD bias is also near zero for MISR over this range of collocation radii. We choose a 12 km radius for these high-resolution products, although a radius up to ~20 km does not appreciably worsen the satellite-AERONET agreement.

The 10 km MODIS AOD products are also for the most part insensitive to collocation radius, with the lone exception of a slightly higher percentage of retrievals within the satellite AOD product error envelopes for a radius of ~20 km (Figure 20b). We thus somewhat arbitrarily choose a 20 km collocation radius for the 10 km products. Like APP, the relative insensitivity of the satellite-AERONET AOD agreement to collocation radius at WB is not surprising, given the altitude homogeneity (Figure 10a) and NDVI homogeneity (Figures 10c, d). Slightly higher AOD in the urbanized region to the east of the WB site (Figure 11a) does not seem to influence the satellite-AERONET AOD agreement.

Figure 20

Statistical Parameters of Satellite Versus AERONET-Measured AOD as a Function of Collocation Radius Centered on the WB AERONET Site

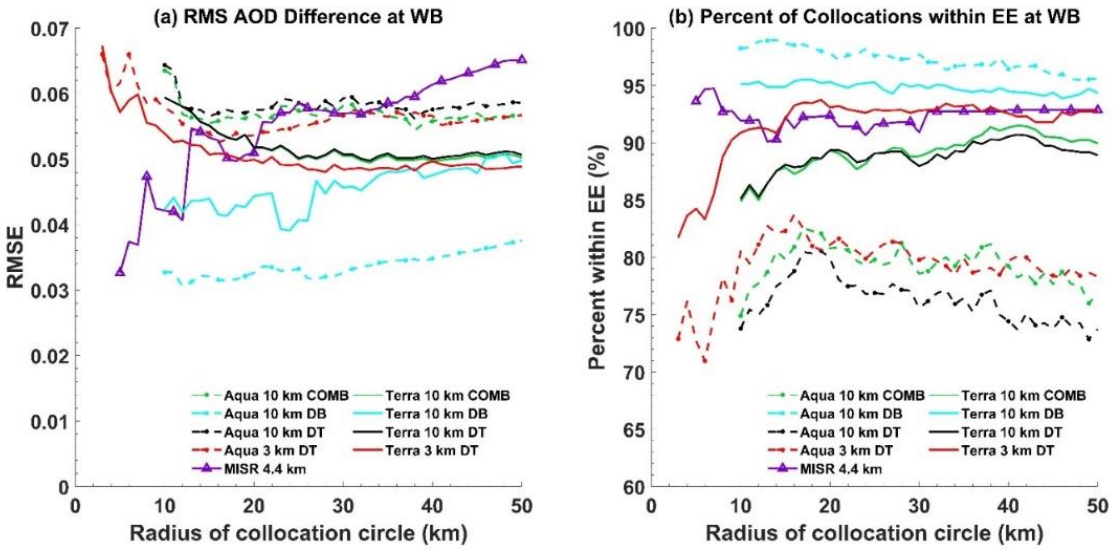

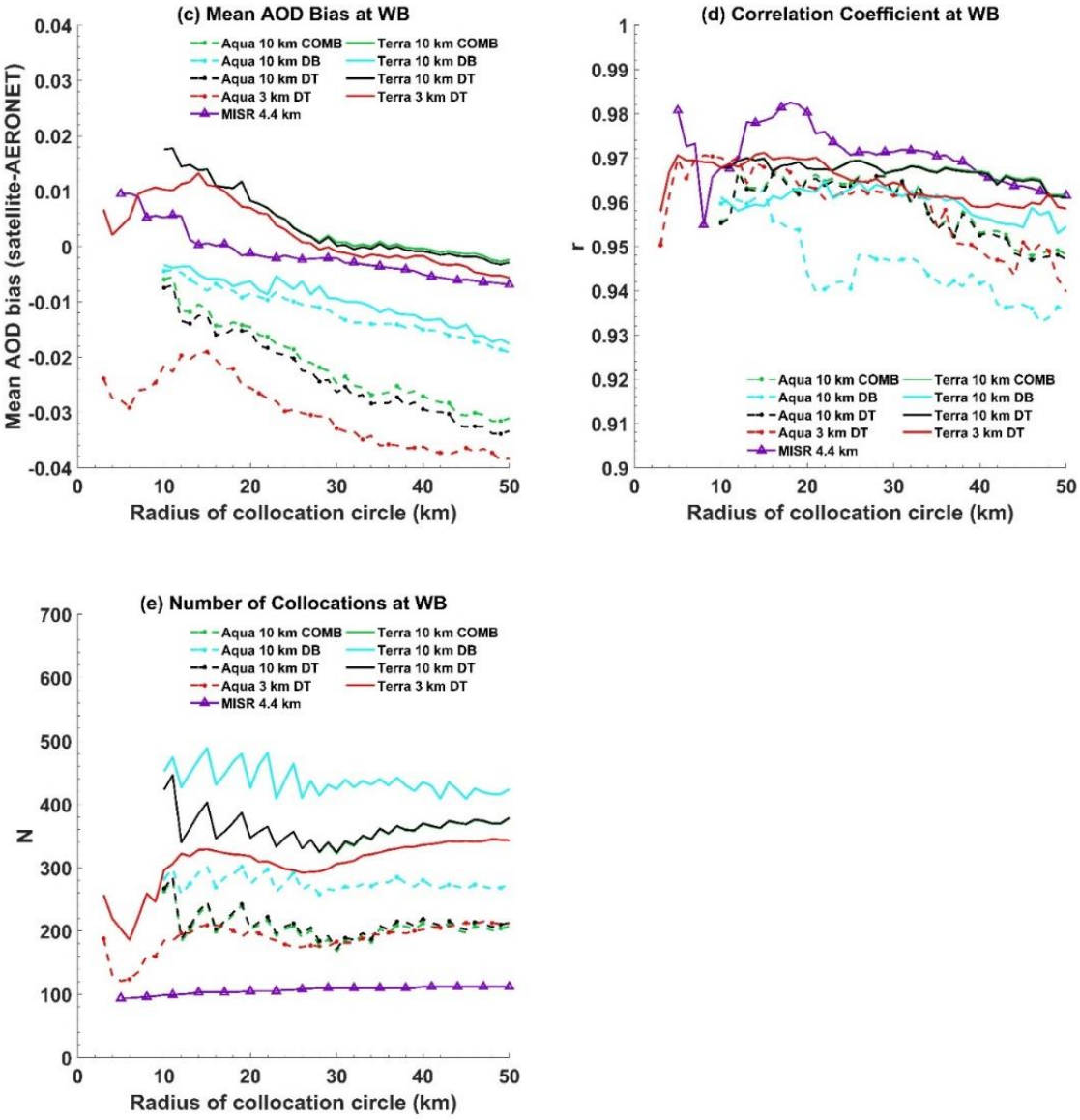

Note. AOD comparisons are made at 550 nm. EE indicates the satellite AOD product expected error envelope. The MODIS DT traces often overlap those of the COMBINED product because the combined product at WB uses DT AOD for nearly all retrievals in this study period.

4.3.3 SPL

The dependence of satellite-sunphotometer AOD agreement at SPL is more sensitive to collocation radius than at the eastern U.S. mountain sites (APP and WB). This is not surprising, given the large range of elevations near the SPL site (Figure 13a) along with the highly inhomogeneous spatial and seasonal NDVI variability (Figures 13c, d). The dependence of AOD agreement on

collocation radius is largest for MISR, especially the RMSE (Figure 21a), the percentage of collocations lying within MISR error envelope (Figure 21b), and the correlation coefficient (Figure 21d). The MISR RMSE increases from 0.04 to ~0.07-0.08 at collocation radii larger than ~20-25 km (Figure 21b) and the correlation coefficient decreases from ~0.85 to between 0.60 and 0.70 (Figure 21d). The percentage of MISR retrievals agreeing with MFRSR to within the MISR expected error envelope decreases steadily from ~80% at 12 km to 65% at 50 km (Figure 21b). The mean MISR AOD bias increases from ~0.02-0.03 to greater than 0.04 with increasing radius. MISR is also the AOD product whose number of collocations is most sensitive to collocation radius, with a gradual increase (by a factor of 2) from 10 km to 50 km. In contrast to MISR, the RMSE, mean AOD bias, and percent of retrievals lying within the expected error envelope become better with increasing collocation radius for the high-resolution MODIS DT products (both Terra and Aqua), up to ~20-25 km (Figures 21a, b). Worse MISR performance and better MODIS DT performance with increasing radius from 10 km to 25 km is likely due to the influence of pixels in the less-vegetated regions west and northeast of SPL, where MISR is biased higher (with respect to MFRSR) and MODIS DT is biased less positive, as discussed in Sect. 4.2.3 (Figure 14). We choose a collocation radius of 12 km for MISR and the MODIS 3 km DT product for consistency with the other sites and because the satellite-sunphotometer AOD bias (Figure 14) becomes less representative of that at the SPL site for r > 12 km. That being said, we note that any radius between 12-20 km could likely be used for these products.

Figure 21

Statistical Parameters of Satellite Versus MFRSR-Measured AOD as a Function of Collocation Radius Centered on the SPL Site

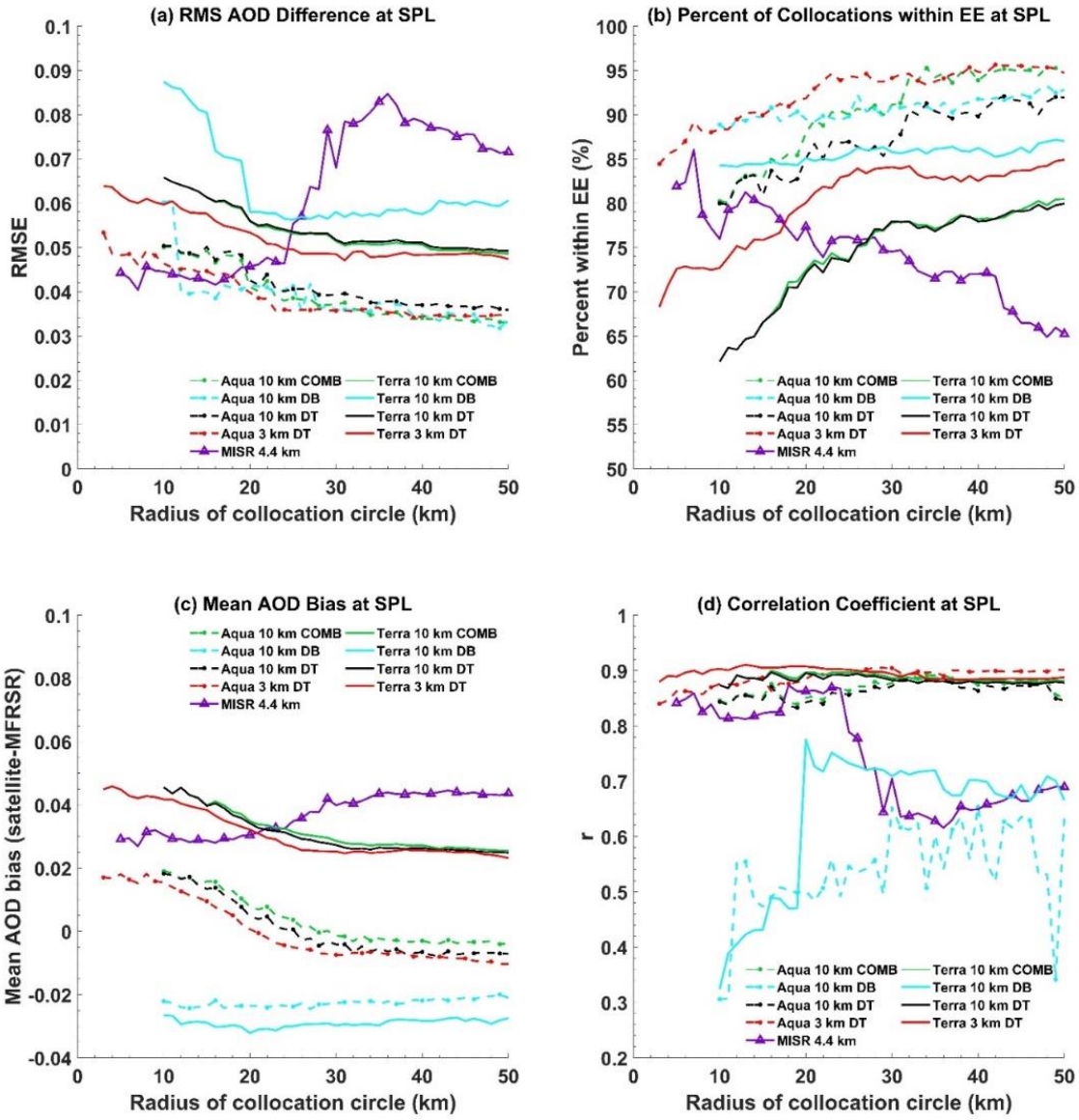

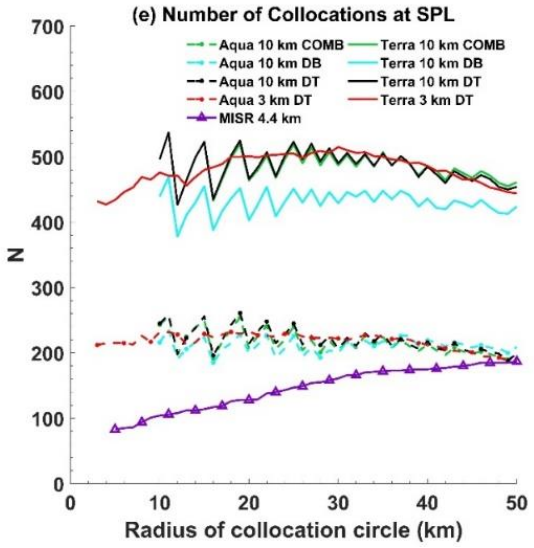

Note. AOD comparisons are made at 550 nm. EE indicates the satellite AOD product expected error envelope. The MODIS COMBINED traces are largely overlapped by those of DT because the combined product at SPL primarily uses DT AOD for all retrievals in this study period.

The MODIS 10 km DT and COMBINED products (which are derived primarily from DT at SPL) agree slightly better with AOD retrieved by the MFRSR when larger collocation radii are used, especially for Terra. This is likely due to the same reasons discussed above for the MODIS 3 km DT products. The percentage of Terra 10 km COMBINED product and DT collocations lying within the expected error envelope increases gradually from ~62% at 10 km to 80% at 50 km (Figure 21b), with a smaller improvement (~10-15%) for the Aqua DT and COMBINED products. The RMS AOD difference (Figure 21a) also exhibits very small improvements with increasing collocation radius, for both Terra and Aqua DT and combined products.

Despite very few pixels containing collocations within ~12 km of SPL, the DB-MFRSR AOD agreement is insensitive to collocation radius. This is not surprising, in light of the smaller spatial variability in mean DB AOD bias (Figure 14) near SPL. The correlation coefficient for Terra and Aqua DB appears to demonstrate modest improvement (especially for Terra) with increasing collocation radius up to 30 km, although still poor (~0.60-0.70).

A drawback of using collocation radius > 20-30 km at SPL is a slight decrease in the number of collocations except for MISR (Figure 21e). Differences in geographic sampling differences between the satellites / sensors (Figure 13) also make comparisons between them more difficult for larger collocation radii. We choose a 30 km collocation radius for the 10 km products due to the slight increase in performance (as compared to 20 km) but note that any radius between 20-30 km could likely be used with minimal effect on agreement with the MFRSR.

4.3.4 RENO

The Reno site is a classic example of the difficulties and subtleties in optimizing satellite-sunphotometer collocation radius over a region with complex terrain, especially through the use of an automated method. Since the number of collocations is larger for more vegetated regions further than ~12 km from the Reno AERONET site (Figure 16) than for pixels at / near the site, the further pixels will be more heavily weighted in the satellite-AERONET collocation statistics. The problem is that the landcover type and NDVI of these further pixels (more vegetated savannas and some evergreen forests) is not representative of that at / near the Reno AERONET site (urban and desert grasslands), leading to a mean satellite-sunphotometer AOD bias that is also not representative of the site (Sect. 4.2.4). This can be seen in Figure 22e, where the number of collocations increases much more rapidly with radius (up to r ~25-30 km) for MODIS DT and DB than for MISR. For this reason, we consider primarily MISR when optimizing the spatial collocation radius for the high spatial resolution AOD products (MISR, MODIS DT 3 km). The percentage of collocations lying within the MISR expected error envelope increases with radius from 10 to 15 km, after which it remains nearly constant (Figure 22a). The correlation between MISR and AERONET decreases slightly (from 0.92 to 0.87) with increasing radius larger than ~12 km. We thus choose a 12 km collocation radius for the high-resolution AOD products. The mean MISR AOD bias and RMS AOD difference do not change much with collocation radius, possibly due to the aggregated effect of near-zero MISR mean AOD bias for pixels in the more vegetated western portion of the surrounding region and the more positive bias in the less vegetated eastern portion (Figure 18), which when combined appear to result in a mean bias

that is comparable to pixels near the site. Poor performance by the Terra and Aqua DT 3 km products at Reno is to be expected, given the brighter, less vegetated surfaces (i.e. lower NDVI, Figure 15c, d) near the site. However, their agreement with AERONET improves with increasing collocation radius (except for the correlation coefficient) due to the inclusion of more vegetated pixels where the DT AOD bias is less positive than that over the less vegetated pixels near the Reno site (Figure 18).

Despite few DB pixels containing frequent collocations within ~12 km of Reno, the DB-AERONET collocation statistics are surprisingly insensitive to collocation radius up to 50 km from Reno. The number of DB-AERONET collocations increases sharply with collocation radius, from ~100 at 12 km to ~500 at 30 km (Figure 22e). The DB AOD becomes less correlated with AERONET with increasing collocation radius, more so for Aqua than for Terra. The correlation coefficient decreases from ~0.95 to ~0.73 for Aqua as collocation radius is increased from 10 km to 50 km while the corresponding decrease is generally less for Terra (0.98 to 0.88, but with a sudden drop to 0.75 at ~47 km). The other statistical indicators such as mean AOD bias and RMS AOD difference are relatively independent of collocation radius, which is consistent with a lack of spatial variability in mean DB-AERONET AOD difference (Figure 18). Like MODIS DB, the MODIS DT 10 km-AERONET collocation statistics are also relatively insensitive to collocation radius.

Reno is the only site where the MODIS COMBINED 10 km product differs significantly from both the DT and DB products, due to use of DB over much of the less-vegetated region east of Reno and DT over the more vegetated region west of Reno (Figure 17). The COMBINED-AERONET AOD agreement improves with increasing collocation radius, with less positive mean AOD bias, smaller RMSE, and higher percent of collocations within the EE envelope as the collocation radius increases from 10 km to ~30 km (Figure 22). This is likely due to the larger number of collocations to the east of Reno (Figure 16), where the mean DB AOD bias is near zero (Figure 18). Since MODIS DT performs poorly for all collocation radii at Reno, we optimize the radius based on the COMBINED and DB products. Based on these considerations, we choose a 30 km collocation radius for the 10 km MODIS products (DT, DB, and COMBINED) at Reno.

Figure 22

Statistical Parameters of Satellite Versus AERONET-Measured AOD as a Function of Collocation Radius Centered on the RENO AERONET Site

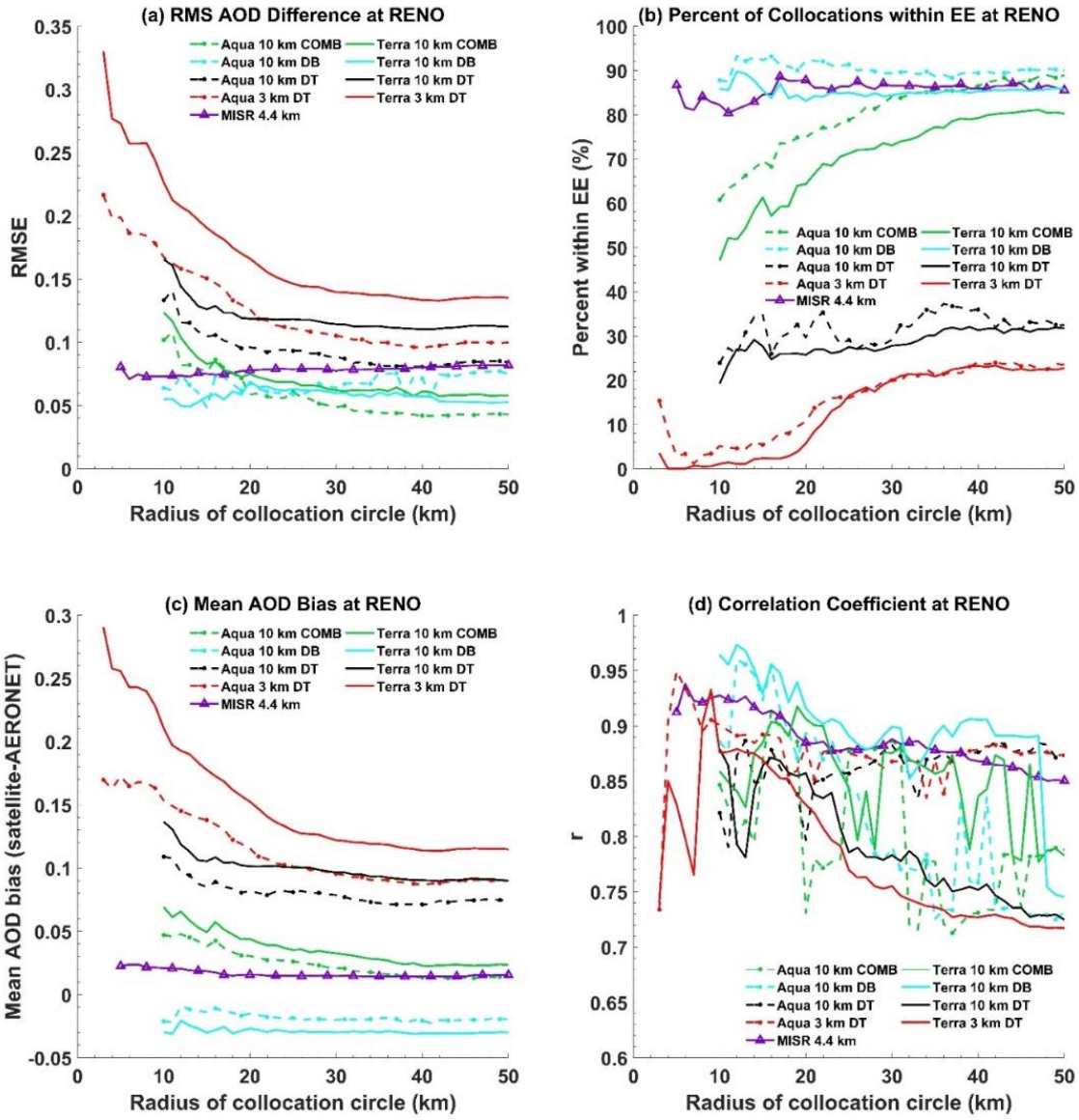

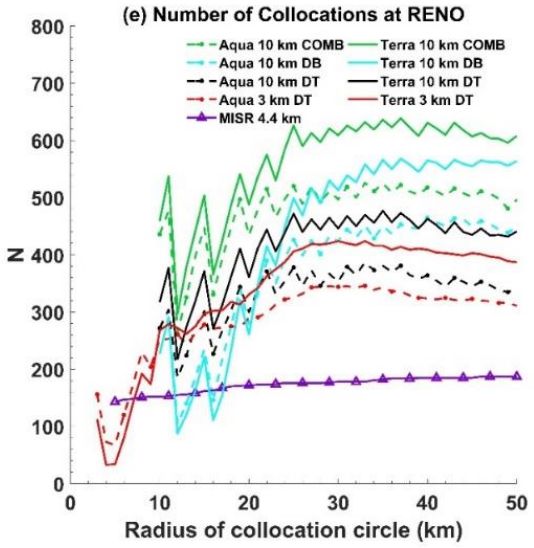

Note. AOD comparisons are made at 550 nm. EE indicates the satellite AOD product expected error envelope.

4.4 Comparison of MISR and MODIS AOD Overall Performance

Collocations are performed utilizing estimates of the 'optimal' spatio-temporal window for each product and site (Sections 4.1-4.3). The overall performance of each MODIS and MISR AOD product is evaluated and results are presented in Table 2.

All satellite AOD products, with exception of DB's large slope underestimation and (to smaller extent) negative mean AOD bias, perform well at APP. The poorer performance of DB at APP is not surprising given the dark, green deciduous forest canopy dominating the region surrounding APP. For the most part, the other satellite AOD products demonstrate a larger dependence on instrument (primarily MODIS Aqua DT versus Terra DT) than on product algorithm or spatial resolution. The nearly identical statistical metrics between the MODIS combined products and DT products indicate that the combined product nearly always selects the DT data. None of the MODIS DT Terra products demonstrate a non-zero mean bias, while those for Aqua are -0.02. The Terra DT-Aqua DT difference is similar to the more positive Terra AOD bias of ~0.03 (relative to that of Aqua) reported for both the MODIS 10 km DT product and 3 km product (Gupta et al., 2018). The Terra DT products also have a greater percentage of collocations lying within the expected error envelope (EE) than Aqua. The percentage of collocations below the EE for all Aqua DT products is greater than the percentage above the EE (underestimation of AOD), while the Terra DT products are more evenly distributed above and below the expected error envelope. Contrary to other studies (Gupta et al., 2018), the MODIS DT 3 km product performs as well as the DT 10 km product at APP. This suggests no sacrifice in accuracy by using the higher-resolution MODIS DT 3 km product at APP. Both the MODIS 10 km and 3 km DT products also perform as well as MISR, with a sampling factor of 3 to 4 times greater based on the number of collocations.

Table 2

Overall Performance of Satellite Retrievals Relative to Ground Truth by Site

Site	Product	Slope	Int[a]	N	r	%<EE[b]	%EE[c]	%>EE[d]	RMSE	Mean Bias
APP	MISR	0.97	0.02	84	0.88	0.0	95.2	4.8	0.03	0.02
APP	Terra COMB	1.20	-0.01	305	0.90	4.6	90.8	4.6	0.04	0.00
APP	Aqua COMB	1.21	-0.03	236	0.90	13.6	84.7	1.7	0.04	-0.02
APP	Terra DB	0.58	0.00	323	0.87	8.0	91.6	0.3	0.04	-0.03
APP	Aqua DB	0.54	0.00	321	0.87	7.8	92.2	0.0	0.04	-0.03
APP	Terra DT 10	1.21	-0.02	308	0.90	5.5	89.9	4.5	0.04	0.00
APP	Aqua DT 10	1.22	-0.04	242	0.89	16.1	82.2	1.7	0.04	-0.02
APP	Terra DT 3	1.24	-0.01	349	0.87	4.0	91.4	4.6	0.04	0.00
APP	Aqua DT 3	1.32	-0.04	324	0.90	11.1	86.7	2.2	0.04	-0.02
WB	MISR	0.83	0.03	100	0.97	3.0	92.0	5.0	0.04	0.01
WB	Terra COMB	1.11	-0.01	347	0.97	3.5	89.3	7.2	0.05	0.01
WB	Aqua COMB	1.24	-0.05	203	0.97	15.3	80.8	3.9	0.06	-0.01
WB	Terra DB	0.85	0.02	426	0.96	1.9	95.3	2.8	0.04	-0.01
WB	Aqua DB	0.90	0.00	274	0.94	1.5	97.8	0.7	0.03	-0.01
WB	Terra DT 10	1.11	-0.01	347	0.97	3.5	89.3	7.2	0.05	0.01
WB	Aqua DT 10	1.25	-0.05	204	0.97	16.2	79.9	3.9	0.06	-0.02
WB	Terra DT 3	1.11	-0.01	322	0.97	1.6	91.3	7.1	0.05	0.01
WB	Aqua DT 3	1.24	-0.05	196	0.97	17.3	81.1	1.5	0.06	-0.02
SPL	MISR	0.83	0.04	108	0.82	0.9	79.6	19.4	0.04	0.03
SPL	Terra COMB	1.15	0.02	487	0.89	0.2	77.8	22.0	0.05	0.03
SPL	Aqua COMB	1.15	-0.01	203	0.88	2.5	91.1	6.4	0.04	0.00
SPL	Terra DB	0.45	0.00	429	0.71	12.8	85.8	1.4	0.06	-0.03

Site	Product	Slope	Int[a]	N	r	%<EE[b]	%EE[c]	%>EE[d]	RMSE	Mean Bias
SPL	Aqua DB	0.32	0.01	200	0.65	9.0	91.0	0.0	0.04	-0.02
SPL	Terra DT 10	1.16	0.02	490	0.88	0.4	78.0	21.6	0.05	0.03
SPL	Aqua DT 10	1.17	-0.01	207	0.87	6.8	87.0	6.3	0.04	0.00
SPL	Terra DT 3	1.19	0.03	471	0.91	0.0	75.2	24.8	0.06	0.04
SPL	Aqua DT 3	1.21	0.00	228	0.87	0.0	89.5	10.5	0.05	0.01
RENO	MISR	0.56	0.05	155	0.92	0.6	81.3	18.1	0.07	0.02
RENO	Terra COMB	0.84	0.04	609	0.88	0.8	73.1	26.1	0.06	0.03
RENO	Aqua COMB	1.05	0.02	497	0.89	1.2	84.1	14.7	0.05	0.02
RENO	Terra DB	0.83	-0.02	513	0.90	15.0	84.4	0.6	0.06	-0.03
RENO	Aqua DB	1.06	-0.02	424	0.79	9.9	89.4	0.7	0.06	-0.02
RENO	Terra DT 10	0.76	0.11	446	0.78	0.2	27.8	72.0	0.11	0.10
RENO	Aqua DT 10	1.11	0.07	353	0.88	0.0	29.2	70.8	0.09	0.08
RENO	Terra DT 3	1.16	0.18	272	0.88	0.0	1.1	98.9	0.21	0.19
RENO	Aqua DT 3	1.37	0.12	261	0.89	0.0	4.6	95.4	0.16	0.15

[a]Intercept

[b]Percent of collocations below the EE.

[c]Percent of collocations within the EE.

[d]Percent of collocations above the EE.

Every satellite product tested demonstrated excellent agreement with ground truth at WB, and the overall results are comparable to those at APP. The correlation coefficients for all products are 0.94 or greater, the highest of any site. Although the MODIS DB products' slopes are still below unity, they are closer than those observed at APP despite the similar surface spectral properties. The sampling frequency for MODIS Terra is generally higher than Aqua at WB, and often higher relative

to Terra at APP. In contrast, the number of collocations for MODIS Aqua at WB is lower than that of APP, particularly for the DT 3 km product. This could be due to more cloudiness during afternoon overpass times at WB than at APP. Similar to APP, the RMS error is highest for MODIS Aqua DT (0.06). The mean AOD bias for the Terra DT products is about 0.03 more positive relative to Aqua (0.01 versus -0.02, respectively), as seen in other studies (Gupta et al., 2018). The results for MODIS combined products are again nearly identical those for the 10 km DT product. The Aqua DT products tend to have more collocations below the EE than above the EE, in contrast to the Terra DT products. The MODIS 3 km products perform as well as the 10 km products, suggesting that again the higher resolution products may be used without compromising on agreement relative to the 10 km products. The results for MISR are like those at APP, although slope is lower, and more collocations fall below the EE.

Despite the larger spatial variability in surface properties (Figure 12) and mean AOD bias (Figure 14) the spatio-temporally optimized collocation results for SPL are, in a broad sense, similar to those for the two Eastern U.S. sites, particularly APP. The MODIS DT products perform well, but we note that there are significantly more DT collocations above the EE at SPL relative to APP and WB, particularly for Terra. The mean AOD bias for Terra DT is 0.03 to 0.04, and between -0.01 and 0.01 for Aqua DT, maintaining the tendency of Terra's positive bias relative to Aqua. The similar performance of MODIS DT 10 km and 3 km products also follows that of APP and WB. The MODIS DB products at SPL have small negative mean AOD biases (-0.03 for Terra and -0.02 for Aqua) and are poorly correlated with MFRSR-measured AOD. The difference in collocation frequency between Terra and Aqua is the greatest at SPL, with Terra generating approximately twice the number of collocations relative to Aqua. MISR-sunphotometer AOD agreement at SPL is comparable to that of Terra DT and is slightly worse than at the eastern U.S. mountain sites, namely (1) a slightly more positive mean AOD bias (0.03); (2) higher percentage of collocations above the expected error envelope (19.4%); and (3) slightly lower correlation (0.82).

Unlike the other three sites, the collocation results for Reno exhibit a strong dependence on instrument, resolution, and algorithm. The MODIS DT 3 km products at Reno are characterized by large mean biases, RMS errors, intercepts, slopes, and possess greater than 95% of the data points above the expected error envelope; the 3 km products are not viable at Reno. The Aqua and Terra DT 10 km products also have ~70% of the collocations falling above the EE and an average mean bias of 0.09. The modestly better performance of the 10 km DT product (relative to 3 km) is likely influenced by a larger collocation radius, which includes pixels from the more vegetated region west of Reno, where the mean DT AOD biases are less positive (Figure 18). Although neither of the 10 km and 3 km DT products are suitable for Reno based on these results, Aqua does outperform Terra in all metrics except number of collocations and percent within the EE. Considering the bright, sparsely vegetated surfaces at Reno (Figure 15), these poor results from the DT algorithm are expected. While the MISR and MODIS DB appear to perform comparably well at Reno (Table 2), this could be due to the larger collocation radius used by the coarser-resolution DB product. Like the other sites, the mean AOD biases for both Terra and Aqua DB are small and negative (-0.03 and -0.02, respectively). Terra DB is also well-correlated with AERONET, while Aqua DB's correlation is somewhat weaker. However, nearly all the DB collocations are from pixels further than 12 km from Reno AERONET site (Figure 18), whereas MISR is able to sample above the urban / desert terrain at / near the AERONET site. The mean MISR AOD bias at Reno (~0.02) and correlation (0.92) are comparable to that at the other three sites, indicating that MISR is able accurately retrieve AOD over various types of heterogeneous U.S. mountain terrain. The MISR RMSE at Reno (0.07), regression slope (0.56), and percentage of collocations lying within MISR EE envelope (~81%) are worse than at the eastern U.S. mountain sites and the AOD for nearly all MISR collocations lying outside of EE is high. The low MISR slope could be impacted by the low AOD at Reno for most of the collocations. The MODIS Aqua COMBINED product outperforms Terra at Reno and is comparable to that of MISR for most statistical measurables (Table 2). This illustrates that while DT and possibly DB are not suitable for retrieving AOD at / near Reno, their combined product is.

4.5 Seasonal Dependence of MISR and MODIS AOD Performance

The satellite-sunphotometer collocation results are stratified by season, with the months May through September corresponding to the warm or summer season, and the months November through March the cold (winter) season, and April and October as transitional months. The winter results are presented in Table 3, while the summer results are in Table 4 below.

Table 3

Winter (Nov-Mar) AOD Collocation Results for the Four Mountainous Sites

Site	Product	Slope	Int[a]	N	r	%<EE[b]	%EE[c]	%>EE[d]	RMSE	Mean Bias
APP	MISR	0.90	0.02	44	0.83	0.0	97.7	2.3	0.03	0.01
APP	Terra COMB	0.99	-0.01	104	0.78	8.7	90.4	1.0	0.03	-0.01
APP	Aqua COMB	1.00	-0.04	66	0.81	30.3	69.7	0.0	0.05	-0.04
APP	Terra DB	0.40	0.01	132	0.77	3.8	96.2	0.0	0.03	-0.02
APP	Aqua DB	0.40	0.01	153	0.74	4.6	95.4	0.0	0.03	-0.02
APP	Terra DT 10	0.98	-0.01	105	0.76	9.5	89.5	1.0	0.03	-0.01
APP	Aqua DT 10	0.98	-0.05	72	0.76	37.5	62.5	0.0	0.06	-0.05
APP	Terra DT 3	0.95	-0.01	118	0.71	7.6	91.5	0.8	0.03	-0.01
APP	Aqua DT 3	1.00	-0.04	124	0.78	20.2	79.8	0.0	0.05	-0.04
WB	MISR	0.96	0.01	37	0.90	0.0	97.3	2.7	0.02	0.01
WB	Terra COMB	0.94	-0.02	129	0.79	8.5	90.7	0.8	0.04	-0.03
WB	Aqua COMB	0.91	-0.04	81	0.82	33.3	66.7	0.0	0.06	-0.05
WB	Terra DB	0.96	0.01	167	0.87	0.0	97.6	2.4	0.02	0.00
WB	Aqua DB	0.91	0.00	145	0.87	0.7	99.3	0.0	0.02	-0.01
WB	Terra DT 10	0.94	-0.02	129	0.79	8.5	90.7	0.8	0.04	-0.03
WB	Aqua DT 10	0.92	-0.04	82	0.82	34.1	65.9	0.0	0.06	-0.05
WB	Terra DT 3	0.98	-0.02	118	0.78	3.4	95.8	0.8	0.04	-0.03
WB	Aqua DT 3	0.89	-0.04	100	0.80	30.0	70.0	0.0	0.06	-0.05
SPL	MISR	0.64	0.02	7	0.61	0.0	100.0	0.0	0.01	0.01
SPL	Terra COMB	-0.65	0.03	9	-0.30	0.0	100.0	0.0	0.03	-0.01
SPL	Aqua COMB	0.34	-0.02	3	0.64	33.3	66.7	0.0	0.05	-0.05
SPL	Terra DB	0.09	0.02	16	0.26	0.0	100.0	0.0	0.01	0.00

Site	Product	Slope	Int[a]	N	r	%<EE[b]	%EE[c]	%>EE[d]	RMSE	Mean Bias
SPL	Aqua DB	0.05	0.02	8	0.27	0.0	100.0	0.0	0.03	-0.02
SPL	Terra DT 10	-0.64	0.03	9	-0.29	0.0	100.0	0.0	0.03	-0.01
SPL	Aqua DT 10	-	-	0	-	-	-	-	-	-
SPL	Terra DT 3	0.74	-0.01	4	0.83	0.0	100.0	0.0	0.01	-0.01
SPL	Aqua DT 3	-	-	0	-	-	-	-	-	-
RENO	MISR	0.60	0.03	24	0.61	0.0	91.7	8.3	0.02	0.01
RENO	Terra COMB	-0.15	0.05	55	-0.11	1.8	81.8	16.4	0.04	0.01
RENO	Aqua COMB	-0.03	0.04	53	-0.02	1.9	94.3	3.8	0.03	0.01
RENO	Terra DB	0.00	0.03	53	0.00	1.9	98.1	0.0	0.03	-0.01
RENO	Aqua DB	0.04	0.02	55	0.16	1.8	98.2	0.0	0.02	-0.01
RENO	Terra DT 10	1.07	0.10	20	0.33	0.0	10.0	90.0	0.11	0.11
RENO	Aqua DT 10	1.82	0.05	17	0.76	0.0	23.5	76.5	0.08	0.08
RENO	Terra DT 3	1.35	0.15	30	0.38	0.0	0.0	100.0	0.16	0.16
RENO	Aqua DT 3	2.38	0.07	25	0.61	0.0	12.0	88.0	0.12	0.11

[a]Intercept.

[b]Percent of collocations below the EE.

[c]Percent of collocations within the EE.

[d]Percent of collocations above the EE.

Table 4

Summer (May-Sept) AOD Collocation Results for the Four Mountainous Sites

Site	Product	Slope	Int[a]	N	r	%<EE[b]	%EE[c]	%>EE[d]	RMSE	Mean Bias
APP	MISR	0.82	0.04	18	0.75	0.0	83.3	16.7	0.05	0.02
APP	Terra COMB	1.15	0.00	120	0.91	0.8	90.8	8.3	0.04	0.02
APP	Aqua COMB	1.15	-0.01	95	0.93	2.1	93.7	4.2	0.04	0.00
APP	Terra DB	0.66	-0.01	98	0.89	17.3	81.6	1.0	0.05	-0.04
APP	Aqua DB	0.61	-0.01	76	0.91	21.1	78.9	0.0	0.06	-0.04
APP	Terra DT 10	1.16	0.00	121	0.91	1.7	90.1	8.3	0.04	0.02
APP	Aqua DT 10	1.15	-0.01	95	0.93	2.1	93.7	4.2	0.04	0.00
APP	Terra DT 3	1.20	0.00	132	0.87	1.5	88.6	9.8	0.05	0.02
APP	Aqua DT 3	1.28	-0.02	108	0.92	1.9	91.7	6.5	0.05	0.01
WB	MISR	0.78	0.05	43	0.97	7.0	86.0	7.0	0.05	0.00
WB	Terra COMB	1.01	0.04	142	0.97	0.0	85.9	14.1	0.06	0.04
WB	Aqua COMB	1.19	-0.02	70	0.97	0.0	91.4	8.6	0.06	0.02
WB	Terra DB	0.81	0.03	163	0.96	3.7	92.0	4.3	0.06	-0.01
WB	Aqua DB	0.86	0.01	66	0.93	3.0	93.9	3.0	0.05	-0.01
WB	Terra DT 10	1.01	0.04	142	0.97	0.0	85.9	14.1	0.06	0.04
WB	Aqua DT 10	1.19	-0.02	70	0.97	0.0	91.4	8.6	0.06	0.02
WB	Terra DT 3	1.01	0.04	129	0.97	0.0	85.3	14.7	0.07	0.04
WB	Aqua DT 3	1.18	-0.02	53	0.98	0.0	94.3	5.7	0.06	0.02
SPL	MISR	0.77	0.05	90	0.80	1.1	75.6	23.3	0.05	0.03
SPL	Terra COMB	1.12	0.02	433	0.89	0.0	75.5	24.5	0.05	0.03
SPL	Aqua COMB	1.12	0.00	179	0.88	1.1	91.6	7.3	0.04	0.00
SPL	Terra DB	0.47	0.00	347	0.72	15.6	82.7	1.7	0.06	-0.04

Site	Product	Slope	Int[a]	N	r	%<EE[b]	%EE[c]	%>EE[d]	RMSE	Mean Bias
SPL	Aqua DB	0.35	0.01	154	0.67	10.4	89.6	0.0	0.04	-0.03
SPL	Terra DT 10	1.12	0.02	434	0.88	0.2	75.6	24.2	0.05	0.03
SPL	Aqua DT 10	1.13	-0.01	182	0.88	3.3	89.6	7.1	0.04	0.00
SPL	Terra DT 3	1.17	0.03	425	0.91	0.0	72.5	27.5	0.06	0.04
SPL	Aqua DT 3	1.17	0.01	201	0.87	0.0	88.1	11.9	0.05	0.02
RENO	MISR	0.54	0.06	98	0.94	1.0	76.5	22.4	0.09	0.02
RENO	Terra COMB	0.84	0.05	435	0.90	0.7	71.0	28.3	0.07	0.04
RENO	Aqua COMB	1.05	0.02	330	0.90	0.6	79.4	20.0	0.05	0.03
RENO	Terra DB	0.85	-0.02	353	0.91	19.5	79.9	0.6	0.07	-0.04
RENO	Aqua DB	1.12	-0.03	263	0.81	12.5	86.3	1.1	0.08	-0.02
RENO	Terra DT 10	0.76	0.11	354	0.79	0.3	31.9	67.8	0.12	0.10
RENO	Aqua DT 10	1.09	0.08	271	0.89	0.0	26.2	73.8	0.09	0.08
RENO	Terra DT 3	1.13	0.19	180	0.89	0.0	1.1	98.9	0.22	0.20
RENO	Aqua DT 3	1.31	0.13	182	0.90	0.0	0.5	99.5	0.17	0.16

[a]Intercept.

[b]Percent of collocations below the EE.

[c]Percent of collocations within the EE.

[d]Percent of collocations above the EE.

While the winter / summer differences in Terra DT performance at APP are small, the seasonal differences are larger for Aqua DT, which performs better in summer. Both MODIS DT products (Terra and Aqua) at APP have a winter mean AOD bias that is more negative by 0.03-0.05 than during summer, where the mean biases are slightly positive (~0.02) for Terra and close to zero for Aqua. The winter mean Aqua AOD biases are -0.05 (-0.04) for the 10 km (3 km) DT product. The

percentage of Aqua DT retrievals within EE and correlation with AERONET AOD are also much lower in winter than summer. Those DT retrievals lying outside EE are nearly always too low in winter and usually too high in summer. The 3 km and 10 km DT products perform similarly to one another, in both winter and in summer. The Terra and Aqua DB AOD products also perform similarly to one another in both winter and summer at APP, with both exhibiting more negative mean AOD bias in summer (-0.04) than in winter (-0.02) and higher summer RMSE (likely due to higher AOD). However, the linear regression parameters (slope, correlation) are better in summer than in winter, albeit still poor. Nearly all the DB collocations with AOD lying outside of EE are low. MISR performs slightly better in winter than summer for all statistical indicators at APP. In contrast to DB, all of MISR retrievals outside EE are high, although there is a small sample size, particularly in summer.

The MODIS DT product performance at WB is very similar to that at APP. with higher correlation in summer and (for Aqua) larger percent within EE. All of the MODIS DT products at WB have small positive mean AOD biases in summer and negative biases in winter, with the mean winter bias more negative by 0.07 than during summer and the Terra DT bias always 0.02 more positive than that of Aqua DT. Similar to APP, the percentage within EE was low for Aqua DT during winter. Nearly all of the Aqua and Terra DT retrievals lying outside of EE are too high in summer and too low in winter. MODIS DB performs well during both summer in winter, with mean AOD bias close to zero for Aqua and Terra DB, along with slopes slightly below 1, high correlation, and over 90% of collocations lying within EE. The lone difference is a larger RMSE in summer than winter for both Aqua and Terra (0.06 versus 0.02), likely due to much higher AOD in summer than in winter. MISR performs well during both summer and winter, with mean AOD biases close to zero, high correlation with AERONET. MISR does have a higher percent of retrievals within the EE and lower RMSE in winter due to lower AOD.

The results for the western U.S. sites (SPL and Reno) are much worse in winter than for the eastern sites. The minimal number of winter collocations at SPL precludes any summer / winter

comparisons. Although the summer / winter discrepancy in number of retrievals at Reno is not as large as at SPL, there are still roughly 4 times more MISR summer retrievals than winter retrievals and at least 5 times more during summer than during winter for MODIS products. MISR possesses a very small positive mean bias in both summer (0.02) and winter (0.01). The RMSE for MISR is 4.5 times larger in summer than in winter (0.09 versus 0.02) and is larger than mean AERONET AOD itself except for August. The percentage of MISR retrievals within EE is higher in winter than summer (91.7% versus 76.5%) but MISR AOD is more correlated with AERONET in summer (0.94 versus 0.61). All MODIS AOD products at Reno are much more correlated with AERONET during summer than winter, with the largest seasonal differences for the COMBINED products (Terra: 0.90 versus -0.11; Aqua: 0.90 versus -0.02) followed by DB (Terra: 0.91 versus 0.00; Aqua: 0.81 versus 0.16). This seems to indicate that the lower RMSE and mean AOD biases in winter at Reno are influenced by lower AOD. We also note the large mean bias present in all Reno DT products year-round, especially at the 3 km resolution.

Chapter 5: Conclusions, Limitations, and Future Work

The following sections draw conclusions from the results presented in Chapter 4, highlight the known assumptions and limitations of the study, and suggest directions that future work might take to build upon this effort.

5.1 Conclusions

Multi-year data of AOD retrieved by MODIS and MISR instruments above four mountainous U.S. sites were collocated with 'ground-truth' AOD measured by sunphotometers at the sites. The primary objectives of this study are to (1) examine the influence of spatial and temporal variability in aerosol and surface properties and topography on satellite / sunphotometer AOD agreement; (2) apply and assess an automated method for optimizing collocation window and radius, in the context of variability in surface properties; and (3) compare the performance of satellite AOD products above the four sites, and examine factors influencing their performance (season, surface properties, etc.). The AOD at the sites is for the most part sufficiently low (< 0.15 at 550 nm) that satellite-retrieved AOD is primarily influenced by surface model assumptions used by the satellite retrieval algorithms.

With the exception of afternoons at SPL, the lack of temporal aerosol variability at the sites near satellite overpass hours leads to insensitivity of satellite / sunphotometer collocations to temporal window sizes of up to ~1-2 hours. The lack of temporal variability likely also implies a fair degree of spatial aerosol homogeneity near the sites. Spatial aerosol homogeneity over a pixel is assumed by the satellite AOD retrieval algorithms and must be examined to properly select an optimal satellite / sunphotometer AOD collocation radius.

The land cover type and NDVI near the heavily forested eastern U.S. mountainous sites (APP and WB) is more uniform than that near the western U.S. sites, leading to spatial variability in mean satellite / sunphotometer AOD differences over 50 km radius circular regions centered at ground sites that are less influenced by surface heterogeneities and more so by elevation differences and higher satellite-measured AOD near urban areas. The MISR and MODIS DB products have relatively small and fairly uniform mean AOD biases (with respect to AERONET) for regions within ~12-20 km of

each site, which avoid the urban pockets and large elevation changes, although small river bodies are still included near WB. The mean AOD bias for MODIS DT 3 km product (and to lesser degree DT 10 km) is more sensitive than those of MODIS DB and MISR to water bodies and suburban terrain near WB. As such, AERONET collocations with MISR or DB should be representative of the ground sites and relatively insensitive to the choice of spatial collocation radius for less than ~20 km while AERONET-DT collocations may be more sensitive to collocation radius at WB, especially for r > 12 km.

All satellite products have small mean AOD biases (relative to ground-truth measurements) above the heavily vegetated APP and WB sites, with magnitudes less than ~0.03-0.04 over the 10-15 km radius circle centered at each ground site. The small mean biases indicate that the surface models and aerosol models lead to AOD that agrees well with AERONET for these sites. While MODIS DT has retrieval gaps for urban and river areas near WB, the MISR and MODIS DB products retrieve over both land cover types. The superior ability of the higher resolution MODIS DT 3 km products to retrieve AOD in heterogeneous terrain (e.g. near small urban areas and rivers near WB) is clearly evident in Figures 10-11 and the mean AOD bias is no higher for DT 3 km than for DT 10 km.

The large spatial heterogeneity in landcover type, NDVI, and (especially at SPL) elevation in the region surrounding the western U.S. mountain sites (SPL and Reno) complicates satellite / sunphotometer collocations in several ways. The heterogeneities result in spatial gaps in collocations at / near each site which usually differ for the various satellite products. These sampling gaps can influence the satellite evaluations if collocation radius is not carefully selected. MODIS products often have gaps over sparsely vegetated (NDVI less than ~0.20) desert terrain. MODIS DB and DT both have gaps over urban surfaces at / near the Reno AERONET site. MISR is able to retrieve over all surface types but does have a gap to the south of SPL site, most likely due to sharp surface elevation gradients.

While the mean satellite-sunphotometer AOD differences at / near the western U.S. sites exhibit less spatial variability for DB, those for DT (and to lesser extent, MISR) follow the spatial

variability in landcover type and NDVI. Mean MODIS DT-sunphotometer AOD differences are most positive over densely vegetated evergreen forests near SPL (NDVI > 0.60) and over sparsely-vegetated desert terrain (NDVI less than ~0.20-0.30) near Reno, with the smallest differences for moderately vegetated terrain (~0.40-0.60) near both sites. Similar to the eastern U.S. sites, the positive bias for Terra DT is ~0.03 higher than for Aqua DT for most landcover types in the regions. The mean MISR-sunphotometer AOD differences are close to zero for NDVI greater than ~0.40 and the differences become increasingly positive over lower NDVI areas, reaching values close to ~0.06 over desert terrain at / near Reno.

An automated algorithm was developed to optimize the temporal window and collocation radius for satellite-based retrievals over the four mountainous U.S. ground sites. The algorithm finds the window and radius which optimize statistical outputs of the satellite / sunphotometer collocations. The relative insensitivity of the statistical outputs of satellite / sunphotometer collocations to temporal window size for all sites is consistent with the lack of diurnal AOD variability near satellite overpass hours at the sites, which in turn likely indicates some degree of spatial aerosol homogeneity near the sites. The statistical outputs of the collocations are relatively insensitive to collocation radius at the eastern U.S. mountain sites (APP and WB) for radii which avoided urban terrain. The algorithm was not as successful at optimizing collocation radius at the more topographically diverse western U.S. mountain sites, especially at Reno. Sampling gaps for all AOD products except MISR at / near the Reno site result in disproportionally large influence on satellite-sunphotometer agreement from pixels further away from the site, where the landcover and satellite AOD bias are not representative of Reno site. The inclusion of these non-representative pixels resulted in ‘improved’ agreement for MODIS DT and DB. The algorithm in its current form is thus inadequate for optimizing collocation radius at these topographically complex sites and ancillary information, such as maps of NDVI, surface type, and mean satellite AOD bias are necessary.

Using the optimized temporal window and collocation radius for each satellite AOD product and site, we compare the performance of the satellite AOD products at each site, both overall and

stratified by season (winter versus summer). The eastern U.S. sites (APP and WB) have comparable numbers of collocations during summer and winter while the number of winter collocations at western U.S. sites (SPL and Reno) is minimal, especially at SPL. As expected, MODIS DT products significantly over-estimate AOD over the desert Reno site, with large mean AOD biases and a large majority of AOD retrievals lying above the EE envelope. The reasonably good regression slopes and correlation with AERONET in summer suggest that the bias is somewhat insensitive to AOD (i.e. an offset) and could be due to over-estimation of the surface contribution to the top-of-atmosphere radiance. The performance of DT at the other sites is rather consistent, where both Terra and Aqua tend to over-estimate AOD by small amounts (0.00-0.04) during summer and under-estimate during the winter (at least at APP and WB). While Aqua DT performs at least as well as Terra during summer, the winter AOD under-estimation is larger for Aqua DT whose mean AOD bias is roughly -0.05 during winter. Terra DT AOD (both 3 km and 10 km) is more positive than that of Aqua DT by ~0.02-0.04 at for all sites / seasons, which is similar to that reported in global evaluations of DT (Gupta et al., 2018). While Gupta et al. (2018) reported better agreement with AERONET for the coarser-resolution 10 km DT product, we find comparable performance between the two products at APP, WB, and SPL sites, which implies that the higher-resolution 3 km product can be used without sacrificing performance.

MODIS DB tends to under-estimate AOD by small amounts (up to ~0.04) at APP, SPL, and Reno, with smaller under-estimates (~0.01) at WB. The Terra / Aqua differences are typically smaller for DB than for DT. The use of the MODIS COMBINED product improves upon the performance of DB and DT at Reno and is close to the performance of MISR. The contribution to the COMBINED product at the other sites is almost exclusively from DT so there is less utility in the COMBINED product at these sites. The ability of MISR to retrieve over nearly all types of landcover likely contributes to its excellent agreement with sunphotometer-measured AOD at all sites, albeit somewhat better at the less topographically challenging eastern U.S. sites. The major disadvantage of MISR is fewer AOD retrievals than MODIS.

5.2 Limitations

It is important to mention some of the assumptions and limitations used in the preceding analysis. Aside from scanning the U.S. Energy Information Administration's state maps for power plants, little information has been gathered regarding the aerosol sources at the sites in this study. There are undoubtedly some anthropogenic sources near the sites, such as in the cities of Reno, NV and Knoxville, TN, however little is assumed regarding natural sources except that the western sites will likely see significant dust from the surrounding arid region in addition to seasonal fire events.

Furthermore, no knowledge of the vertical distribution of aerosols is presented for the sites; any aerosol plumes measured may be either local or long-range transport. It is possible that some of the surface-based measurements are only indicative of the column at that location, and satellite-retrieved AOD is accurate over nearby pixels reported as biased which do not contain the same aerosol as that sampled at the ground station. This has a significant potential to occur where the topography creates natural barriers to aerosol transport. Sub-pixel horizontal aerosol homogeneity is assumed by the satellite retrieval algorithms, yet no measurements of the horizontal distribution of aerosols are available to back this claim. No knowledge of the dominant wind and weather patterns at the sites accounted for, which may alter the transportation and deposition of aerosols.

It has been assumed that the land cover has not changed significantly since 2004, which may not be true for all sites. The January and June NDVI maps were also taken from the year 2004, so they may not be accurate given that climate change, changes in land use, and human population growth have inevitably altered the landscape. An interannual average for each site is recommended for any future work.

5.3 Future Work

This study shows that there is an opportunity for improvement when performing aerosol retrievals over arid, mountainous regions. It is the author's desire that future students and scientists take up this endeavor, as it supports the critical understanding of the Earth's changing environment. Following are several areas upon which this work may be improved and / or built-upon.

First, a detailed study of the relationship between satellite agreement with ground truth as a function of per-pixel NDVI could be performed. In such a project, the full-resolution NDVI files for the entire study period would be needed, and the collocation algorithm would then match each satellite pixel with an averaged (or interpolated) NDVI value for each collocation. This would necessitate that all pixels are returned for each collocation, as is done to create the AOD bias maps in chapter 4 above. Alternatively, rather than just matching the per-pixel NDVI, a filter could be used to only include high or low NDVI pixels in the spatial average for each collocation. Similarly, filters could be made for IGBP land cover type or elevation.

In this study, satellite-sunphotometer agreement was analyzed over regions that are topographically complex and / or possess heterogeneous surface properties. Future work may benefit from placing these results in the context of satellite-sunphotometer collocations over flat, homogeneous regions where retrievals are expected to perform well. This approach could assist in identifying surface properties and other parameters influencing satellite-sunphotometer agreement.

There are many SDS fields available within the satellite data files, and one area to explore further would be the effects of the satellite viewing geometry on the agreement, such as glint angle, scattering angle, etc. In-situ and remote sensing measurements could also be used to constrain MISR aerosol type, which was one of the objectives of the original form of this thesis. MISR results may also benefit from the use of the “legacy aerosol retrieval success flag per mixture” SDS as a proxy for a QA flag during the collocation process.

Finally, geostationary satellites equipped to perform aerosol retrievals could provide additional collocations with ground-truth instrumentation relative to polar-orbiting satellites, since there would be no “dead time” between overpasses for each site. The spatial distribution of aerosols over time could be estimated with much greater temporal precision. However, such a system would need careful engineering to achieve the same (or better) spatial resolution as polar-orbiting platforms. Global coverage would also not be possible without a network of geostationary satellites.

Bibliography

Ackerman, A. S. (2000). Reduction of tropical cloudiness by soot. *Science*, *288*(5468), 1042–1047. https://doi.org/10.1126/science.288.5468.1042

Albrecht, B. A. (1989). Aerosols, cloud microphysics, and fractional cloudiness. *Science*, *245*(4923), 1227–1230. https://doi.org/10.1126/science.245.4923.1227

Alexandrov, M. D., Lacis, A. A., Carlson, B. E., & Cairns, B. (2008). Characterization of atmospheric aerosols using MFRSR measurements. *Journal of Geophysical Research*, *113*(D8), 38. https://doi.org/10.1029/2007JD009388

Bodhaine, B. A., Wood, N. B., Dutton, E. G., & Slusser, J. R. (1999). On Rayleigh optical depth calculations. *Journal of Atmospheric and Oceanic Technology*, *16*(11), 1854–1861. https://doi.org/10.1175/1520-0426(1999)016%3C1854:ORODC%3E2.0.CO;2

Chu, D. A., Kaufman, Y. J., Zibordi, G., Chern, J. D., Mao, J., Li, C., & Holben, B. N. (2003). Global monitoring of air pollution over land from the Earth Observing System-Terra Moderate Resolution Imaging Spectroradiometer (MODIS). *Journal of Geophysical Research*, *108*(D21), 32,141. https://doi.org/10.1029/2002JD003179

Didan, K. (2015). *MOD13Q1 MODIS/Terra vegetation indices 16-Day L3 global 250m SIN grid* (V006) [Data set]. NASA EOSDIS Land Processes DAAC. https://doi.org/10.5067/MODIS/MOD13Q1.006

Dubovik, O., Holben, B. N., Lapyonok, T., Sinyuk, A., Mishchenko, M. I., Yang, P., & Slutsker, I. (2002). Non-spherical aerosol retrieval method employing light scattering by spheroids. *Geophysical Research Letters*, *29*(10), 54-1-54-4. https://doi.org/10.1029/2001GL014506

Dubovik, O., Smirnov, A., Holben, B. N., King, M. D., Kaufman, Y. J., Eck, T. F., & Slutsker, I. (2000). Accuracy assessments of aerosol optical properties retrieved from Aerosol Robotic Network (AERONET) Sun and sky radiance measurements. *Journal of Geophysical Research*, *105*(D8), 9791–9806. https://doi.org/10.1029/2000JD900040

Eck, T. F., Holben, B. N., Reid, J. S., Dubovik, O., Smirnov, A., & O'Neill, N. T., Slutsker, I., & Kinne, S. (1999). Wavelength dependence of the optical depth of biomass burning, urban, and desert dust aerosols. *Journal of Geophysical Research*, *104*(D24), 31333–31349. https://doi.org/10.1029/1999JD900923

Friedl, M., & Sulla-Menashe, D. (2019). *MCD12Q1 MODIS/Terra+Aqua land cover type yearly L3 global 500m SIN grid* (V006) [Data set]. NASA EOSDIS Land Processes DAAC. https://doi.org/10.5067/MODIS/MCD12Q1.006

Garay, M. J., Kalashnikova, O. V., & Bull, M. A. (2017). Development and assessment of a higher-spatial-resolution (4.4 km) MISR aerosol optical depth product using AERONET-DRAGON data. *Atmospheric Chemistry and Physics*, *17*(8), 5095–5106. https://doi.org/10.5194/acp-17-5095-2017

Goldstein, A. H., Koven, C. D., Heald, C. L., & Fung, I. Y. (2009). Biogenic carbon and anthropogenic pollutants combine to form a cooling haze over the southeastern United States. *Proceedings of the National Academy of Sciences of the United States of America*, *106*(22), 8835–8840. https://doi.org/10.1073/pnas.0904128106

Gupta, P., Remer, L. A., Levy, R. C., & Mattoo, S. (2018). Validation of MODIS 3km land aerosol optical depth from NASA's EOS Terra and Aqua missions. *Atmospheric Measurement Techniques*, *11*(5), 3145–3159. https://doi.org/10.5194/amt-11-3145-2018

Hallar, A. G., Petersen, R., Andrews, E., Michalsky, J., McCubbin, I. B., & Ogren, J. A. (2015). Contributions of dust and biomass burning to aerosols at a Colorado mountain-top site. *Atmospheric Chemistry and Physics*, *15*(23), 13665–13679. https://doi.org/10.5194/acp-15-13665-2015

Hansen, J. E., Lacis, A. A., Lee, P., & Wang, W.-C. (1980). Climatic effects of atmospheric aerosols. *Annals of the New York Academy of Sciences*, *338*(1), 575–587. https://doi.org/10.1111/j.1749-6632.1980.tb17151.x

Harrison, L., Michalsky, J., & Berndt, J. (1994). Automated multifilter rotating shadow-band radiometer: an instrument for optical depth and radiation measurements. *Applied Optics*, *33*(22), 5118–5125. https://doi.org/10.1364/AO.33.005118

Haywood, J. M., & Shine, K. P. (1995). The effect of anthropogenic sulfate and soot aerosol on the clear sky planetary radiation budget. *Geophysical Research Letters*, *22*(5), 603–606. https://doi.org/10.1029/95GL00075

Holben, B. N., Eck, T. F., & Fraser, R. S. (1991). Temporal and spatial variability of aerosol optical depth in the Sahel region in relation to vegetation remote sensing. *International Journal of Remote Sensing*, *12*(6), 1147–1163. https://doi.org/10.1080/01431169108929719

Holben, B. N., Eck, T.F., Slutsker, I., Tanré, D., Buis, J.P., Setzer, A., Vermote, E., Reagan, J.A., Kaufman, Y.J., Nakajima, T., Lavenu, F., Jankowiak, I., & Smirnov, A. (1998). AERONET – a federated instrument network and data archive for aerosol characterization. *Remote Sensing of Environment*, *66*(1), 1–16. https://doi.org/10.1016/S0034-4257(98)00031-5

Hsu, N. C., Jeong, M.-J., Bettenhausen, C., Sayer, A. M., Hansell, R., Seftor, C. S., Huang, J., & Tsay, S.-C. (2013). Enhanced Deep Blue aerosol retrieval algorithm: The second generation. *Journal of Geophysical Research: Atmospheres*, *118*(16), 9296–9315. https://doi.org/10.1002/jgrd.50712

Huete, A., Justice, C., & van Leeuwen, W. (1999). MODIS vegetation index (MOD13) algorithm theoretical basis document [Unpublished document]. https://modis.gsfc.nasa.gov/data/atbd/atbd_mod13.pdf

Ichoku, C., Chu, D. A., Mattoo, S., Kaufman, Y. J., Remer, L. A., Tanré, D., Slutsker, I., & Holben, B. N. (2002). A spatio-temporal approach for global validation and analysis of MODIS aerosol products, *Geophysical Research Letters*, 29(12), doi:10.1029/2001GL013206

Intergovernmental Panel on Climate Change. (2014). Anthropogenic and natural radiative forcing. In *Climate Change 2013 – The Physical Science Basis: Working Group I Contribution to the Fifth Assessment Report of the Intergovernmental Panel on Climate Change* (pp. 659-740). Cambridge University Press. https://doi.org/10.1017/CBO9781107415324.018

Kahn, R. A. (2012). Reducing the uncertainties in direct aerosol radiative forcing. *Surveys in Geophysics*, *33*(3-4), 701–721. https://doi.org/10.1007/s10712-011-9153-z

Kahn, R. A., & Gaitley, B. J. (2015). An analysis of global aerosol type as retrieved by MISR. *Journal of Geophysical Research: Atmospheres*, *120*(9), 4248–4281. https://doi.org/10.1002/2015JD023322

Kahn, R. A., Gaitley, B. J., Garay, M. J., Diner, D. J., Eck, T. F., Smirnov, A., & Holben, B. N. (2010). Multiangle Imaging SpectroRadiometer global aerosol product assessment by comparison with the Aerosol Robotic Network. *Journal of Geophysical Research*, *115*(D23), 20673. https://doi.org/10.1029/2010JD014601

Kaufman, Y. J., Setzer, A., Ward, D., Tanre, D., Holben, B. N., Menzel, P., Pereira, M. C., & Rasmussen, R (1992). Biomass burning Airborne and Spaceborne Experiment in the Amazonas (BASE-A). *Journal of Geophysical Research*, *97*(D13), 14581. https://doi.org/10.1029/92JD00275

Kaufman, Y. J., Tanré, D., Remer, L. A., Vermote, E. F., Chu, A., & Holben, B. N. (1997). Operational remote sensing of tropospheric aerosol over land from EOS moderate resolution imaging spectroradiometer. *Journal of Geophysical Research*, *102*(D14), 17051–17067. https://doi.org/10.1029/96JD03988

Kovacs, T. (2006). Comparing MODIS and AERONET aerosol optical depth at varying separation distances to assess ground-based validation strategies for spaceborne lidar. *Journal of Geophysical Research*, *111*(D24), D10S07. https://doi.org/10.1029/2006JD007349

Levy, R. C., Mattoo, S., Munchak, L. A., Remer, L. A., Sayer, A. M., Patadia, F., & Hsu, N. C. (2013). The Collection 6 MODIS aerosol products over land and ocean. *Atmospheric Measurement Techniques*, *6*(11), 2989–3034. https://doi.org/10.5194/amt-6-2989-2013

Levy, R. C., Remer, L. A., & Dubovik, O. (2007a). Global aerosol optical properties and application to Moderate Resolution Imaging Spectroradiometer aerosol retrieval over land. *Journal of Geophysical Research*, *112*(D13). https://doi.org/10.1029/2006JD007815

Levy, R. C., Remer, L. A., Kleidman, R. G., Mattoo, S., Ichoku, C., Kahn, R., & Eck, T. F. (2010). Global evaluation of the Collection 5 MODIS dark-target aerosol products over land. *Atmospheric Chemistry and Physics*, *10*(21), 10399–10420. https://doi.org/10.5194/acp-10-10399-2010

Levy, R. C., Remer, L. A., Mattoo, S., Vermote, E. F., & Kaufman, Y. J. (2007b). Second-generation operational algorithm: Retrieval of aerosol properties over land from inversion of Moderate Resolution Imaging Spectroradiometer spectral reflectance. *Journal of Geophysical Research*, *112*(D13). https://doi.org/10.1029/2006JD007811

Levy, R. C., Remer, L. A., Tanre, D., Mattoo, S., & Kaufman, Y. J. (2009). Algorithm for remote sensing of tropospheric aerosol over dark targets from MODIS: Collections 005 and 051 [Unpublished document]. https://modis-atmosphere.gsfc.nasa.gov/sites/default/files/ModAtmo/ATBD_MOD04_C005_rev2_0.pdf

Link, M., Zhou, Y., Taubman, B., Sherman, J., Morrow, H., Krintz, I., Robertson, L., Cook, R., Stocks, J., West, M., & Sive, B. C. (2015). A characterization of volatile organic compounds and secondary organic aerosol at a mountain site in the Southeastern United States. *Journal of Atmospheric Chemistry*, *72*(2), 81–104. https://doi.org/10.1007/s10874-015-9305-5

Martonchik, J. V., & Diner, D. J. (1992). Retrieval of aerosol optical properties from multi-angle satellite imagery. *IEEE Transactions on Geoscience and Remote Sensing*, *30*(2), 223–230. https://doi.org/10.1109/36.134073

McComiskey, A., Schwartz, S. E., Schmid, B., Guan, H., Lewis, E. R., Ricchiazzi, P., & Ogren, J. A. (2008). Direct aerosol forcing: Calculation from observables and sensitivities to inputs. *Journal of Geophysical Research*, *113*(D9), 26793. https://doi.org/10.1029/2007JD009170

Michalsky, J. (2002). Broadband shortwave calibration results from the Atmospheric Radiation Measurement Enhanced Shortwave Experiment II. *Journal of Geophysical Research*, *107*(D16), 4743. https://doi.org/10.1029/2001JD001231

Michalsky, J. J., Schlemmer, J. A., Berkheiser, W. E., Berndt, J. L., Harrison, L. C., Laulainen, N. S., Larson, N. R., & Barnard, J. C. (2001). Multiyear measurements of aerosol optical depth in the Atmospheric Radiation Measurement and Quantitative Links programs. *Journal of Geophysical Research*, *106*(D11), 12099–12107. https://doi.org/10.1029/2001JD900096

Pincus, R., & Baker, M. B. (1994). Effect of precipitation on the albedo susceptibility of clouds in the marine boundary layer. *Nature*, *372*(6503), 250–252. https://doi.org/10.1038/372250a0

Sayer, A. M., Hsu, N. C., Lee, J., Kim, W. V., & Dutcher, S. T. (2019). Validation, stability, and consistency of MODIS Collection 6.1 and VIIRS Version 1 Deep Blue aerosol data over land. *Journal of Geophysical Research: Atmospheres*, *124*(8), 4658–4688. https://doi.org/10.1029/2018JD029598

Sayer, A. M., Munchak, L. A., Hsu, N. C., Levy, R. C., Bettenhausen, C., & Jeong, M.-J. (2014), MODIS Collection 6 aerosol products: Comparison between Aqua's e-Deep Blue, Dark Target, and "merged" data sets, and usage recommendations, *Journal of Geophysical Research: Atmospheres*, *119*(24), 13,965–13,989, doi:10.1002/2014JD022453.

Shaw, G. E. (1983). Sun photometry. *Bulletin of the American Meteorological Society*, *64*(1), 4–10. https://doi.org/10.1175/1520-0477(1983)064%3C0004:SP%3E2.0.CO;2

Sherman, J. P., Gupta, P., Levy, R. C., & Sherman, P. J. (2016). An evaluation of MODIS-Retrieved aerosol optical depth over a mountainous AERONET site in the southeastern US. *Aerosol and Air Quality Research*, *16*(12), 3243–3255. https://doi.org/10.4209/aaqr.2015.09.0568

Sherman, J. P., & McComiskey, A. (2018). Measurement-based climatology of aerosol direct radiative effect, its sensitivities, and uncertainties from a background southeast US site. *Atmospheric Chemistry and Physics*, *18*(6), 4131–4152. https://doi.org/10.5194/acp-18-4131-2018

Sherman, J. P., Sheridan, P. J., Ogren, J. A., Andrews, E., Hageman, D., Schmeisser, L., Jefferson, A., & Sharma, S. (2015). A multi-year study of lower tropospheric aerosol variability and systematic relationships from four North American regions. *Atmospheric Chemistry and Physics*, *15*(21), 12487–12517. https://doi.org/10.5194/acp-15-12487-2015

Twomey, S. (1977). The influence of pollution on the shortwave albedo of clouds. *Journal of the Atmospheric Sciences*, *34*(7), 1149–1152. https://doi.org/10.1175/1520-0469(1977)034<1149:TIOPOT>2.0.CO;2

Val Martin, M., Logan, J. A., Kahn, R. A., Leung, F.-Y., Nelson, D. L., & Diner, D. J. (2010). Smoke injection heights from fires in North America: analysis of 5 years of satellite observations. *Atmospheric Chemistry and Physics*, *10*(4), 1491–1510. https://doi.org/10.5194/acp-10-1491-2010

VanCuren, R. A., & Cahill, T. A. (2002). Asian aerosols in North America: Frequency and concentration of fine dust. *Journal of Geophysical Research*, *107*(D24), 367. https://doi.org/10.1029/2002JD002204

Van Donkelaar, A., Martin, R. V., Brauer, M., Hsu, N. C., Kahn, R. A., Levy, R. C., Lyapustin, A., Sayer, A. M., & Winker, D. M. (2016). Global Estimates of Fine Particulate Matter using a Combined Geophysical-Statistical Method with Information from Satellites, Models, and Monitors. *Environmental Science & Technology*, *50*(7), 3762–3772. https://doi.org/10.1021/acs.est.5b05833

Yu, H., Remer, L. A., Chin, M., Bian, H., Tan, Q., Yuan, T., & Zhang, Y. (2012). Aerosols from overseas rival domestic emissions over North America. *Science*, *337*(6094), 566–569. https://doi.org/10.1126/science.1217576

Zhao, T. X.-P., Stowe, L. L., Smirnov, A., Crosby, D., Sapper, J., & McClain, C. R. (2002). Development of a global validation package for satellite oceanic aerosol optical thickness retrieval based on AERONET observations and its application to NOAA/NESDIS operational aerosol retrievals. *Journal of the Atmospheric Sciences*, *59*(3), 294–312. https://doi.org/10.1175/1520-0469(2002)059<0294:DOAGVP>2.0.CO;2

Vita

Ian Krintz was born in Hampton, Virginia to Ann Fahres and Edwin Krintz Jr. He received his B.S. in Applied Physics from Appalachian State University in 2014. In 2016, he enrolled in the Engineering Physics program at Appalachian State University and then dual enrolled in 2018 in the Mechatronics and Smart Technologies program at Management Center Innsbruck in Austria. Both Master's degrees were awarded in 2021.

Mr. Krintz is a member of Sigma Pi Sigma and worked throughout his years at Appalachian State University as a member of the AppalAIR research team. He resides in Asheville, North Carolina with his wife Jessica and their two cats, Sid and Captain.